# Golden Goal Collaborates with Flamingo in Synaptic-Layer Targeting in the *Drosophila* Visual System

**Sandra Müller**
**PhD thesis**

from the faculty of biology of the Ludwig-Maximilians-Universität München

completed at the Max Planck Institute of Neurobiology

# Golden Goal Collaborates with Flamingo in Synaptic-Layer Targeting in the *Drosophila* Visual System

Dissertation der Fakultät für Biologie der Ludwigs-Maximilians-Universität München

Angefertigt am Max-Planck-Institut für Neurobiologie, Forschungsgruppe Neuronale Konnektivität (Takashi Suzuki)

Vorgelegt von Sandra Müller

Datum der mündlichen Prüfung: 14. Juli 2011

| | |
|---|---|
| Erstgutachter: | Prof. Dr. Rüdiger Klein |
| Zweitgutachter: | Prof. Dr. Parsch |

## Ehrenwörtliche Versicherung

Hiermit, erkläre ich, dass ich die vorliegende Dissertation selbständig und ohne unerlaubte Hilfe angefertigt habe. Ich habe mich dabei keiner anderen als der von mir ausdrücklich bezeichneten Hilfen und Quellen bedient.

## Erklärung

Ich erkläre hiermit, daß ich mich nicht anderweitig ohne Erfolg einer Doktorprüfung unterzogen habe. Die Dissertation wurde in ihrer jetzigen oder ähnlichen Form bei keiner anderen Hochschule eingereicht und hat noch keinen sonstigen Prüfungszwecken gedient.

München, Juli 2011

Sandra Müller

Die vorliegende Arbeit wurde zwischen Oktober 2007 und März 2011 unter der Leitung von Dr. Takashi Suzuki am Max-Planck-Institut für Neurobiologie in Martinstried durchgeführt.

**Publication from the work presented in this dissertation**

Hakeda-Suzuki S[*], Berger-Müller S[*], Tomasi T, Usui T, Horiuchi SY, Uemura T, Suzuki T. Golden Goal collaborates with Flamingo in conferring synaptic-layer specificity in the visual system. *Nat Neurosci*. 2011 Mar;14(3):314-23. Epub 2011 Feb 13.

[*]Equal contribution

*A mes parents…*

# TABLE OF CONTENT


Table of content 1
Index of figures 3
List of abbreviations 4
Abstract 7

**1. INTRODUCTION 8**

1.1 Molecular mechanisms of axon pathfinding 9
1.2 Mechanisms involved in synaptic specificity 12
1.3 The *Drosophila* visual system as a model for layer-specific targeting 14
1.4 Cell-surface molecules involved in R cells synaptic specificity 21
1.5 Phenotypic similarities between Gogo and Fmi 24
1.6 The thesis project 27

**2. MATERIAL AND METHOD 28**

2.1 Molecular biology 28
2.2 Cell culture-based assays 36
2.3 Biochemistry 40
2.4 *Drosophila* genetics and immunohistochemical staining 42

**3. RESULTS 50**

3.1 *gogo* and *fmi* genetically interact in R8 photoreceptor axons 50
3.2 *gogo* and *fmi* act in the same pathway 51
3.3 Gogo and Fmi co-accumulate at cell-cell contacts in cultured cells 52
3.4 Gogo ectopic expression induces Fmi mislocalization in wing cells 55
3.5 Gogo and Fmi interact *in cis* 58
3.6 Gogo/Fmi direct interaction could not be detected by co-immunopreciptation 61
3.7 Gogo forms oligomers 64
3.8 The BiFC assay showed unspecific fluorescent signal 65
3.9 *in situ* PLA generates unspecific background signal in S2 cells 67
3.10 Gogo does not modify the adhesive properties of Fmi in cultured cells 70
3.11 Gogo and Fmi collaborate to mediate M3 recognition 71
3.12 Fmi is required in L3 for R8 axon targeting 73

**4. DISCUSSION 80**

4.1 Gogo and Fmi interaction in neuronal development 80
4.2 Physical interaction between Gogo and Fmi 82
4.3 How does Gogo collaborate with Fmi in R8 axons? 86
4.4 Asymmetric Fmi homophilic interactions between R8s and target cells 88
4.5 How do Gogo and Fmi confer synaptic-layer specificity? 91
4.6 Redundant mechanisms for R8 targeting 93

4.7 Concluding remarks and general considerations about axon targeting 95

Supplemental figures 96
References 98
Acknowledgements 105
Curriculum vitae 106

## INDEX OF FIGURES

**Figure 1.1** Molecular mechanisms of axon pathfinding
**Figure 1.2** Mechanisms of synaptic specificity
**Figure 1.3** The adult *Drosophila* visual system
**Figure 1.4** Development of the visual system during the 3rd instar larval stage
**Figure 1.5** The two axon targeting steps of R7 and R8 photoreceptors
**Figure 1.6** Gogo and Fmi protein structure and mutant phenotypes in R8 photoreceptors
**Figure 2.1** The FLICK system and FRTs used to generate *fmi* and *gogo* knock-out
**Figure 3.1** Loss-of-function interaction between *gogo* and *fmi* in R8 photoreceptor axons
**Figure 3.2** The R8 phenotype is not enhanced in the double mutant for *gogo* and *fmi*
**Figure 3.3** Gogo and Fmi colocalize at cell-cell contacts
**Figure 3.4** Gogo interacts with Fmi in wing epithelial cells
**Figure 3.5** Adherens junctions are not disrupted in *gogo*-overexpressing cells
**Figure 3.6** Gogo and Fmi do not interact in *trans* in S2 cells
**Figure 3.7** Gogo does not relocalize Fmi in *trans* in wing cells
**Figure 3.8** Gogo recruits Fmi on lateral membranes of wing cells in *cis*
**Figure 3.9** Attempts to co-immunoprecipitate Gogo and Fmi
**Figure 3.10** Gogo forms oligomers in S2 cells
**Figure 3.11** The BiFC assay generates unspecific signal in transfected S2 cells
**Figure 3.12** PLA shows unspecific interactions of transmembrane proteins
**Figure 3.13** Gogo does not modulate Fmi homophilic interactions in S2 cells
**Figure 3.14** Gogo and Fmi collaborate in the recognition of the M3 layer
**Figure 3.15** Fmi is required in L3 neurons for R8 axon targeting to M3
**Figure 3.16** Monitoring of cells that undergo FLP-out with drivers used in *fmi* brain FLICK
**Figure 3.17** The synaptic layers of the medulla are not disrupted in *fmi* brain FLICK flies
**Figure 3.18** Fmi staining at the mid-pupal stage in *fmi* brain FLICK flies
**Figure 4.1** Phenotype summary and model

## LIST OF ABBREVIATIONS

| | |
|---|---|
| APF | after puparium formation |
| Big-2 | Brefeldin A-inhibited guanine nucleotide-exchange |
| BiFC | bimolecular fluorescence complementation |
| BMP | bone morphogenetic protein |
| cAMP | cyclic adenosine monophosphate |
| Caps | Capricious |
| cdc42 | cell division control protein 42 homolog |
| cGMP | cyclic guanosin monophosphate |
| CAM | cell adhesion molecule |
| CNS | central nervous system |
| CUB | complement subcomponents Clr/Cls, Uegf, Bmpl |
| DCC | deleted in colorectal carcinoma |
| Dscam | Down syndrome cell adhesion molecule |
| DSP | Dithiobis(succinimidyl propionate) |
| DTSSP | 3,3´-Dithiobis(sulfosuccinimidylpropionate) |
| E-Cad | E-Cadherin |
| EGF | epidermal growth factor |
| ElaV | embryonic lethal abnormal vision |
| Eph | Ephrin receptor |
| FLICK | FRTs located in *cis* for conditional knock-out |
| FLP | Flipase |
| Fmi | Flamingo |
| Fz | Frizzled |
| FRT | Flipase recognition target |
| Fwd | forward |
| Gal | genes induced by galactose |
| Gcm | glial cells missing |
| GMR | glass multiple reporter |
| Gogo | Golden Goal |
| GPCR | G-protein coupled receptor |
| GPI | glycophosphatidylinositol |
| GTPase | guanosine triphosphatase |
| HRM | hormone receptor domain |

| | |
|---|---|
| Ig | Immunoglobulin |
| Kirre | Kin of Irre |
| L1-L5 | lamina neurons 1 to 5 |
| LacZ | β-galactosidase |
| LAR | leukocyte common antigen-related |
| M1-M10 | medulla layers 1 to 10 |
| N-Cad | N-Cadherin |
| NGS | normal goat serum |
| OE | overexpression |
| PBS | phosphate saline buffer |
| PCA | protein complementation assay |
| PCP | planar cell polarity |
| PKA | protein kinase A |
| PKC | protein kinase C |
| PLA | proximity ligation assay |
| PTP69D | protein tyrosine phosphatase 69D |
| R1-R8 | retinula cells (photoreceptors) 1 to 8 |
| Rev | reverse |
| Repo | reverse polarity |
| Rac | Ras-related C3 botulinum toxin substrate |
| Rh | Rhodopsin |
| S2 | Schneider 2 cells |
| Src | Sarcoplasmic |
| Sema | Semaphorin |
| Seq | Sequoia |
| Shh | Sonic hedgehog |
| TSB1 | Thrombospondin 1 |
| UAS | upsteam activated sequence |
| Unc | Uncoordinated |
| UV | ultraviolet |
| Vang | Vang Gogh |
| Wnt | wingless and Int |

## ABSTRACT

Neuronal connections have to be established with extreme precision to allow proper information processing in the brain. Synaptic contacts are often organized in layers where neurons that have similar functions converge. How is synaptic-layer specificity achieved during development? In the *Drosophila* visual system, two different types of photoreceptors (R7 and R8) that respond to distinct wavelengths form connections in separate layers in the medulla. The atypical cadherin Flamingo (Fmi) and the putative receptor Golden Goal (Gogo) have a specific role in R8 axon targeting, whereas R7 are not affected in the mutants. R8 axons lacking *fmi* or *gogo* have a very similar phenotype: during mid-pupal stages, they fail to extend from their temporary target to their final layer. This suggested a potential interaction of these two genes in the final step of R8 axon targeting. We showed that *gogo* and *fmi* interact genetically in photoreceptor axons in loss-of-function and gain-of-function experiments. The R8 phenotype was not more severe in the double mutant, suggesting that *gogo* and *fmi* act in the same pathway. Our attempts to co-immunoprecipitate Gogo and Fmi were not successful, and assays to test protein-protein interactions in intact cells (bimolecular fluorescence complementation and proximity ligation assay) showed high unspecific background. Although we were not able to demonstrate a direct binding between Gogo and Fmi, we could show that they mutually influence their localization in cultured cells and *in vivo*. In pupal wings, Gogo ectopic expression induced the relocalization of Fmi in the same cell but not in adjacent cells, indicating that Gogo and Fmi interact in *cis*. R7 axons co-overexpressing Gogo and Fmi often stopped at the R8-recipient layer, suggesting that Gogo and Fmi collaborate to recognize the target cells of R8 photoreceptors. In addition, removing *fmi* from the target area induced premature R8 axon stopping, similarly to the phenotype observed in *fmi* mutant R8 photoreceptors. This result indicates that Fmi mediates R8 targeting via homophilic axon-target interactions. We further showed the requirement of *fmi* in lamina neurons L3 whose branches are restricted to the R8-target layer, suggesting that these neurons are the guidance target cells of R8 axons. Overall, we propose that asymmetric homotypic interactions between Gogo and Fmi in R8 photoreceptors and Fmi in their target layer govern the specificity of R8 axon targeting.

# 1. INTRODUCTION

The intricate architecture of neuronal circuits constitutes a functional network that allows sensory perception and complex behavior. In the developing nervous system, neuronal connections are established with astounding precision and fidelity, which is essential to form well-defined neural circuits and ensure proper information processing in the brain. Synaptic connections are often organized in characteristic neuropile structures, where synapses between neurons that have similar functional properties are clustered (Huberman et al.; Luo and Flanagan, 2007). For instance, olfactory sensory neurons which express identical olfactory receptors innervate the same spherical structures termed glomeruli. Similarly, in the visual system, photoreceptors which respond to the same feature of the visual input connect to the same layers in the brain.

The question of how axons navigate towards and select their appropriate target remains a challenging issue in neurobiology. Differentiating neurons extend their axons to the target region through an environment containing numerous axons and dendrites of other neurons, sometimes over long distances. Along their way, axons have to make various decisions, including stopping at intermediate positions to allow the development of their target, turning, bundling or defasciculating from other neurons. Once within the target field, axons select their synaptic partners among processes of many different neurons. In some cases, neuronal activity then refines the pattern of synaptic connections (Zou et al., 2004).

A specialized region at the tip of extending axons, the growth cone, mediates axonal growth in specific directions. Growth cones are highly motile structures that can sense, integrate and respond to different types of guidance signals: attractive or repulsive, which can act either at short or long-range. Signal transduction of these extracellular cues ultimately triggers guidance decisions such as growth, stopping, or turning by remodeling the cytoskeleton at the growth cone. Which are the molecular cues that instruct axons where to grow and what are the signaling mechanisms that lead to growth cone movements? After reaching the target field, how do axons choose their appropriate target among the numerous neurons that are in close proximity? These questions have been extensively studied and conserved mechanisms have emerged.

## 1.1 Molecular mechanisms of axon pathfinding

Trajectories followed by axons can often be divided into segments: axons grow linearly towards intermediate targets, where they have to decide how to continue their journey. Pioneer axons first innervate the developing nervous system when the cellular environment is still relatively simple. Other axons then follow this first axonal tract by fasciculation, which simplifies their task in an ever more crowded environment (**Fig1.1**).

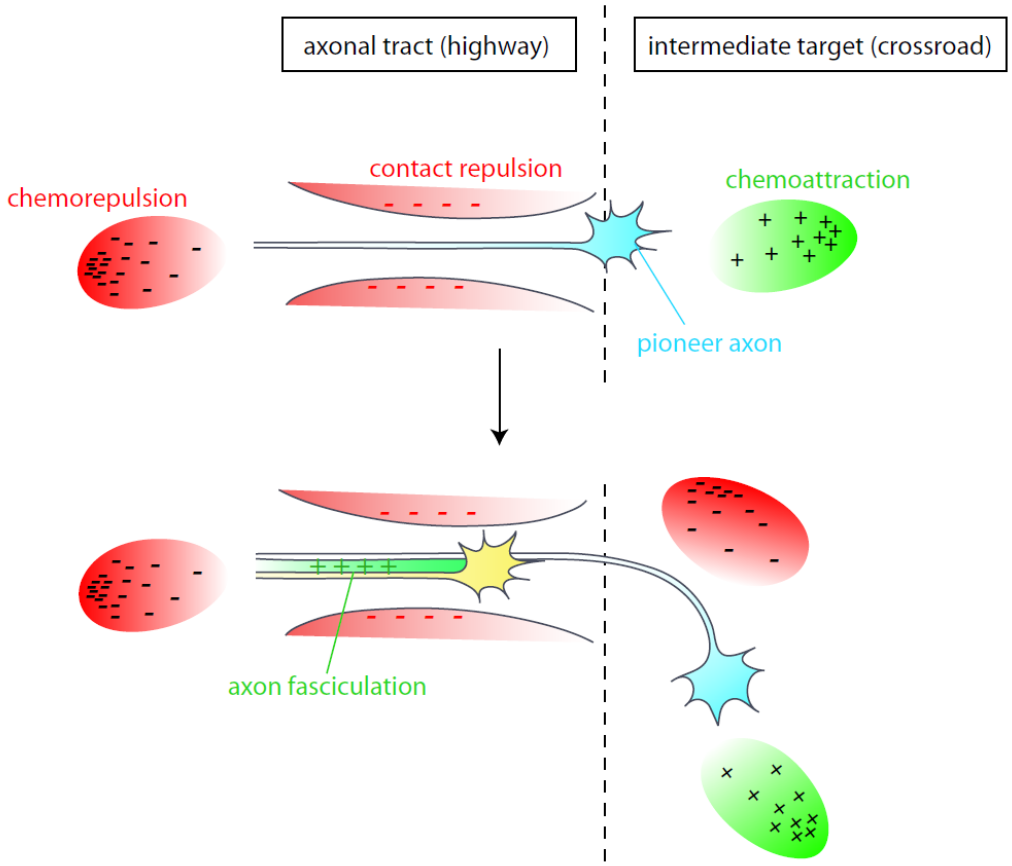


**Figure1.1 Molecular mechanisms of axon pathfinding**
Axonal trajectories can often be divided in distinct segments, consisting of "highways" where axonal extension is linear, and "crossroads" (or decision points) at intermediate targets, where axons choose their direction for the next segment of the trajectory. Pioneer axons find their way in the developing nervous system by responding to attractive or repulsive guidance forces, which can act at short or long distances. Later in development, migrating growth cones can follow the tracts of pioneer axons by selective fasciculation. The expression of guidance cues changes over time, allowing a dynamic regulation of axon guidance.

As early as in 1893, Ramon y Cajal proposed that growth cones might be guided by attractive gradients of diffusible factors emanating from their synaptic targets. However, before the 1990's, only few axon guidance molecules were discovered. The development of *in vitro* assays for the study of guidance cues in vertebrates and the numerous genetic studies in invertebrates allowed the identification of several conserved families of guidance proteins. Among these, the four "classical" axon guidance molecules, the Netrins, the Semaphorins, the Ephrins and the Slits families, were the most studied, although morphogens and cell adhesion molecules are also involved in axon pathfinding and target selection.

- Netrin was the first diffusible guidance molecule to be identified (Hedgecock et al., 1990; Mitchell et al., 1996; Serafini et al., 1996). Netrins can act either as attractants or repellants depending on the receptor they activate: DCC/Frazzled mediates attraction, whereas Unc5 is repulsive, also in combination with DCC (Culotti and Merz, 1998; Hedgecock et al., 1990; Keleman and Dickson, 2001). Recently, DSCAM has been shown to be another receptor for Netrin that contributes to axon guidance during development (Andrews et al., 2008; Ly et al., 2008).

- Slit proteins have been shown to be involved in the guidance of commissural axons at the CNS midline both in invertebrates and vertebrates. Slits act mainly as repellants via the Roundabout (Robo) receptors (Battye et al., 1999; Kidd et al., 1999; Kidd et al., 1998; Seeger et al., 1993).

- Semaphorins constitute a large family of axon guidance molecules divided in eight classes according to their structure. They can be either associated to the membrane or secreted, and have different receptors, the best characterized being Plexins and Neuropilins (Yazdani and Terman, 2006).

- Ephrins are membrane-bound guidance molecules that can be either GPI-anchored or transmembrane proteins. Ephrins are the ligands for the Eph family of receptor tyrosine kinases. Ligand/receptor binding can lead to the classical "forward signaling" through Eph, but also to "reverse signaling" where the ligand itself generate intracellular response (Dickson, 2002). Ephrin signaling often depends on receptor endocytosis and cleavage (Bashaw and Klein, 2010).

- Morphogen family proteins, known to regulate cell fate by gradients, have been shown to be also involved in axon pathfinding and topographic mapping (Zou and Lyuksyutova, 2007). For example, BMPs, Shh, and the Wnt family guide commissural

axons in the vertebrate spinal cord (Augsburger et al., 1999; Charron et al., 2003; Lyuksyutova et al., 2003).

- Cell adhesion molecules (CAMs) of the immunoglobulin (Ig) and cadherin superfamily are also involved in axon pathfinding. For instance, Fasciclin II, a member of the Ig superfamily, promotes the formation of axonal tracts by homophilic adhesion (Harrelson and Goodman, 1988). A case of axon guidance, rather than axon fasciculation, mediated by CAMs have been recently reported in *Drosophila*, where heterophilic interactions between the Ig superfamily members Beaten path (on the surface of motor neurons) and Sidestep (on the surface of cells along the way to the target) regulates axon pathfinding (Siebert et al., 2009).

Interestingly, many axon guidance molecules can mediate both axonal attraction and repulsion, and some of them can act at long and short-range. How is the axonal response to guidance molecules regulated? Signaling pathways activated by guidance cues trigger cytoskeleton reorganization in the growth cone. Attractive signals initiate intracellular events that finally lead to actin polymerization in the filopodia of growth cones and axonal extension toward the positive source. By contrast, repulsive cues support F-actin disassembly, what prevents motility in this direction. Guidance cues also regulate the polymerization, depolymerization or stabilization of microtubules (Bouquet and Nothias, 2007).

The second messengers calcium and cyclic nucleotides (cAMP and cGMP) have been shown to be involved in axon guidance signaling and to affect guidance responses. Downstream targets include kinases such as PKA, PKC and Src, or Rho-GTPases (Bashaw and Klein, 2010).

The role of Rho-GTPases in guidance receptor signaling and the consequences of their activation on the cytoskeleton have been well studied. The best characterized members of the Rho-GTPases family are Rho, Rac and cdc42. They are differentially regulated by axon guidance cues: Rho mainly promotes growth cone repulsion, whereas Rac and cdc42 rather mediate attraction (Bouquet and Nothias, 2007).

Recent studies suggest that local asymmetric translation of β-actin in the growth cone may be a driving force for axon turning (Leung et al., 2006; Yao et al., 2006). Interestingly, it has also been proposed that $Ca^{2+}$-dependent exocytosis and endocytosis participate in growth cone attraction and repulsion respectively (Tojima et al., 2007; Tojima et al., 2010).

## 1.2 Mechanisms involved in synaptic specificity

Once axons have reached their target field by responding to repulsive or attractive cues, they have to choose their proper synaptic target. It is difficult to separate axon pathfinding from synaptic targeting, since long-range cues guide axons to their target field, which is a prerequisite for correct synaptic partner selection. In addition, several of the axon guidance molecules listed above are also involved in synaptic targeting by acting at short-range. However, the formation of specific synaptic connections requires additional molecular mechanisms to fine-tune synaptic connection patterns.

One intuitive mechanism for axon-target recognition is molecular matching: cell adhesion molecules (CAMs) are expressed in a restrictive subset of axons and their corresponding synaptic partners, and specifically recognize each other by homophilic or heterophilic binding (**Fig1**.**2A**). This concept is nicely illustrated by the chick retina, where synaptic matchmaking is achieved by the homophilic adhesion molecules Sidekicks and Dscams (Yamagata and Sanes, 2008; Yamagata et al., 2002). Additionnally, a temporal coding of CAMs expression in axons or in their target add specificity to synaptic connections. The two major classes of cell adhesion molecules involved in synaptic targeting are the cadherins and the immunoglobulin superfamily (Shapiro et al., 2007; Takeichi, 2007).

CAMs can also function in axon sorting: similar axons that mediate the same information converge into the same target by adhesion (**Fig1**.**2B**). This strategy has been demonstrated in the mouse olfactory system, where Kirrel and Big-2 cell adhesion molecules mediate axon convergence into glomeruli (Kaneko-Goto et al., 2008; Serizawa et al., 2006).

The restricted expression of repellants in a subset of axons and target neurons can also participate in synaptic specificity (**Fig1**.**2D**). In the mouse spinal cord for instance, repellant signaling, induced by the recognition of Sema in a subset of motor neurons and Plexin in a subset of sensory neurons, regulates synaptic specificity by prohibiting inappropriate synapses (Pecho-Vrieseling et al., 2009).

Another way to specify synaptic connections is by interactions among afferents. This is the case for example in the *Drosophila* visual system, where the complex connection pattern of photoreceptors in the lamina is orchestrated by interactions between afferent growth cones just before they enter the target area (Chen and Clandinin, 2008; Clandinin and Zipursky, 2000; Sanes and Yamagata, 2009).

In the target field, axons can also stop at intermediate targets, in some cases to synchronize with the development of their synaptic partners. In the layered structure of the *Drosophila* medulla neuropile for example, photoreceptor targeting occurs in a two-step manner: axons stop at superficial layers for some hours before they extend towards their final synaptic partners (Ting et al., 2005).

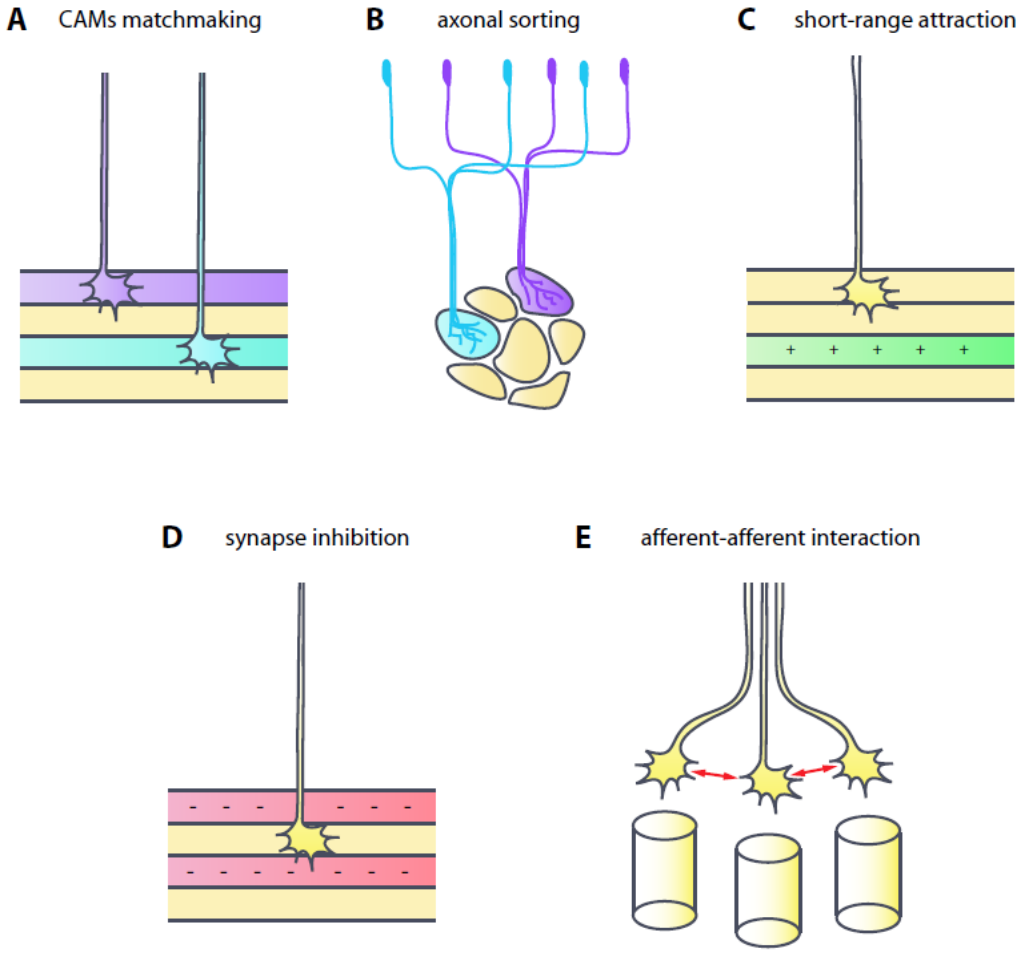


**Figure 1.2 Mechanisms of synaptic specificity**
(**A**) Cell adhesion molecules regulate synaptic specificity using their binding specificity. CAMs are expressed in a restricted number of axons and target cells. An axon expressing a single CAM target the layer which express the same CAM (homophilic binding) or a CAM that specifically bind to it (heterophilic binding). (**B**) A common way to regulate synaptic specificity in the olfactory system is by axonal sorting. Axons from olfactory neurons that express the same olfactory receptor fasciculate and innervate a single glomerulus. (**C**) Axon targeting can be mediated by diffusible or membrane-bound attractive cues that act at short-range. (**D**) Synapse formation can be restricted to specific area by synapse inhibition using repulsive cues. (**E**) Afferent-afferent interactions, in defascicling axon bundles for example, can regulate targeting specificity.

## 1.3 The *Drosophila* visual system as a model for layer-specific targeting

Although many advances have been made in understanding how axons target their synaptic partners, the high level of specificity of synaptic connections cannot be explained by the rather small amount of characterized axon guidance molecules. Our lab is trying to explore in more details how synaptic specificity is achieved using the *Drosophila* visual system as a model.

Already a century ago, Cajal noticed striking similarities between the neuronal circuits of flies and vertebrates visual systems (Cajal and Sanchez, 1915). Across animals, a prominent feature of the visual system is its organization in radial and layered structures. Nearby photoreceptors in the input field connect to adjacent target in higher brain centers, forming a radial arrangements of connections. This ordered projection of neurons, called topographic map, preserves the spatial relationships between the visual word and its representation in the brain. In addition, photoreceptor neurons which respond to different features of a visual stimulus, like color or brightness, form synapses in distinct layers (or laminae). Thus, each lamina contains synapses between neurons that have similar function and decodes similar features of the visual input.

In vertebrates, many regions of the brain and spinal cord can be divided into anatomical laminae which underlie the spatial and functional organization of synapses. Since the optic ganglia in the *Drosophila* visual system present a layered structure, this system is an attractive model to study the formation of synaptic layers (Astigarraga et al.; Mast et al., 2006; Sanes and Zipursky, 2010).

### 1.3.1 The adult *Drosophila* visual system

The fly visual system comprises the retina and four optic ganglia: the lamina, the medulla, the lobula and the lobula plate (**Fig1**.**3A**). The retina is made of about 750 hexagonal units called ommatidia. Each ommatidium contains 8 photoreceptors, or retinula cells (R1-R8). The outer photoreceptor cells R1-R6 express Rhodopsin 1 (Rh1) which responds to a broad spectrum of visible light. These photoreceptors mediate motion detection and form connections in the first optic ganglion, the lamina. The inner photoreceptors R7 and R8, which mediate color vision, project their axons through the lamina and target the second optic ganglion, the medulla. R7s express the UV-sensitive

opsins Rh3 or Rh4, whereas R8s express the opsins Rh5 or Rh6, which respond to blue and green visual inputs, respectively.

The lamina and the medulla are organized in radial synaptic units called cartridges and columns, respectively. Photoreceptors which see the same point in space innervate the same lamina cartridge for R1-R6 and the same medulla column for R7 and R8. Due to the curvature of the eye, R1-R6 photoreceptors from the same ommatidium do not see the same point in space. Therefore, one lamina cartridge receives input from six photoreceptors whose cell bodies belong to six neighboring ommatidia. R cells axons from the same ommatidium form a bundle in the retina, but then defasciculate and form a complex stereotyped connection pattern in the lamina, ensuring that axons from R cells which see a single point in space converge in one lamina cartridge (**Fig1**.**3B**). This superposition of axonal inputs increases light detection sensitivity. R1-R6 form synaptic connections with lamina neurons L1-L5, amacrine cells and centrifugal interneurons (Meinertzhagen and Sorra, 2001). In the medulla, each column is innervated by 50-60 neurons, namely photoreceptors R7 and R8, lamina neurons (L1-L5), medulla intrinsic neurons (Mi), transmedulla neurons (Tm and TmY), and distal medulla neurons (Dm) (Fischbach and Dittrich, 1989). All these neurons innervate the medulla layers M1-M10 with stereotypic connection patterns (**Fig1**.**3A**). R7 and R8 connect to M6 and M3, respectively. Transmedulla neurons transmit visual information to the two other optic ganglia, the lobula and the lobula plate. Complex patterns of connections relay this processed information from the lobula complex to higher brain centers.

The circuit underlying vision in *Drosophila* is of extreme complexity. What are the developmental steps that lead to these precise connection patterns in the adult eye?

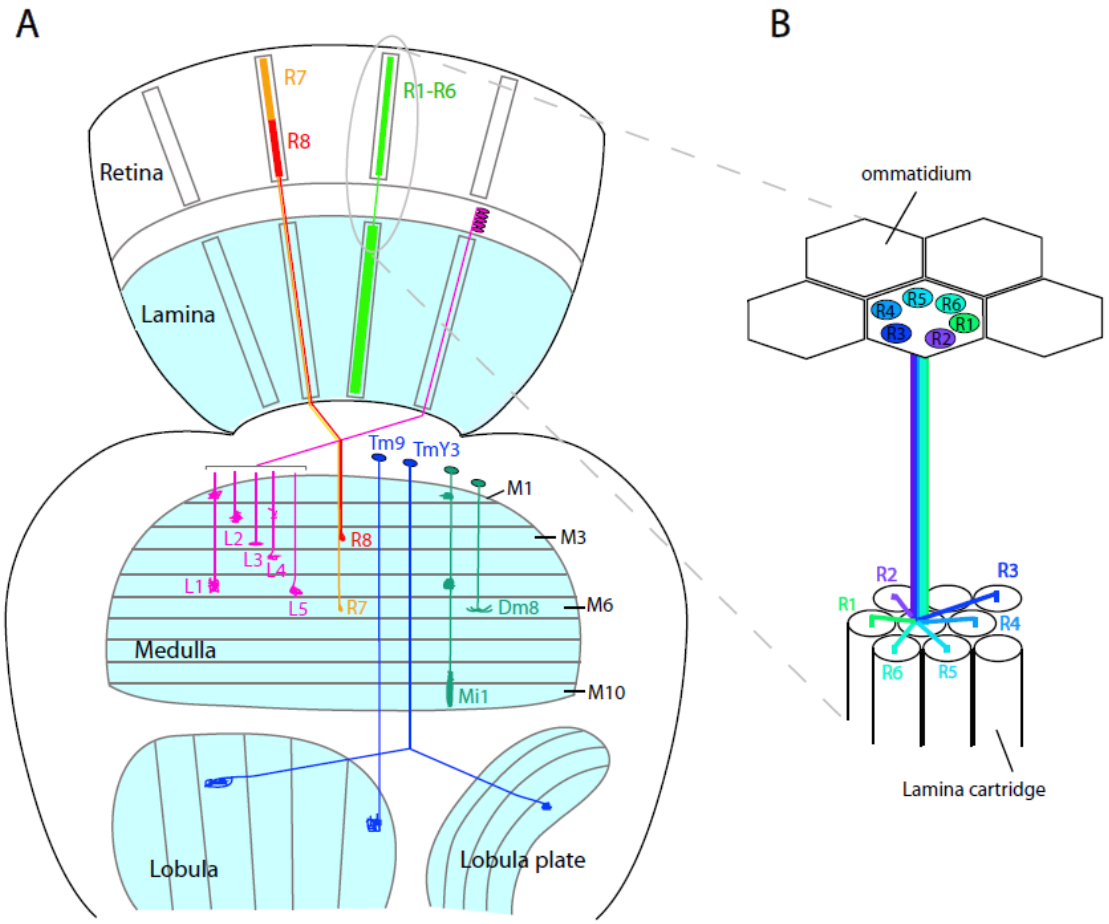


**Figure 1.3 The adult *Drosophila* visual system**
(**A**) The *Drosophila* visual system consists of the retina and four optic ganglia (blue areas): the lamina, the medulla, the lobula and the lobula plate. The photoreceptor cells (R1-R8) innervate different optic ganglion in the brain: R1-R6 target the lamina, whereas R7 and R8 connect to distinct layers in the medulla (M6 and M3, respectively). The lamina neurons (L1-L5), lying between the retina and the lamina, project their axons to the medulla and develop stereotyped neuronal processes in distinct medulla layers. Neurons whose nuclei are situated above the medulla can be classified in different categories: the medulla intrinsic neurons (Mi) which only innervate the medulla, the transmedulla neurons (Tm) that connects the medulla to the lobula, the TmY neurons whose axons connect the medulla layers with the lobula and lobula plate, and the amacrine distal medulla intrinsic neurons (Dm) branching in the distal medulla. Examples for each of these classes are depicted. (**B**) Due to the curvature of the eye, R1-R6 photoreceptors from the same ommatidium do not “see” the same point in space. Thus, a complex connection pattern is necessary to ensure that one lamina cartridge is innervated by axons that detect the same spatial input. R1-R6 axons that emerge from a single ommatidium form a fascicle, but unbundle just above the lamina and select distinct lamina cartridges, allowing a topographic projection of the visual input to the brain. (Adapted from Hadjieconomou et al., 2010)

### 1.3.2 Visual system development

The eye disc originates from an infolding of embryonic ectoderm that forms a simple epithelial sac and remains proliferative and unpatterned until the third instar larval stage (Wolff and Ready, 1993). At 40h before pupation, cells start to differentiate at the posterior side of the eye disc. This transition is marked by the formation of an indentation along the dorsal-ventral axis, called the morphogenetic furrow, which moves anteriorly (**Fig1**.**4**). Ahead of the furrow, cells are mitotic and unpatterned. Behind the furrow, R8 photoreceptors differentiate first. Then the photoreceptor types R2/R5 are specified, followed by R3/R4, then R1/R6, and finally R7. Photoreceptor axon outgrowth from the retina occurs sequentially following the wave of cellular differentiation in the larval eye disc. The pioneer R8 axons grow towards the optic lobe through a narrow tube-like structure called the optic stalk. At the end of the optic stalk, axons separate but retain their positions according to the retina, thus forming a topographic map. R8 axonal tracts act as a scaffold for the other photoreceptor axons. Indeed, R1-R7 axons fasciculate with the R8 axon from the same ommatidium and follow its trajectory until they reach the lamina. R8 axons, and later R7 axons, continue their journey towards the developing medulla, and finally pause at intermediate targets in superficial layers of the medulla during early pupal stages. R1-R6s temporarily terminate between two layers of glial cells in the developing lamina which provide a stop signal that prevents them to grow further in the optic lobe (Poeck et al., 2001).

R cells majorly influence the optic lobe development by inducing the growth, the differentiation, and the recruitment into columns of lamina neurons via the secretion of Hedgehog and the EGF-like ligand Spitz (Huang and Kunes, 1996; Huang et al., 1998). Then, L1-L5 axons bundle with R1-R6 axons to form a columnar structure (lamina cartridge). Hence, the temporal wave of R axon outgrowth in the optic lobe and the matched assembly of lamina cartridges are the major mechanisms for retinotopic map formation along the anterior-posterior axis. Besides, the dorso-ventral retinotopy is mediated by the Wnt4 ligand (Sato et al., 2006). Conversely, the development of medulla and lobula neurons seems to be largely independent from the innervation by sensory neurons (Fischbach, 1983).

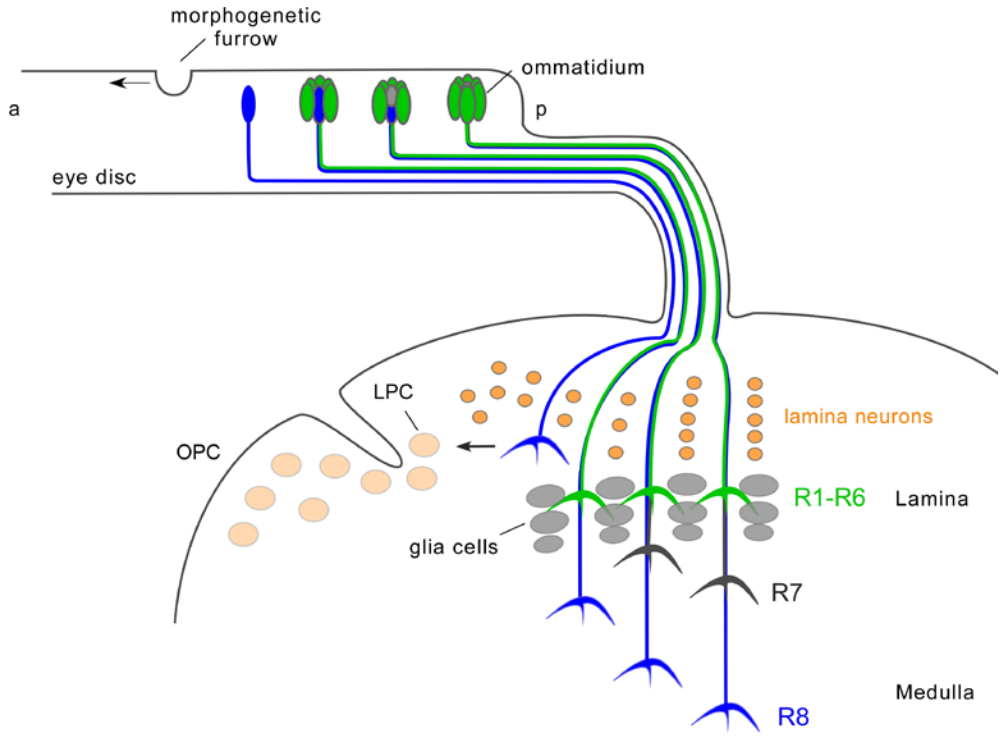


**Figure 1.4 Development of the visual system during the 3rd instar larval stage**
A wave of photoreceptor cell differentiation initiates at the posterior side of the eye disc and sweeps anteriorly following the morphogenetic furrow. R8 photoreceptors differentiate first, followed by R1-R6s, and finally R7s. Axonal extension into the brain occurs in the same order as cell specification. R8 axons are thus pioneers, and R1-R7 axons from the same ommatidium use R8 axonal tracts to find their way through the optic stalk and to the optic ganglia R1-R6s stop in the lamina between two layers of glial cells, and induce the proliferation, differentiation, and recruitment into columns of lamina precursor neurons (LPC). R8 axons extend through the lamina and project to the medulla, followed by R7 axons. OPC: outer proliferation center; a: anterior; p: posterior. (Adapted from Moses, 2002)

During pupal development, the optic lobe undergoes an intense reorganization: the developing optic ganglia move, and the lamina becomes centered below the retina. Additionally, the 90° rotation of the medulla leads to the formation of the optic chiasm (Meinertzhagen and Hanson, 1993).

As explained above, due to the curvature of the eye, the convergence of R1-R6 axons which see the same point in space to a single lamina cartridge requires a complex regulation of synaptic targeting. R1-R6 larval axons from the same ommatidia innervate the lamina as a bundle. During mid-pupal stages, R1-R6 axons defasciculate and extend in different directions. They select their appropriate cartridge, elongate centripetally, and finally form synapses along the lamina cartridges.

The column-targeting of R7 and R8 in the medulla is simpler, since the pair of R7/R8 in each ommatidium sees the same point in space. However, R7s and R8s target different medulla layers, M6 and M3 respectively. This specific targeting occurs in two steps (**Fig1.5**). First, at around 24h APF, R8 axons pause at the most superficial layer of the medulla, while R7 overtake R8 axons and stop at a deeper layer (**Fig1.5B**). At the same time, lamina neurons grow and establish stereotyped arborizations in specific medulla layers, which increases the distance between the R7- and R8-temporary layers. The stepwise targeting of photoreceptor axons allows their coordination with the formation of synaptic target layers. At 50h APF, R8s start to extend thin filopodia towards their final target layers, while their growth cones stay at the temporary layer (**Fig1.5C**). Finally, at 60h APF, R8 axons growth cones have reached their final target layer, and later retract their filopodia. R7 growth cones also arrive at the final layer around 60h APF, but it is not clear whether they migrate actively or are pulled by insertion of ingrowing medulla processes. Subsequently, R7 and R8 axons develop mature terminals and undergo synaptogenesis. Although synapses are often enriched in the tip of axons at their final target layer, synaptic contacts are also formed along the axonal shaft in R8s (Takemura et al., 2008).

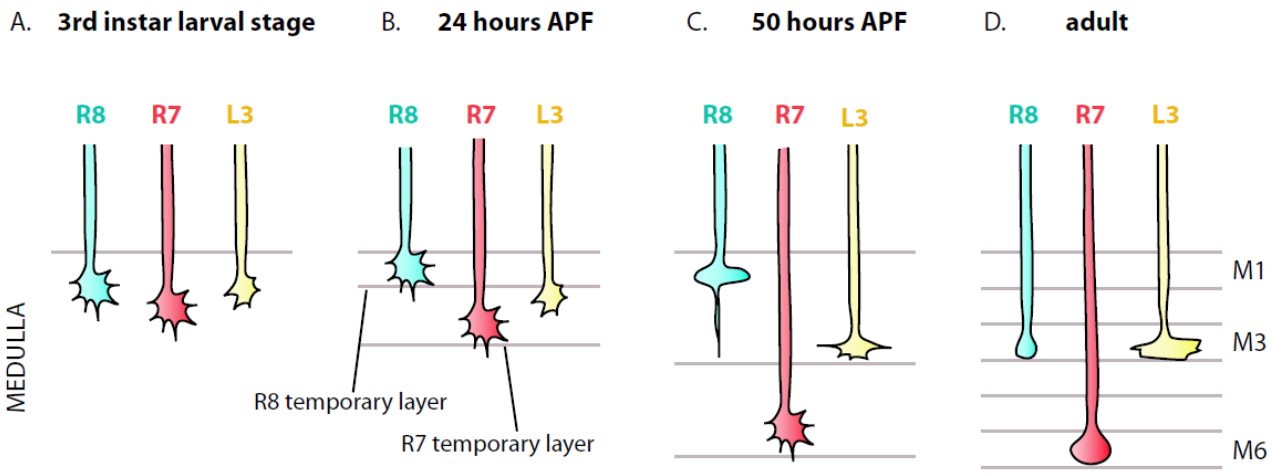


**Figure 1.5 The two axon targeting steps of R7 and R8 photoreceptors**
R7 axons are represented in red, R8 axons in blue, and L3 in yellow as an example of lamina neurons innervating the medulla. (**A**) During the 3rd instar larval stage, R8 axons first innervate a superficial layer in the medulla. They are followed by R7 axons, which slightly overtake R8 growth cones. L3 axons then extend from the lamina and target the same layer as R8 in the medulla. (**B**) At 24h APF, R7 and R8 have reached their respective temporary layer. L3 growth cones insert

between these two layers. (**C**) At around 50h APF, R8 axons form thin protrusions that target their future final layer, while R7 axons extend further in the medulla and L3 growth cones reach the layer targeted by R8s. (**D**) In the adults, R7 and R8 termini appear as small blobs in the M6 and M3 layers, respectively, whereas L3 axonal tips are flat axonal processes at the proximal part of M3.

## 1.4 Cell-surface molecules involved in R cells synaptic specificity

The development of the *Drosophila* visual system presents the major features described above underlying axon targeting, namely topographic mapping, column and layer targeting, axon fasciculation/defasciculation, and intermediate targets. Therefore, the *Drosophila* visual system provides an excellent model to study how these different processes are regulated. In vertebrates, neuronal activity is required to refine the pattern of synaptic connections. However, synaptic connections in the *Drosophila* visual system seems to be determined only genetically, since they are not dependent on vesicle release or electric activity (Hiesinger et al., 2006). What are the molecules involved in column selection in the lamina and layer targeting in the medulla? A number of cell-surface regulators of these processes have been identified.

The transmembrane proteins Flamingo (Fmi), N-Cadherin (N-Cad) and Leukocyte-antigen-related (LAR) have been shown to play a role in lamina cartridge targeting of photoreceptor cells. The atypical cadherin Flamingo (Fmi) have been identified as a major player in R1-R6 target selection (Lee et al., 2003). Chen and colleagues analyzed the targeting phenotype of R1-R6 in flies with a single *fmi* mutant or Fmi-overexpressing cell within an ommatidium. From this study, they proposed that Fmi mediates R1-R6 targeting in a non-autonomous way, and that the balance of Fmi homophilic interaction between afferent axons regulates the extension of growth cone to the appropriate direction (Chen and Clandinin, 2008). The typical cadherin N-Cadherin (N-Cad) is required for the defasciculation of R1-R6 axon bundles (Lee et al., 2001). Additionally, in mosaic *N-Cad* mutant flies, wild-type photoreceptor growth cones preferentially target N-Cad-expressing target cells, suggesting that N-Cad homophilic interaction stabilize the association between R cells and the lamina target neurons (Prakash et al., 2005). R cells mutant for the receptor tyrosine phophatase LAR also fail to unbundle when they innervate the lamina, but unlike N-Cad, LAR is not required in target cells (Clandinin et al., 2001; Prakash et al., 2009).

Interestingly, all these three cell-surface molecules are also involved in synaptic-layer selection in the medulla: LAR and N-Cadherin are required for R7 targeting, whereas Fmi mediates R8 targeting. In *N-Cad* mutants, R7 axons stop at the R8 targeting layer M3 instead of M6 (Lee et al., 2001). N-Cad regulates both the temporary and final

layer-targeting of R7 axons (Nern et al., 2005; Ting et al., 2005). Since N-Cad is expressed in the medulla, axon-target homophilic interaction could be involved in photoreceptor targeting. However, it is difficult to assess the requirement of N-Cad in the target area for R7 targeting to the M6 layer, since lamina neurons require N-Cad to target their proper medulla layers (Nern et al., 2008). In any case, since N-Cad is expressed in both R7 and R8 as well as in many medulla layers, it cannot account for the specificity of R7 targeting the M6 layer. Additionally, R7 targeting depends on the receptor tyrosine phosphatase LAR and PTP69D (Clandinin et al., 2001; Garrity et al., 1999; Maurel-Zaffran et al., 2001; Newsome et al., 2000). In both *LAR* and *PTP69D* mutants, R7 axons terminate at the M3 layer. *LAR* mutant R7 axons initially target their temporary layer, but then withdraw to the M3, suggesting a possible role of LAR in stabilizing connections.

On R8 photoreceptors, three transmembrane proteins have been identified as regulators of axon targeting: Fmi, the putative receptor Gogo (Berger et al., 2008; Tomasi et al., 2008), and the leucine-rich repeats cell adhesion molecule Capricious (Caps) (Shinza-Kameda et al., 2006; Shishido et al., 1998). Adult flies lacking *fmi* or *gogo* in photoreceptor cells show strong R8 targeting defects: R8 axons form bundles and often stop at the temporary layer M1 (Lee et al., 2003; Senti et al., 2003; Tomasi et al., 2008). Gogo overexpression lead to R8 stopping at the M1 layer, suggesting that Gogo promotes the recognition of the R8 temporary layer M1 (Tomasi et al., 2008). Gogo and Fmi function in R8 but are not required in R7, although they are expressed in both photoreceptor subtypes. Fmi is also expressed in several medulla layers, suggesting homophilic axon-target interactions. However, since Fmi and Gogo are broadly expressed, it is not clear how they can mediate the specificity of R8 targeting to the M3 layer. Conversely, the homophilic cell-adhesion molecule Caps is expressed specifically in R8s, and in distal medulla layers including the R8-recepient layer but not the R7-target layer. R8 axons lacking Caps abnormally terminate above or below the M3 layer. Importantly, R7 overexpressing Caps undershoot their correct target layer M6 and stop at the R8-recipient layer M3, suggesting that Caps has an instructive role for M3 targeting. From its expression pattern, and from the fact that Caps mediates homophilic adhesion in cultured cells, one can imagine that Caps interacts homophilically between R8 and neurons at the M3 layer. However, Caps requirement in target cells of R8s has not been tested, and Caps does not interact homophilically between the axons of olfactory receptor neurons and the dendrites of projection neurons (Hong et al., 2009).

In summary, axon targeting in the lamina and the medulla are mediated by partially overlapping cell-surface molecules which are expressed broadly. Thus, the molecular mechanisms underlying the specificity of photoreceptor connections remain obscure. To explain the layer-targeting specificity of R7 and R8, the “temporal targeting competence” model has been proposed: the Zn finger transcription factor sequoia (Seq) would sequentially regulate the competence of R8 and R7 growth cone to respond to broadly expressed cell adhesion molecules (Petrovic and Hummel, 2008). During the first targeting step, Seq expression appears as consecutive peaks (first in R8, then in R7) that match the sequential target layer innervation of R8 and R7 axons. In Sequoia mutants, both R7 and R8 axons abnormally terminate at superficial medulla layer, whereas prolonged expression in R8s leads to their targeting to M6. How Seq regulates “axonal competence” is however not clear, although the control of N-Cadherin expression level seems to be involved. Additionnally, Seq is expressed during the first targeting step only; thus, it does not explain how targeting specificity is achieved during the final layer targeting. Consequently, more detailed analysis is needed to decipher the molecular mechanisms that are responsible for synaptic specificity.

## 1.5 Phenotypic similarities between Gogo and Fmi

As mentioned above, Fmi is an atypical cadherin involved in the targeting of R8 axons. Fmi is a large transmembrane protein that contains numerous domains, including cadherin repeats which are thought to mediate homophilic adhesion, and a 7-transmembrane domain similar to G-protein coupled receptors (GPCR), which make this cadherin "atypical" (**Fig1**.**6A**). Since Fmi is expressed in R7 and R8 and in several medulla layers during R8 axon targeting, it is difficult to understand how Fmi mediates layer-specific targeting of R8 photoreceptor axons. We thus wanted to explore further the mechanism by which Fmi mediates the targeting of R8 axons. Interestingly, we noticed that *gogo* mutants have a very similar phenotype to *fmi* mutants in photoreceptor axon guidance (Lee et al., 2003; Senti et al., 2003; Tomasi et al., 2008). *gogo* codes for a transmembrane protein containing a CUB and a TSP1 domain that are known to function in axon guidance (**Fig1**.**6A**). In both *gogo* and *fmi* mutant larvae, R8 photoreceptor axons seem to lose repulsive interactions, leading to unevenly spaced axon shafts and growth cones, and to the formation of axon bundles. In the adult, both mutants show severe defects in R8 axons: they tangle up and most often stop at the superficial M1 layer (**Fig1**.**6B**). Therefore, the idea that *gogo* and *fmi* could act together in R8 axon guidance emerged.

We thus wanted to know whether the phenotypes seen in adult are the result of the same targeting defects during development. The *gogo* and *fmi* mutant phenotypes were analyzed in early to mid-pupal stages when R8 axons target their intermediate and their final layers in the medulla (Hakeda-Suzuki et al., 2011). In both mutants, the most prominent phenotype was the failure of R8 axons to extend their filopodia toward their final layer M3 at 50h APF, suggesting a common role of *gogo* and *fmi* in the guidance of R8 axons during the second targeting step (**Fig1**.**6B**).

Fmi is a multifunctional protein that is also required in R1-R6 photoreceptor targeting (Lee et al., 2003), in dendritic formation (Gao et al., 2000; Kimura et al., 2006), and in planar cell polarity (PCP) (Chae et al., 1999; Usui et al., 1999). We therefore checked whether *gogo* is also involved in these different processes (Hakeda-Suzuki et al., 2011). We found that *gogo* has a lamina cartridge selection phenotype: like in *fmi* mutants, cartridges contain a variable number of photoreceptor termini. Moreover, *gogo* is also involved in dendritic formation of multiple dendrites (md) neurons in the embryo, and md dendrites overgrow and cross the dorsal midline like in *fmi* mutants (Gao et al.,

2000; Hakeda-Suzuki et al., 2011). In contrast to *fmi*, *gogo* did not show a PCP phenotype and is not expressed in wing cells when PCP is established (data not shown).

Additionally, Gogo and Fmi share similarities in their expression pattern. Particularly in third instar larvae, Gogo and Fmi staining are essentially overlapping, and a strong signal was observed in the youngest photoreceptor axons innervating the optic lobe. Importantly, Fmi, but not Gogo, was also detected in the target area from the third instar larvae to the first half of the pupal stage (Hakeda-Suzuki et al., 2011).

Overall, the phenotypic similarities and overlapping expression patterns of Gogo and Fmi suggests that these two genes may collaborate during neuronal development.

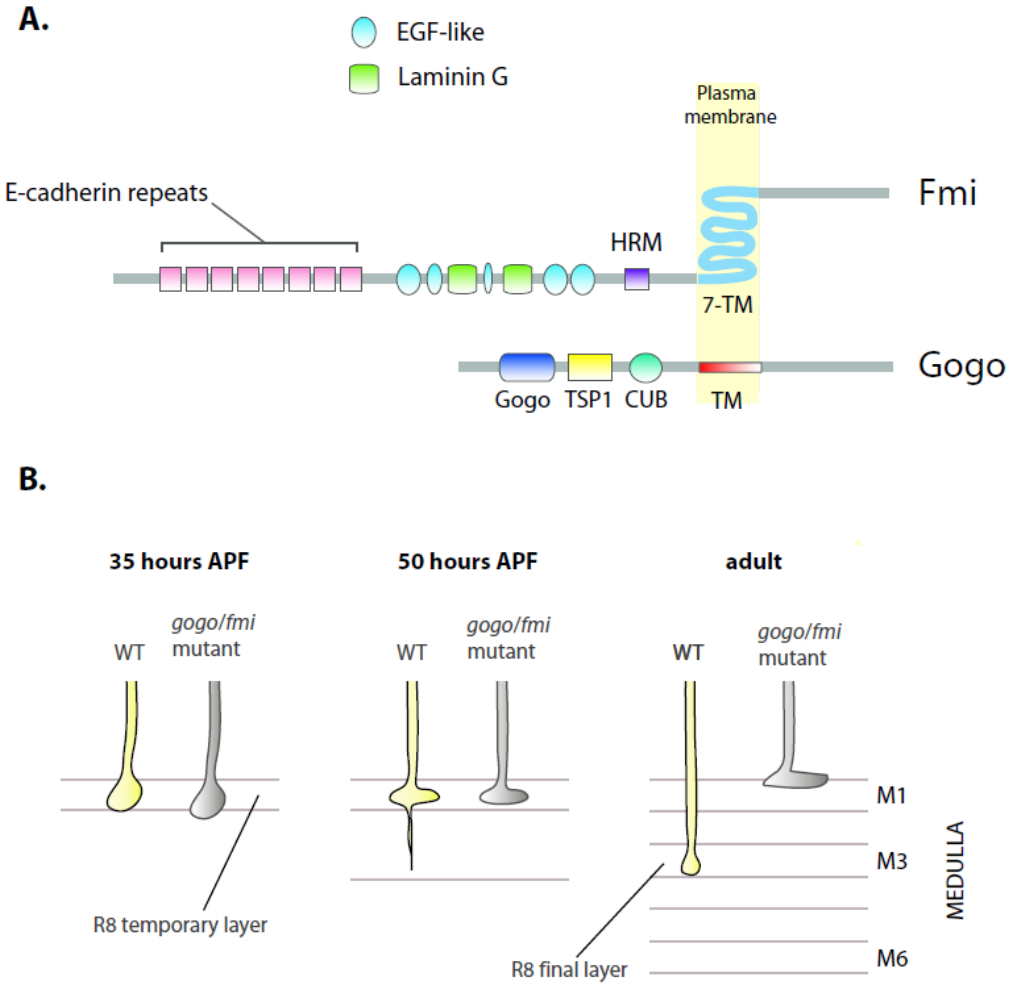


**Figure 1.6 Gogo and Fmi protein structure and mutant phenotypes in R8 photoreceptors**
(**A**) Structural domains of the Fmi and Gogo proteins. The atypical cadherin Fmi contains 8 cadherin repeats, EGF-like and Laminin G domains, a Hormone Receptor Motif (HRM), and a

seven-pass transmembrane domain (7-TM) similar to GPCR. Gogo extracellular part consists in a conserved Gogo domain (predicted to form four Ig-like folds), and TSP1 and CUB domains (both conserved in axon guidance molecules). The CUB domain is not required for R8 axon guidance, whereas the TSP1 and Gogo domains are crucial, as well as the cytoplasmic domain. (**B**) The *gogo* and *fmi* mutant phenotypes in R8 axon targeting during pupal development. At 35h APF, *gogo* and *fmi* mutant axons usually target the proper temporary layer, despite some overshooting. The most striking phenotype is visible at 50h APF, when wild type R8 axons extend thin filopodia towards the final target layer. In both *fmi* and *gogo* mutant, R8s fail to form these protusions. In adults, *gogo* and *fmi* mutant R8 axons abnormally stop at the M1 instead of the M3 layer.

## 1.6 The thesis project

Although a number of cell-surface molecules necessary for layer-specific targeting have been found in the *Drosophila* visual system, it is still not well understood how the specificity of synaptic connections is achieved by broadly expressed guidance cues. Since *gogo* and *fmi* have similar expression patterns and striking phenotypic similarities, we wondered if these two molecules closely work together and provide a combinatorial code of cell-surface proteins underlying the specificity of synaptic-layer targeting.

Therefore, the first goal of this project was to check whether *gogo* and *fmi* interact genetically and if they act in the same pathway. In addition, we wished to determine if Gogo and Fmi physically bind to each other, by analyzing their colocalization and by biochemical and cell-based assays. Furthermore, using *in vitro* and *in vivo* experiments, we wanted to find out how *gogo* and *fmi* collaborate and mediate targeting specificity of R8 photoreceptor axons. Finally, we wondered if Fmi was the ligand in target area of photoreceptor axons, and which cells in the medulla are responsible for R8 targeting.

The thesis project was conducted in team together with Satoko Suzuki. Satoko performed the genetic loss-of-function interaction between *gogo* and *fmi* (**Fig3.1**) and the double mutant (**Fig3.2**). We also collaborated in the miscolocalization of Fmi in wing cells (**Fig3.4, Fig3.6, Fig3.7**). Satoko participated in the gain-of-function interaction (**Fig3.14**), performed the *gcm*-FLICK (**Fig3.15b**,**f, Fig3.16b**,**d**, **Fig3.17b,d, Fig3.18b,e**). The figures presented in the supplemental information were made by Satoko.

# 2. MATERIAL AND METHOD

## 2.1 Molecular biology

### 2.1.1 Bacteria strains

**DH5α**

Genotype: F$^-$ φ80*lac*ZΔM15 Δ(*lac*ZYA-*arg*F) U169 *rec*A1 *end*A1 *hsd*R17 ($r_k$-, $m_k$+) *pho*A *sup*E44 λ$^-$ *thi*$^-$1 *gyr*A96 *rel*A1

**DB3.1**

Genotype: *e14$^-$ (McrA$^-$) □(mcrCB-hsdSMR-mrr)171 endA1 supE44 thi$^-$1 gyrA96 relA1 lac recB recJ sbcC umuC::Tn5* (Kan$^r$) *uvrC* [F' *proAB lacI$^q$ZΔM15 Tn10* (Tet$^r$)]
DB3.1 bacteria were used for the amplification of ccdB containing plasmids, since they are not sensitive to CcdB effects.

### 2.1.2 Media for bacteria

**LB medium**

Bacto-Tryptone 10 g/l
Bacto-Yeast extract 5 g/l
NaCl 5 g/l
pH 7.5
optional:
75 µg/ml Ampicillin
50 µg/ml Kanamycin

**LB plates**

LB medium 1 L
Bacto-Agar 15 g
optional:
75 µg/ml Ampicillin
50 µg/ml Kanamycin

### 2.1.3 Oligonucleotides

The following table indicates the primers used for the construction of expression vectors. All primers were ordered from the Metabion Company (Martinsried, Germany) with normal “desalted” purification and at a dilution of 100pmol/µl concentration.

| Primer name | Sequence | Use |
|---|---|---|
| SIGHA GW1 | GGGGACAAGTTTGTACAAAAAAGCAGGCTCAGCCACCATGGCCCTGTGCAGCGGCGGCAGC | attB1+kozak+SIGHA 5’ fwd |
| Unc5 GW3 | GGGGACCACTTTGTACAAGAAAGCTGGGTCAATCCACAAAGGGCCTATGGTTTC | unc5 3’+attB2 rev |
| TS089 | GCGCGCGGCCGCGGTACCGTCGACCCCGGGGGATCCACCATGGACA | Not+Kpn+Sal+VC fwd |
| TS097 | GCGCTCTAGATACCGGTCTTGTACAATTCATCCATACC | VC+stop+XbaI rev |
| TS088 | GCGCGCGGCCGCGGTACCGTCGACCCCGGGGGATCCACCATGGTGA | Not+Kpn+Sal+VNm9 fwd |
| TS112 | GCGCTCTAGATACCGGTGGCCATGATGTATACATTGTG | VNm9+stop+XbaI rev |
| TS092 | GCGCGCGGCCGCATGCGGAAAAACTCAAAGGAAATGGCGGC | NotI+gogo 5’ start fwd |
| TS093 | GCGCGGTACCCACGGCCACTTCCTTTGACTTCGGC | KpnI+ gogo 3’ rev |
| SB16 | GCGCGCGGCCGCATGGCCTCACCGTTGACCCGC | NotI+mcd8 5’ fwd |
| SB17 | GCGCGGTACCGCGGCTGTGGTAGCAGATGAGAGTGAT | KpnI+mcd8 3’ fwd rev |

### 2.1.4 Plasmids used for cloning

| Plasmid name | Description | Source |
|---|---|---|
| pUAS-SIGHA-Unc5d | UAS promoter, signal peptide from *wingless*, N-terminal HA-tag, Unc5d | Barry Dickson |
| pDONR™ 221 | Donor vector | Invitrogen |
| pKSWB-GFP | Destination vector with UAS promoter and C-terminal fusion of GFP | Stephan Ohler |
| pDEST13 | Destination vector with UAS promoter and C-terminal fusion of GFP | Stephan Ohler |
| pTS130 | Entry clone containing $Gogo^{Ecto}$::$Unc5^{TM+cyto}$ | Takashi Suzuki |
| pTT2 | Entry clone containing *gogo*ΔN-D | Tatiana Tomasi |
| pTT3 | Entry clone containing *gogo*ΔN-E | Tatiana Tomasi |
| pTT4 | Entry clone containing *gogo*ΔN-F | Tatiana Tomasi |
| pTT5 | Entry clone containing *gogo*ΔN-B | Tatiana Tomasi |
| pTT6 | Entry clone containing *gogo*ΔN-C | Tatiana Tomasi |
| pTT7 | Entry clone containing *gogo*ΔN-A | Tatiana Tomasi |
| pTT20 | Entry clone containing *gogo*ΔN-G | Tatiana Tomasi |
| pMT/V5his A | Metallothionein promoter, C-terminal V5 and His tags | Invitrogen |
| pUAS-*fmi*-EYFP | UAS promoter, *fmi*, C-terminal EYFP | Tadashi Uemura |
| pUAS-mCD8-KO-myc | UAS promoter, mCD8, C-terminal Kusabira-Orange and myc | Satoko Suzuki |
| pUAST | UAS promoter | Andrea Brand |
| pCS2-VC | Venus residues 155 -238 in PCS2 | Tom Kerppola |
| pCS2-VNm9 | Venus residues 1-154 with T153M mutation in pCS2 | Tom Kerppola |
| pUAS-*gogo*-myc | UAS promoter, *gogo* tagged with myc in C-terminal | Stephan Ohler |

### 2.1.5 Strategies used for molecular cloning

The following expression vectors were constructed:
pUAS-*unc5*-GFP
pUAS-*gogo*$^{Ecto}$::*Unc5*$^{TM+Cyto}$-GFP
pUAS-*gogo*ΔNA-GFP
pUAS-*gogo*ΔNB-GFP
pUAS-*gogo*ΔNC-GFP
pUAS-*gogo*ΔND-GFP
pUAS-*gogo*ΔNE-GFP
pUAS-*gogo*ΔNF-GFP
pUAS-*gogo*ΔNG-GFP
pMT-*fmi*-V5
pUAS-*gogo*-VC
pUAS-*fmi*-VN
pUAS-*mCD8*-VC

The pUAS-Unc5-GFP plasmid was generated by amplifying Unc5 from the pUAS-Unc5-HA plasmid with primers containing attB sequences (SIGHA GW1 and Unc5 GW3). This fragment was inserted in the donor vector pDONR211 by BP reaction, and recombined into the destination vector pKSWB-GFP by LR reaction.
For the UAS-Gogo$^{Ecto}$::Unc5$^{TM+cyto}$-GFP plasmid, the entry clone (TS130), containing the residues 1-399 of Gogo and 502-1072 of Unc5, was recombined to the destination vector pKSWB-GFP by LR reaction.
Unc5 related constructs contain the additional residues SF (HindIII) after the transmembrane domain, since they were amplified from the UAS-SIGHA-Unc5d plasmid.
For pUAS-*gogo*ΔNA-GFP, pUAS-*gogo*ΔNB-GFP, pUAS-*gogo*ΔNC-GFP, pUAS-*gogo*ΔND-GFP, pUAS-*gogo*ΔNF-GFP, LR reaction were performed between the destination vector pDest13 and pTT7, pTT5, pTT6, pTT2, and pTT4, respectively. pUAS-*gogo*ΔNE-GFP and pUAS-*gogo*ΔNG-GFP were constructed by LR reaction with the destination vector pKSWB-GFP, and pTT3 and pTT20, respectively.
For pMT-*fmi*-V5, the *fmi* DNA was cut from pUAS-*fmi*-EYFP with NotI and SalI, and cloned into pMT/V5-His A with NotI and XhoI.

For the BiFC constructs, VC (C-terminal part of Venus) was amplified from pCS2-VC with TS089 and TS097, cut with NotI and XbaI, and inserted into pUAST between the NotI and XbaI sites. VN (N-terminal part of Venus) was amplified from pCS2-VNm9 with TS088 and TS112, and cut with NotI and XbaI. The vector pUAST was cut with EcoRV and religated to remove a part containing a SalI site (which prevents the subsequent insertion of Fmi in the vector). This vector was then cut with NotI and XbaI, and the VN cut PCR product was ligated between these restriction sites.
*gogo* coding sequence was amplified from pUAS-*gogo*-myc with TS092 and TS093 and cut with NotI and Asp718 (Asp718 recognizes KpnI restriction site). mCD8 was amplified from pUAS-mCD8-KO-myc with SB016 and SB017 and cut with NotI and Asp718. These inserts were ligated into pUAS-VC cut with NotI and Asp718. Fmi was cut from pUAS-*fmi*-EYFP with NotI and SalI, and inserted in pUAS-VNm9 cut with the same enzymes.

### 2.1.6 Standard cloning methods

**Polymerase chain reaction (PCR)**

- Reaction mix

25µl 2x iProof High-Fidelity Polymerase Master Mix (Biorad)
2.5µl primer sense (10mM)
2.5µl primer antisense (10mM)
1µl template (50ng/µl)
19µl dd$H_2O$

- Standard PCR program

1. 98°C 30sec
2. 98°C 10sec
3. annealing temperature : from 58-70°C 30sec
4. 72°C 30sec/kb
5. Step 2 to 4 for 34 more cycles
6. 72°C 10min

**PCR purification**

To purify PCR products, the PCR reaction was cleaned using the PCR purification kit from Qiagen according to the manufacturer's intructions.

**DNA digestion by restriction enzymes**

To digest plasmids or PCR constructs, the following reaction was used:
1µg DNA
1µl enzyme
5µl 10X buffer
$H_2O$ (to 50µl)
The reaction was incubated for 1h30 at 37°C.

**DNA gel electrophoresis**

Depending on the size of the DNA fragment to be separated, the agarose concentration in TAE buffer ranged from 0.5%-2.0%. Ethidium bromide was added to the melted agarose to a final concentration of 0.5µg/ml before pouring it in the mold. The DNA gel was run in 1xTAE buffer. The loading buffer was added to the DNA sample before electrophoresis.

6x loading buffer
0.25% Bromphenol blue
0.25% Xylene Cyanol
30% Glycerol
100mM Tris pH 7.5
100mM EDTA pH 8.0
$H_2O$

50xTAE (2l)
484g Tris base
50mM EDTA pH 8.0
114.2ml glacial acetic acid
$H_2O$
adjust pH 8.5 with gl. ac. acid

**DNA extraction from agarose gels**

To purify specific DNA fragments, DNA was separated on an agarose gel. The band of interest was cut out from the gel using a sterile razor blade and purified using Qiagen Gel Extraction Kit as described in the company's manual. DNA was eluted in 30µl EB buffer.

**Ligation**

The following reaction was used to ligate an insert in a plasmid:
100ng plasmid
300ng insert
3µl 10X ligase buffer

1µl T4 ligase
$H_2O$ (to 30µl)
The reaction was incubated at 25°C for 2h to overnight.
The ratio plasmid/insert can be optimized (from 1:1 to 1:6).

### 2.1.7 Cloning with the Gateway recombination system

PCR products containing attB recombination sites were inserted into the donor vector by BP reaction, performed as follow:
1-2µl attB-PCR product (final amount: 50-150ng)
1µl pDONR™ vector (supercoiled, 150 ng/µl)
To 4µl TE Buffer, pH 8.0
1µl BP Clonase™ II enzyme mix
The reaction was incubated for 2h to overnight at 25°C. 1µl of Proteinase K was added to terminate the reaction, and samples were incubated for 10min at 37°C.

The following LR reaction was used to recombined the entry vector with the destination vector, leading to the generation of the expression clone:
1-2µl Entry clone (final amount: 50-100ng)
1µl destination vector (supercoiled, 150 ng/µl)
to 4µl TE Buffer, pH 8.0
1µl LR Clonase™ II enzyme mix
The reaction was incubated for 2h to overnight at 25°C. 1µl of Proteinase K was added to terminate the reaction, and samples were incubated for 10min at 37°C.

### 2.1.8 Transformation and plasmid preparation

After thawing 100µl competent bacteria from a -80°C stock on ice, the bacteria were incubated with ~100ng of DNA on ice for 30min. The cells were heat-shocked at 42°C for 90sec and immediately returned on ice for 1-2min. To allow expression of resistance genes in transformed bacteria, the cells were shaken for 1h at 37°C after the addition of 750µl of LB medium. Afterwards, bacteria were plated on LB plates containing selective antibiotics and incubated overnight at 37°C.

Single colonies were picked up from the Petri dish and grown in LB medium containing the proper antibiotic. Bacterial plasmids were purified using the Qiagen Kits as described in the manual provided by the company. For Mini-Preps and Midipreps, 5ml and 50ml of overnight bacteria culture were used, respectively. After plasmid preparation, the DNA concentration was determined using a spectrophotometer (NanoDrop 1000 Spectrophotometer, PeqLab).

## 2.2 Cell culture-based assays

### 2.2.1 Media for S2 cells

Schneider's Drosophila medium (Promocell)
10 % heat-inactivated Fetal Calf Serum
50 units Penicillin/ml
50 µg Streptomycin/ml

### 2.2.2 Cell culture and transfection

The Schneider's line 2 (S2) cell line is derived from a primary culture of late stage *Drosophila melanogaster* embryos (Schneider, 1972). Many characteristics of the S2 cell line suggest that they are derived from macrophage-like lineage.

S2 cells were maintained in a 25°C incubator without $CO_2$, in Schneider's medium (PromoCell GmbH) supplemented with 10% heat-inactivated FCS, 2mM glutamine, 100 units/ml penicillin, and 100µg/ml streptomycin. Cells were passaged every 3-4 days at a 1:2,5 dilution.

For transient transfection, cells were seeded at $10^6$ cells/ml in 6-well plates (2ml per well). After 16h, cells were transfected with Cellfectin (Invitrogen) according to the manufacturer instructions. Per well, 1-2µg of plasmid and 10µl of Lipofectamine were used. The DNA and Cellfectin were separately diluted in 100µl of serum free medium (without antibiotics), mixed together, and incubated at room temperature for 30min. Cells were washed with serum-free medium, 0.8ml of serum free medium were added to each well, and the transfection mix was added dropwise. After 5-6h incubation, the transfection mix was removed and cells were grown in complete medium (2ml/well).

All expression constructs contained the UAS promoter, except Fmi-V5 which was under the metallothionein (MT) promoter. UAS was activated by co-transfection with pActin5C-Gal4, and MT by incubation with copper sulfate (500µM). The time of expression depended on the type of the experiment.

The following plasmids were used for S2 cells transfection:
pActin-*gal4* (Jürgen Knoblich)
pUAS-*gogo*-myc (Stephan Ohler)

pUAS-*gogo*-GFP (Stephan Ohler)
pUAS-*gogo*ΔC-GFP (Stephan Ohler)
pUAS-*gogo*$^{Ecto}$::*Unc5*$^{TM+Cyto}$-GFP
pUAS-*fmi* (Tadashi Uemura)
pUAS-*fmi*ΔC (Tadashi Uemura)
pUAS-*E-cadherin*-GFP (Hiroki Oda)
pUAS-*unc5*-GFP
pUAS-*citrine* (Tadashi Uemura)
pUAS-*dsRed* (Gaia Tavosanis)
pUAS-*mcd8*-GFP (Satoko Suzuki)
pUAS-*N-Cad* (Tadashi Uemura)
pUAS-*gogo*-VC
pUAS-*fmi*-VN
pUAS-*mCD8*-VC
pMT-*fmi*-V5
pUAS-HA-fmi$^{EctoΔCad}$ (Satoko Suzuki)
pUAS-GogoΔN-myc (Stephan Ohler)
pUAS-mCD8-KO-myc (Satoko Suzuki)

### 2.2.3 Immunocytochemical staining

Cells were attached to slides coated with poly-L-lysine (µ-slide IV 0.4, IBIDI) for 1hr, washed 2 times with 100µl PBS, fixed for 30min at 37°C with paraformaldehyde (4% in PBS), washed 2 times with PBS, permeabilized with 0.1% Triton X-100 in PBS for 3min, washed 2 times with PBS, and incubated with 5% NGS in PBS for 30min. Cells were incubated for 1h30 with the primary antibody, washed 3 times in PBS, and incubated for 1h with the secondary antibody. The following primary antibodies were used: mouse anti-Fmi (#74; 1:50, DSHB), rabbit anti-Gogo (1:20), rat anti-mCD8 (MCD0800, 1:400, Invitrogen), and rabbit anti-GFP Alexa Fluor488-conjugated (Molecular Probes, 1:300). Alexa Fluor-conjugated secondary antibodies (488, 568, 633; Molecular Probes) were used at 1:300.

.

### 2.2.4 Cell aggregation assay

72hr after transfection, cells were diluted to obtain a concentration of $10^6$ cells/ml and agitated on a rotary shaker for 2hr. To concentrate the samples, cells were centrifuged at 1000g for 1min and resuspended in 1/10 of the initial medium volume. The immunostaining was performed as described above.
To quantify protein accumulation at cell-cell contacts, we used Photoshop to calculate the fluorescence intensities of selected areas at cell-cell borders and on membranes which were not contacting other cells. The background fluorescence was subtracted, and the ratio of the fluorescence intensities between cell-cell contact membranes and free membranes was calculated.

### 2.2.5 Bimolecular Fluorescent Complementation (BiFC) assay

S2 cells were transfected with VN and VC-tagged constructs with Act-Gal4 using a low concentration of DNA to avoid unspecific binding (0.02µg per well in 24-well plates). 48h after transfection, cells were transferred to slides, fixed, and stained as decribed above.

### 2.2.6 Proximity Ligation Assay (PLA)

Since secondary PLA probes exist only against mouse and rabbit antibody, primary PLA probes were made for rat anti-N-Cad (Ex#8, DSHB) and rat anti-mCD8 (MCD0800, Invitrogen) using the Duolink probemaker kit (Olink Bioscience). 40µl of N-Cad antibody were diluted in 800µl of PBS, and purified using a microcon filter (YM-3, cut-off 3,000 MW, Millipore) by centrifugation at 10,000g for 50min. 100µl of rat anti-mCD8 were concentrated using the same procedure (final volume of 20µl). 2µl of conjugation buffer was added to 20µl of antibody at 1mg/ml. The mix was added to the vial of activated oligonucleotide (Duolink II PLUS or MINUS) and incubated at room temperature overnight. 2µl of stop reagent was added, and the reaction was incubated at room temperature for 30min. 24µl of storage solution was added, and probes were kept at 4°C.
The PLA was conducted as described in the Duolink II Fluorescence user's manual (Olink Bioscience). 72hrs after transfection, cells were fixed and blocked as described

above and incubated with the PLA probes. The PLA reaction was done according to the DuolinkII Fluorescence protocol (Olink Bioscience). Slides were incubated with non-conjugated primary antibody (diluted in 5% NGS in PBS) for 1h30 at room temperature, washed 3X with buffer A, and incubated with the PLA probe (diluted in the Antibody Diluent) for 1h. Sildes were washed 3X with buffer A and incubated with the ligation mix (1µl ligase, 8µl of 5X ligation stock, 31µl of high purity water) for 30min at 37°C. Slides were washed 3X with buffer A, and incubated with the amplification mix (0.5µl of polymerase, 8µl of amplification stock, 31,5ml of high purity water) for 80min at 37°C. Slides were washed 3X in buffer B for 2min, and Vectashield was added. For the quantification, the number of PLA dots per cells were counted on at least 15 cells in 3 independent experiments.

## 2.3 Biochemistry

### 2.3.1 Co-immunoprecipitation

48hr after transfection, cells were washed twice in PBS, and lysed with a dounce homogenizer in lysis buffer (1% NP-40, 150mM NaCl, 50mM Tris, pH 7.5) containing protease inhibitors (Roche). After centrifugation at 13,000g for 15min, the protein concentration was determined using the Bradford method (Protein Assay, Biorad). 250 µg of lysate diluted in lysis buffer was incubated with 20µl of anti-myc, anti-V5, or anti-HA agarose beads (Sigma) for 2hr at 4°C. The beads were washed three times with 750µl of lysis buffer and incubated with Leammli loading buffer at 65°C for 30min. The beads were removed by centrifugation before loading on a polyacrylamide gel. Myc-tagged constructs were detected by mouse anti-Myc (9E10, 1:100, Santa Cruz), Gogo-GFP by mouse anti-GFP (JL-8, 1:1000, Clonetech), Fmi-V5 by mouse anti-Fmi (#74; 1:50, DSHB) or mouse anti-V5 (1:5000, Invitrogen), HA-Fmi$^{EctoΔCad}$ by rat anti-HA (3F10, 1:1000, Roche).
For co-immunoprecipitation in larvae, 150µg of proteins were used (corresponding to approximately 100 dissected brains).

For crosslink experiments, 48h after transfection, cells were washed twice in PBS, and incubated with 2ml of DTSSP (1mM in PBS, Pierce) for 30min at room temperature. To quench the reaction, 20µl of stop solution was added (1M Tris, pH7.5) and cells were incubated for 15min at room temperature. Cells were then lysed and treated as described above. For non-reducing conditions in the Gogo oligomerization experiment, samples were incubated with NuPAGE® LDS Sample Buffer (Invitrogen) with or without NuPAGE® reducing agent dithiothreitol (Invitrogen).

### 2.3.2 Western blot analysis

Protein samples were incubated for 30min at 65°C with the loading buffer. Proteins were separated by SDS-PAGE on a 7% or 3-7% Tris-acetate gel (Invitrogen) in Novex Tris-acetate SDS running buffer (invitrogen). Gels were run at 150V for 1-1h30 until the loading dye run out. Proteins were blotted on a Hybond ECL Nitrocellulose membrane (Amersham) overnight with 90mA/gel. Protein transfer was check by Ponceau staining (0.1% Ponceau S, 5% acetic acid). Membranes were washed briefly with water and

incubated with blocking solution (5% milk powder in PBS) for 1h. The primary antibody was applied in blocking solution overnight at 4°C in a wet chamber on a shaker. The membrane was washed 3 times for 10 min with PBS. The secondary antibody was diluted in PBS and membranes were incubated for 1h30 at room temperature under agitation. The membrane was washed 3 times for 10 min with PBS. The membrane was incubated in ECL solution (GE Healthcare) for 1min, transferred to a western blot cassette, and exposed to Hyperfilm ECL (Amersham).

To stain the nitrocellulose membrane, the following primary antibodies were used: anti-GFP (JL-8, Clontech, 1:2000), anti-myc (9E10, Santa Cruz, 1:100), rat anti-HA (3F10, 1:1000, Roche), mouse anti-V5 (1:5000, Invitrogen), and mouse anti-Fmi (#74; 1:50, DSHB). As secondary antibodies, the following HRP-conjugated antibodies were used: ECL™ HRP-conjugated anti-mouse (1:5000, NA931V, GE Healthcare), ECL™ HRP-conjugated anti-rat (1:3000, NA935V, GE Healthcare), and HRP-conjugated anti-rabbit (1:1000, Bethyl laboratories).

Loading buffer

100mM Tris pH 6.8
40g/l SDS
20% Glycerol
0.25g/l Bromphenol Blue
200mM β-Mercaptoethanol

## 2.4 *Drosophila* genetics and immunohistochemical staining

### 2.4.1 Fly maintenance

Flies were cultured in vials, or in bottles for expansion with ~2 cm of fly food covering the bottom part. Vials/bottles were put into cardboard boxes and stored in incubators with controlled temperature and humidity. Humidity was held constantly between 60 and 70%, while the temperature was set to 25ºC for expanding flies, including crossings, and to 18ºC for maintaining the stocks. For collecting virgins or analyze the markers, flies were anaesthetized with $CO_2$, transferred to a $CO_2$ pad and examined with a stereomicroscope (Leica MS5, Leica MZ9.5, Leica PM IL fluorescence microscope, Olympus SZX16)

**Standard Drosophila medium**

For 50L medium, 585g Agar was dissolved in 30l of water by heating the mixture to the boiling point; meanwhile 3 kg corn flour and 750 g yeast (Femipan Inc.) were mixed with water to obtain a homogeneous broth. As soon as the agar was dissolved, 4 kg molasses and corn flour/yeast were added. The mélange was filled up with water to 50l and cooked at 96°C for 1,5h. 315ml Propionic acid and 120g Methylparaben were added after the mixture had cooled down to 60 °C.

**Blue Yeast paste**

Instant dry yeast (Femipan Inc.) was mixed with Instant blue Drosophila medium (Fisher Scientific) and water.

For all experiments, flies were grown at 25ºC unless indicated. The co-overexpression of *gogo* and *fmi* transgenes was carried out at 20°C to reduced the expression level of Gogo and Fmi. To generate clones overexpressing *gogo* in the wing, flies were heat-shocked for 30min at 37°C at day 3 after egg laying (AEL). To produce *fmi* mutant clones in the wing disc, larvae were heat-shocked for 1h at 37°C at day 3 AEL.

### 2.4.2 Drosophila stock lines

The stock lines used to establish new lines are listed in the following table.

| Genotype | Description/Use | Source |
|---|---|---|
| $w^{1118}$ | $w^-$ control flies | Bloomington |
| GMR-FLP mCD8-GFP/FM7 | Balancer 1st | Larry Zipursky |
| yw ; Pin/CyO, $y^+$ | Balancer 2nd | Barry Dickson |
| yw ; MKRS/TM6B, $y^+$ | Balancer 3rd | Barry Dickson |
| yw eyFLP2 C-LacZ; Sp/CyO, $y^+$; MKRS/TM6B, $y^+$ | Double balancer | Takashi Suzuki |
| *w*; Sco/Cyo; MKRS/TM6B | Double balancer | Bloomington Stock |
| *w/yw*; (UAS-*gogo*T2)/CKG; (Caps-GAl4 y99)/TM6, $y^+$ | Double balancer | Gaia Tavosanis |
| eyFL2 C-LacZ; FRT82B | Recombination on the 2R | Barry Dickson |
| *Rh6*-GFP-myc *ey*3.5 FLP; Pin/CyO | R8-specific marker + FLPase under R cells specific promoter | Satoko Suzuki |
| *w*; ; *Rh6*-GFP-myc/ TM3 | R8-specific marker | Takashi Suzuki |
| *Rh4*-GFP-myc *ey3.5* FLP; *Sco*/CyO; MKRS/TM6B | R7-specific marker + FLPase under R cells specific promoter | Satoko Suzuki |
| *yw ey*FLP2; *gogo*[H1675] FRT80/TM6B, $y^+$ | *gogo* mutant | Takashi Suzuki |
| *w*; <*gogo*</TM6B | *gogo* FLICK | Satoko Suzuki |
| *w*; *fmi*[E86] | *fmi* hypomorph | Tadashi Uemura |
| *yw*; *actin*>y stop>Gal4 U-mCD8GFP/ CyO; (*ato*-t-myc Y99)/TM6B, $y^+$ | *gogo* OE in wings | Akinao Nose |
| *w* ; UAS-*gogo*T1 | *gogo* OE | Barry Dickson |
| *w* ; UAS-*gogo*T2 | *gogo* OE | Stephan Ohler |
| *yw*; FRT42B *fmi*[E59]/ CyO, $y^+$ | *fmi* mutant | Kirsten Senti |

| | | |
|---|---|---|
| *w* ; FRT42B *tub*-Gal 80/CyO | used for *fmi* wing clones | Liqun Luo, Barry Dickson |
| *yw*; GMR-GAL4 | R cells driver | Barry Dickson |
| *yw*; ; UAS-*fmi* | *fmi* OE | Tadashi Uemura |
| GMR-FLP mCD8-GFP/FM7 | used for R7 OE | Larry Zipursky |
| *w*; FRT82B tub-Gal 80/TM3, Sb | R7 OE | Liqun Luo, Barry Dickson |
| *w*; UAS-nlsGFP/(CyO); *Act*<stop<nlacZ/(TM6B) | used for monitoring FLP-out events | Bloomington Stock |
| *w*; ; 9-9-Gal4 | L3 driver | Iris Salecker |
| *w*; *Repo*-Gal4/TM3, Sb | Glial cell driver | Gaia Tavosanis |
| *Rh6*-GFP UAS-FLP; *fmi*[E59] AUS-FLP/CDGY | Used for brain FLICK | Satoko Suzuki |
| *yw*; <*fmi*<[2]/CyO | *fmi* FLICK | Satoko Suzuki |
| *Rh6*-GFP; <fmi<[2]/CDGY | *fmi* FLICK | Satoko Suzuki |
| *ey*FLP2 glass-LacZ *Rh6*-GFP; GMR-Gal4 UAS-*gogo*/ CyO | *gogo* overexpression | Tatiana Tomasi |
| *ey*FLP2 glass-LacZ *Rh6*-GFP; GMR-Gal4 UAS-*gogo*ΔC | *gogo*ΔC overexpression | Tatiana Tomasi |
| *yw*; sp/CyO; U-*fmi*ΔC(III) | *fmi*ΔC overexpression | Tadao Usui |
| GMR-*gogo*-myc (IIA), GMR-*gogo*-myc (IIB); GMR-*gogo*-myc (IIIA) | Co-immunoprecipitation | Stephan Ohler |

### 2.4.3 Established stock lines

The newly generated stock lines are listed below. Unrelevant transgenes are indicated in brackets.

| Genotype | Description/Use |
|---|---|
| *hs*FLP; FRT42D *fmi*[E59] UAS-*gogo*T1 | used for Gogo OE in wings |
| FRT42D *tub*-Gal80 (GMR-mCD8-mKOmyc); Act-Gal4 | used for Gogo OE in wings |
| *hs*FLP; FRT42D *fmi*[E59] | used for Gogo OE in wings |
| FRT42D UAS-mCD8-mKOmyc UAS-*gogo*T1/CyO; *Act*-Gal4 | used for Gogo OE in wings |
| GMR-FLP UAS-mCD8-GFP; FRT82D Gal80 | used for R7 specific OE |
| GMR-Gal4 UAS-gogoT1; UAS-*fmi* FRT82B | used for R7 specific OE |
| *w*; (FRT42D) *fmi*[E59] UAS-FLP/CyO; Rh6-GFP/TM6B | used for brain FLICK |
| <*fmi*<[2]/CyO; *Repo*-Gal-4/TM6B | used for brain FLICK |
| <*fmi*<[2]/CyO; 9-9-Gal-4/TM6B | used for L3 FLICK |
| <*fmi*<[2]/CKG; 9-9-Gal-4/TM6B | Brain FLICK |

### 2.4.3 List of genotypes used in all figures

The genotypes non-related to the experiments are in indicated in brackets.

**Fig3.1a-c** *Rh6*-GFP/*Rh6*-GFP, *ey*3.5FLP; *fmi*[E86]/<*fmi*<[1]

**Fig3.1b-d** *Rh6*-GFP/*Rh6*-GFP, *ey*3.5FLP; *fmi*[E86]/<*fmi*<[1]; *gogo*[H1675] (FRT80B)

**Fig3.2a** *Rh6*-GFP/*Rh6*-GFP, *ey*3.5FLP; *gogo*[H1675] (FRT80B)/<*gogo*<

**Fig3.2b** *Rh6*-GFP/*Rh6*-GFP, *ey*3.5FLP; (FRT42D) *fmi*[E59] /<*fmi*<[1]

**Fig3.3c** *Rh6*-GFP/*Rh6*-GFP, *ey*3.5FLP; (FRT42D) *fmi*[E59] /<*fmi*<[1]; *gogo*[H1675] (FRT80B)/<*gogo*<

**Fig3.4a-d** *hsFLP*/+; UAS-*gogo*T2/Act<$y^+$<Gal4

**Fig3.5a-d** *hsFLP*/+; UAS-*gogo*T2/Act<$y^+$<Gal4

**Fig3.7a-d** *hsFLP*/+; FRT42D *fmi*[E59] UAS-GogoT2/FRT42D tub-Gal80 (GMR-mCD8mKOmyc) ; Act-Gal4/+

| | |
|---|---|
| **Fig3.8a-d** | *hsFLP*/+; FRT42D *fmi*[E59] / FRT42D UAS-mCD8-mKOmyc, UAS-*gogo*T1; *Act*-Gal4/+ |
| **Fig3.14a** | *Rh4*-GFP; GMR-Gal4/+; UAS-*fmi*/+ |
| **Fig3.14b** | Rh4-GFP; GMR-Gal4, UAS-*gogo*T1/+ |
| **Fig3.14c** | Rh4-GFP; GMR-Gal4, UAS-*gogo*T1/+; UAS-*fmi*/+ |
| **Fig3.14d** | GMR-FLP, UAS-mCD8GFP/+; GMR-Gal4, UAS-*gogo*T1/+; UAS-*fmi*, FRT82B/ FRT82B, *tub*-Gal80 |
| **Fig3.15a,e** | (FRT42D) *fmi*[E59] UAS-FLP/<*fmi*<[2]; *Rh6*-GFP/+ |
| **Fig3.15b,f** | *Rh6*-GFP, UAS-FLP/*Rh6*-GFP; (FRT42D) *fmi*[E59] UAS-FLP/<fmi<[2], *gcm*-Gal4 |
| **Fig3.15c,g** | (FRT42D) *fmi*[E59] UAS-FLP/<*fmi*<[2]; *Rh6*-GFP/*Repo*-Gal-4 |
| **Fig3.15d,h** | (FRT42D) *fmi*[E59] UAS-FLP/<*fmi*<[2]; *Rh6*-GFP/9-9-Gal-4 |
| **Fig3.16b,d** | UAS-FLP/+; *gcm*-Gal4/(UAS-nlsGFP); *Act*<stop<nLacZ |
| **Fig3.16c,e** | UAS-FLP(II)**/+;** *Repo*-Gal4/*Act*<stop<nLacZ |
| **Fig3.16d,f** | UAS-FLP(II)**/+;** 9-9-Gal4/*Act*<stop<nLacZ |
| **Fig3.17a** | *Rh6*-GFP; (FRT42D) *fmi*[E59]/<fmi<[2], *gcm*-Gal4 |
| **Fig3.17b** | *Rh6*-GFP, UAS-FLP/*Rh6*-GFP; (FRT42D) *fmi*[E59] UAS-FLP/<fmi<[2], *gcm*-Gal4 |
| **Fig3.17c** | (FRT42D) *fmi*[E59] UAS-FLP/<*fmi*<[2]; *Rh6*-GFP/9-9-Gal-4 |
| **Fig3.17d** | (WT) w; FRT42/FRT42 *tub*-Gal80; *dac*FLP *9-9*Gal4/UAS-mCD8-GFP |
| **Fig3.17d** | (fmi) w; FRT42 *fmi*[E59]/FRT42 *tub*-Gal80; *dac*FLP *9-9*Gal4/UAS-mCD8-GFP |
| **Fig3.18a,d** | *Rh6*-GFP; (FRT42D) *fmi*[E59]/<fmi<[2], *gcm*-Gal4 |
| **Fig3.18b,e** | *Rh6*-GFP, UAS-FLP/*Rh6*-GFP; (FRT42D) *fmi*[E59] UAS-FLP/<fmi<[2], *gcm*-Gal4 |
| **Fig3.18c,f** | (FRT42D) *fmi*[E59] UAS-FLP/<*fmi*<[2]; *Rh6*-GFP/9-9-Gal-4 |
| **Sup Fig1** | (*Rh6*-GFP), *ey*3.5FLP; FRT42D *fmi*[E59]/FRT42D GMR-mCD8-mKO-myc (*tub*-Gal80) |
| **Sup Fig2a,d** | *Rh4*-GFP,(*ey*3.5FLP)/*Rh4*-GFP;GMR-Gal4,UAS-gogoΔC/UAS-fmiΔIntra (II) |
| **Sup Fig2b,e** | *Rh4*-GFP,(*ey*3.5FLP)/*Rh4*-GFP;GMR-Gal4,UAS-gogoΔC/+; UAS-fmi/+ |
| **Sup Fig2c,f** | *Rh4*-GFP,(*ey*3.5FLP)/*Rh4*-GFP;GMR-Gal4,UAS-gogoT1/UAS-fmiΔIntra (II) |

### 2.4.4 Whole mount brain and wing disc staining

Whole mount brain antibody stainings were performed in pupae and adult flies. To perform the dissection at a precise pupal stage, white pupae that just formed the puparium were transferred into a new vial (0 hours APF) and were kept at 25°C until the desired stage. Pupal cases were carefully removed around the head region before dissection. Before brain dissection, adult flies were anesthetized with $CO_2$ and transferred into 70% EtOH for 30s. Brains were dissected in 0,1% PBT solution (0,1% Triton X100 in PBS), tracheas were removed, and brains were kept on ice until fixation. Dissected brains were fixed with 4% paraformaldehyde on a shaker for 30-35min, and then washed 3 times for 10min in 0.1% PBT. The brains were blocked for 30min in 0.1% PBT with 5% NGS and then stained on a shaker from overnight up to 2 days at 4°C. The primary antibody was diluted in 0.1% PBT containing 5% NGS. After washing the brains 3 times for 10min in 0.1% PBT, the secondary antibody diluted in 0.1% PBT was applied for 2-4 hours. The brains were washed 3 times for 10min in 0.1% PBT, and incubated with Vectashield Mounting Medium (Vector Laboratories Inc.) for 15 min. To mount the brains in the correct orientation for observing the medulla, a small gap of ~1.5 fold the size of the brain was created using two coverslips on a glass slide. The brains were carefully pushed toward the gap until they fall in the proper orientation.

Wing discs were dissected out at 28h APF in 4% paraformldehyde. The pupal case around the head was removed, and a hole was created in the head to allow the fixative to enter the body. Pupae were extracted from the pupal case, and a hole was done at the hindge between the cell body and the wing to let the fixative penetrate into the wing dics. After 15 min of fixation, the wing disc was pulled out of the ensheathing membrane. Wing discs were fixed overnight in 4% paraformaldehyde, and stained as described for the brain.

The following primary antibobies were used: rabbit anti-GFP Alexa Fluor488-conjugated (Molecular Probes, 1:300), chicken anti-β-gal (Abcam, 1:1000), mouse Ab24B10 (DSHB, 1:50), rat anti-Elav (DSHB 7E8A10, 1:100), rat anti-*D*NCadherin (Ex#8, DSHB, 1:50), mouse anti-Fmi (#74, DSHB, 1 :20). Alexa Fluor-conjugated secondary antibodies (488, 568, 633; Molecular Probes) were used at 1:300.

Images were acquired with Leica SP2 or Olympus FV1000 Confocal Microscopes and processed with Adobe Photoshop.

### 2.4.5 Agarose sections

For agarose sections, fly heads were detached from the body and the proboscis was removed. Fly heads were fixed with 4% formaldehyde overnight, washed 3 times in PBS, and transferred to a Petri dish. A solution of 7% agarose in PBS was heated up until the agarose has been dissolve. The agarose was let at room temperature for 5-10min to remove the air bubbles. Then, the agarose was poured in the Petri dish, and the fly heads were detached from the bottom of the dish using a pipette tip. The dish was kept at 4°C until it solidifies. Pyramids were cut from the agarose gel (the fly heads should be on the top of the pyramid and in the desired orientation). 50-80 μm sections were cut using a vibrating blade microtome (Leica VT1000S). This was followed by standard antibody staining procedures.

### 2.4.6 The FLICK system

The FLICk system is a new method for generating mutants developed by Satoko Suzuki (Hakeda-Suzuki at al., 2011). FLICK stands for **F**RTs **L**ocated **I**n *cis* for **C**onditional **K**nock-out). In the FLICK system, the gene to be knocked-out is flanked by a pair of FRTs. The fragment surrounded by the two FRTs can be excised by FLPase. By combining this chromosome with a mutant allele, one can generate mutant cells where and when FLPase is expressed (deletion/mutation), whereas cells which do not express FLPase are wild type (WT/mutation) (**Fig2.1**). FRT insertions used for flanking the genes of interest were selected from the Exelexis collection.

**a**

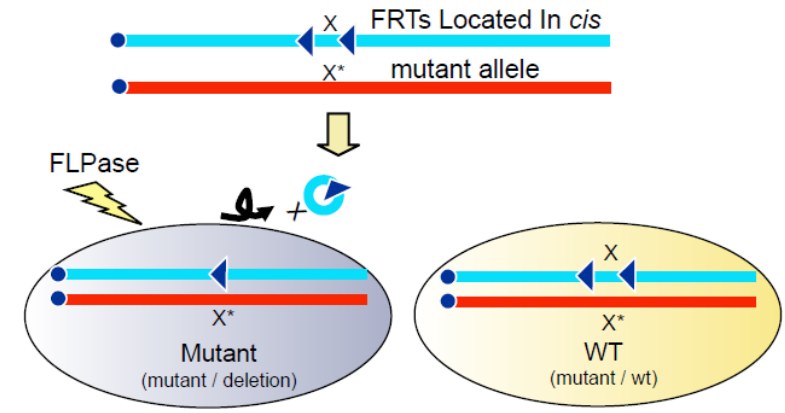


**b**

| | left FRT | right FRT | distance between two FRTs |
|---|---|---|---|
| <*fmi*<[1] | P{XP}lola[d10398] | PBac{WH}stan[f00907] | 177kb |
| <*fmi*<[2] | PBac{RB}git[e04690] | PBac{WH}stan[f00907] | 74kb |
| <*gogo*< | PBac{WH}CG7668[f03604] | PBac{WH}CG5618[f05961] | 352kb |

**Fig2.1 The FLICK system and FLICK alleles used to generate *fmi* and *gogo* knock-out.**
(**a**) Schematic representation of the FLICK system. When FLPase is expressed, the DNA fragment containing the gene to be knocked out is excised, generating mutant cells (mutant/deletion). (**b**)The table shows the FRT used for making *fmi* and *gogo* FLICK flies on the left and right side of the genes, and the distance between these FRTs.

# 3. RESULTS

## 3.1 *gogo* and *fmi* genetically interact in R8 photoreceptor axons

Since *gogo* and *fmi* have very similar phenotypes in R8 axon targeting, we wanted to test if they genetically interact in photoreceptors axons. We first checked the genetic interaction in loss-of-function experiments, using a hypomorphic allele of *fmi* (*fmi*[E86]) which induces a single amino-acid change (D1297N). In order to generate *fmi* hypomorphic mutants only in photoreceptors, we used the FLICK system (see material and methods). Using this technique, we obtained mosaic flies that express only the Fmi hypomorphic protein in photoreceptors, and both hypomorphic and wild type Fmi in the rest of the animal. These flies showed a mild phenotype in R8 axons: they occasionally innervated neighboring columns and form bundles with other R8 axons (**Fig3.1a,c,e**). When one copy of *gogo* was removed in this background, the incidence of the R8 bundling phenotype was enhanced (**Fig3.1b,d,e**). This indicated that *gogo* and *fmi* interact genetically in R8 photoreceptor axons.

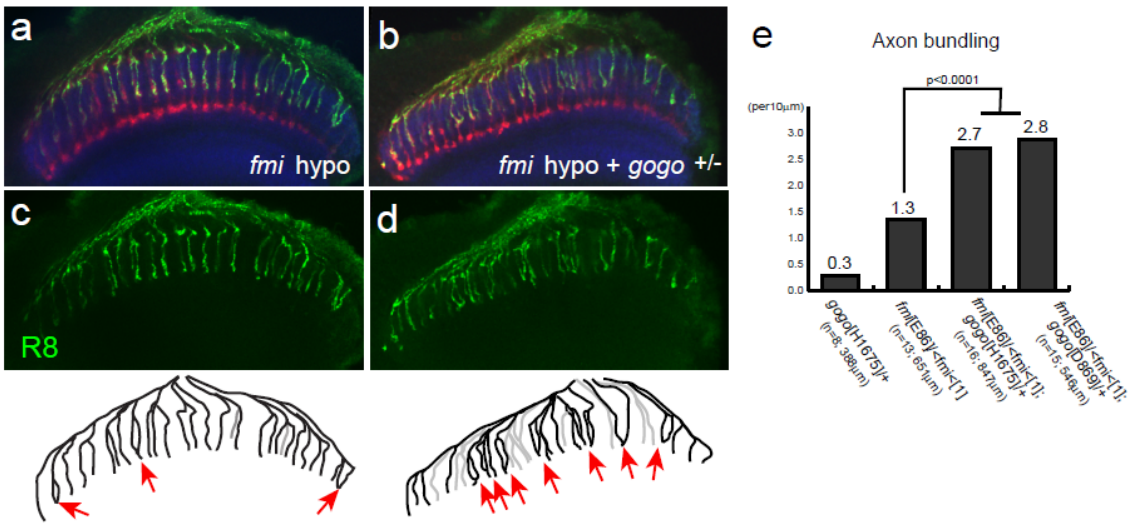


**Figure 3.1 Loss-of-function interaction between *gogo* and *fmi* in R8 photoreceptor axons**
R7 and R8 axons in the medulla are stained with 24B10 antibody (red), R8s with *Rh6*-GFP (green), and medulla layers with anti-NCad (blue). (**a**,**c**) Flies that have *fmi* hypomorphic photoreceptor cells (ey3.5FLP *fmi*[E86] FLICK) showed a mild R8 axon bundling phenotype. (**b**,**d**) When one copy of *gogo* was removed in this *fmi* hypomorphic background, the incidence of the R8 axon bundling increased significantly. The tracing of R8 axons in focus (black) and out of focus (grey) is shown below each panel. Bundling axons are indicated with red arrows. (**e**) Quantification of R8 axon bundles per 10µm of medulla in *gogo* mutants (*gogo*[H1675]), *fmi* hypomorphic flies, and flies containing the combination one copy of two different *gogo* null alleles (*gogo*[H1675] and *gogo*[H1675]) with *fmi* hypomorph (P<0.0001, two tailed *t* test).

## 3.2 *gogo* and *fmi* act in the same pathway

Since *gogo* and *fmi* interact genetically, we wondered if they work in the same or parallel pathways. To answer this question, we generated a double mutant for *gogo* and *fmi* only in photoreceptor cells using the FLICK system. In theory, if these two genes work in independent pathways, their deletion should have an additive effect on the R8 phenotype. On the contrary, if *gogo* and *fmi* act exclusively in a single pathway, there should not be any phenotypic difference between the single and the double mutants. We observed that the phenotype in R8 photoreceptor axons was not more severe in the double mutant than the single *gogo* and *fmi* mutants (**Fig3.2**), indicating that *gogo* and *fmi* act in the same pathway.

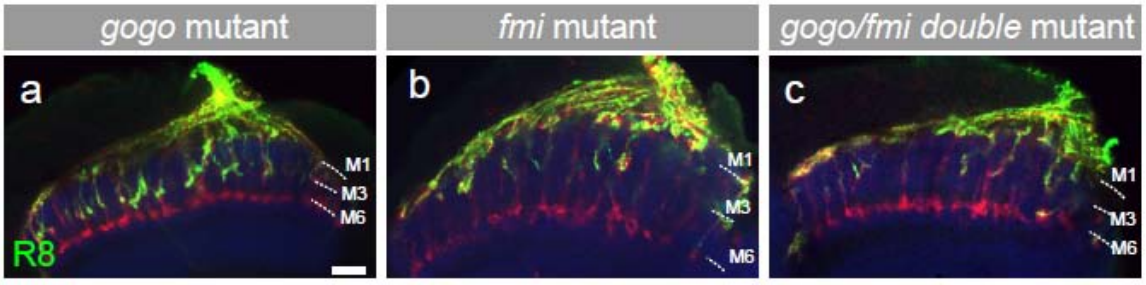


**Figure 3.2 The R8 phenotype is not enhanced in the double mutant for *gogo* and *fmi***
(**a**–**c**) Mutants in photoreceptor cells were generated using *ey*3.5FLP FLICK. R7 and R8 axons in the medulla are stained with 24B10 antibody (red), R8 axons with *Rh6*-GFP (green), and medulla layers with anti-NCad (blue). The R8 axon bundling and stopping phenotype observed in *gogo* and *fmi* single mutants was not enhanced in the double mutant, indicating that *gogo* and *fmi* belong to the same pathway. Scale bar: 20μm.

### 3.3 Gogo and Fmi co-accumulate at cell-cell contacts in cultured cells

Because Gogo and Fmi interact genetically in R8 photoreceptor axons and seem to belong to the same molecular pathway, we asked whether they bind physically. Aggregation assay in *Drosophila* S2 cells is commonly used to test the adhesion properties of cell-surface molecules (Dworak et al., 2001; Malaga-Trillo et al., 2009; Yonekura et al., 2006). Cultured S2 cells usually do not aggregate at low concentrations. S2 cells transfected with Fmi form aggregates due to Fmi homophilic interactions (Usui et al., 1999). Within such cell clusters, Fmi often accumulates at sites of cell-cell contacts. The transmembrane PCP proteins Vang Gogh (Vang) and Frizzled (Fz), known to form complexes with Fmi at the boundaries of wing cells, have been shown to colocalize with Fmi at cell-cell contact in S2 cells (Strutt and Strutt, 2008). We therefore applied this assay to test the physical interaction of Gogo and Fmi. Gogo-expressing cells do not generate the formation of aggregates, suggesting that Gogo does not bind homophilically (Tomasi et al., 2008). When Gogo and Fmi were co-expressed, Gogo was enriched at sites of cell contacts together with Fmi (**Fig3**.**3a–c**), suggesting that Fmi recruits Gogo at cell boundaries. To confirm that this effect was specific to Fmi, we cotransfected Gogo with another cadherin E-Cad, which mediates strong S2 cells aggregation and accumulates at cell-cell borders. Gogo did not colocalize with E-Cad (**Fig3.3d–f**). Conversely, we tested whether Fmi could recruit other transmembrane proteins at cell boundaries. To this end, we co-transfected Fmi with Unc5, which structurally resembles Gogo (Keleman and Dickson, 2001). Unc5 did not co-accumulate with Fmi (**Fig3.3g–i**). These data indicates that the recruitment of Gogo by Fmi at cell-cell contacts is specific. To quantify these results, we calculated for each cell border the “cell-cell contact accumulation ratio”, defined as the ratio of fluorescence intensities between membranes at cell-cell borders and membranes which does not contact other cells (**Fig3.3p**).

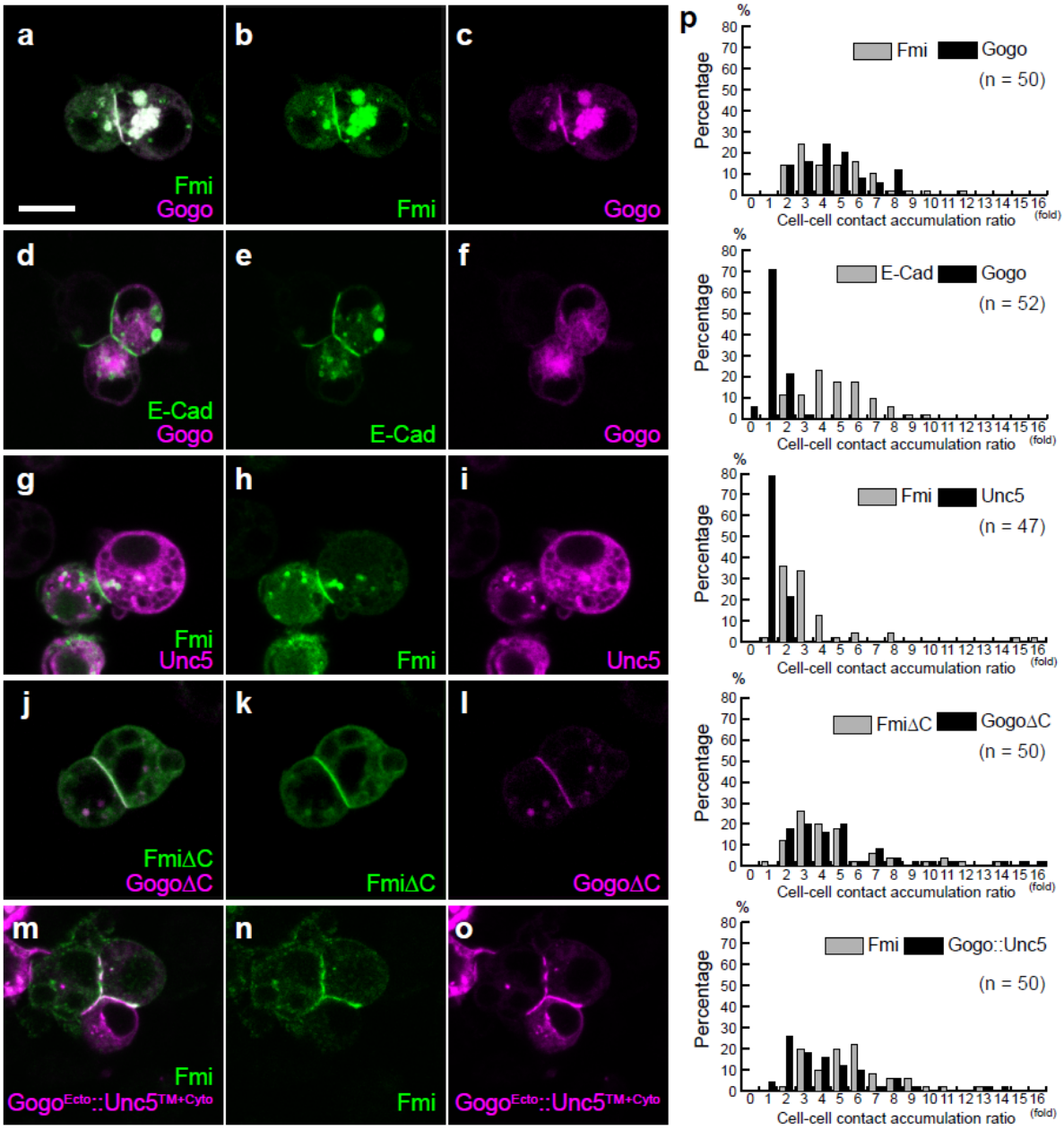


**Figure 3.3 Gogo and Fmi colocalize at cell-cell contacts**
(**a**–**o**) Protein accumulation at cell boundaries in transienlty transfected S2 cells subjected to aggregation assay. All cells are co-transfected with the *Act*-Gal4 driver. Cells co-transfected with Fmi and Gogo-myc (**a**–**c**), E-Cad-GFP and Gogo-myc (**d**–**f**), Fmi and Unc5-GFP (**g**–**i**), FmiΔC-myc and GogoΔC-GFP (**j**–**l**), and Fmi and Gogo$^{Ecto}$::Unc5$^{TM+Cyto}$-GFP (**m**–**o**). Fmi recruits Gogo at cell-cell contacts (**a**–**c**), whereas Gogo does not colocalize with E-cad (**d**–**f**), nor does Unc5 colocalize with Fmi (**g**–**i**). FmiΔC can recruit GogoΔC (**j**–**l**) and Fmi recruits the chimera Gogo$^{Ecto}$::Unc5$^{TM+Cyto}$ (**m**–**o**), which suggests that the ectodomains of Gogo and Fmi mediate their colocalization. Scale bar: 10µm. (**p**) Quantification of the accumulation of each protein are shown on the right side of each panel. The cell-cell contact accumulation ratio is defined as the ratio of the fluorescence intensity at the cell-cell border to the fluorescence intensity at the membrane which does not contact other cells. The sample size is indicated with n.

We then tried to figure out which parts of the proteins were involved in the co-localization. We first used deletion constructs that lacks Gogo and Fmi intracellular domains (GogoΔC and FmiΔC). We found that Gogo colocalizes with Fmi without the cytoplasmic portion of both proteins, indicating that the co-localization is mediated by their transmembrane or extracellular domains (**Fig3.3j–l**). To distinguish between these two possibilities, we generated a chimeric protein consisting of the extracellular domain of Gogo and the transmembrane and cytoplasmic domains of Unc5 ($Gogo^{Ecto}$::$Unc5^{TM+Cyto}$). This chimera successfully colocalized with Fmi at cell-cell contacts (**Fig3.3m–o**), suggesting that the ectodomain of Gogo mediates the colocalization with Fmi.

We generated Gogo constructs lacking different extracellular domains and tested them in the aggregation assay to map down the site that mediate the co-accumulation with Fmi. Unfortunately, we could not determine which domain was required, since the co-accumulation was not as clear as for the other constructs, and some results were contradictory, indicating that several domains are involved in the interaction with Fmi or that the trafficking to the cell membrane was affected for some Gogo deletions.

In any case, we could show that Fmi is able to recruit Gogo at cell-cell contacts. This strongly suggests that Gogo and Fmi work in close proximity, and that their association underlies the genetic interaction observed in photoreceptor targeting.

### 3.4 Gogo ectopic expression induces Fmi mislocalization in wing cells

Since Fmi was able to relocalize Gogo to cell boundaries in cultured S2 cells, we wanted to know whether Gogo and Fmi can also influence their localizations *in vivo*. To this end, we used the wing epithelial cells, where Fmi localization is easily visible. These cells are large, have a hexagonal shape, and their cell boundaries are well-organized. During mid-pupal stages, Fmi has a precise localization which is important for its function in the establishment of planar cell polarity: Fmi accumulates at the apical pole of wing epithelial cells, and only at the proximal and distal cell borders, leading to a characteristic "zigzag" localization (Usui et al., 1999). To check whether Fmi and Gogo localizations are dependent on each other in this context, we generated cell clones that ectopically expressed Gogo in wing cells, and stained Gogo and Fmi proteins at 28h APF. In these clones, Gogo was localized everywhere on the cell membrane of wing cells (**Fig3.4a,b**). Strikingly, the nice zigzag Fmi localization at the apical pole of wild type cells was disrupted in Gogo-overexpressing clones (**Fig3.4c**). More basally, Fmi co-localized with Gogo on the entire surface of lateral membranes in Gogo-overexpressing cells, whereas Fmi staining was not detected in the basal part of wild type cells (**Fig3.4d,e**). These results indicate that Gogo binds to Fmi and recruits it to lateral membranes of wing epithelial cells.

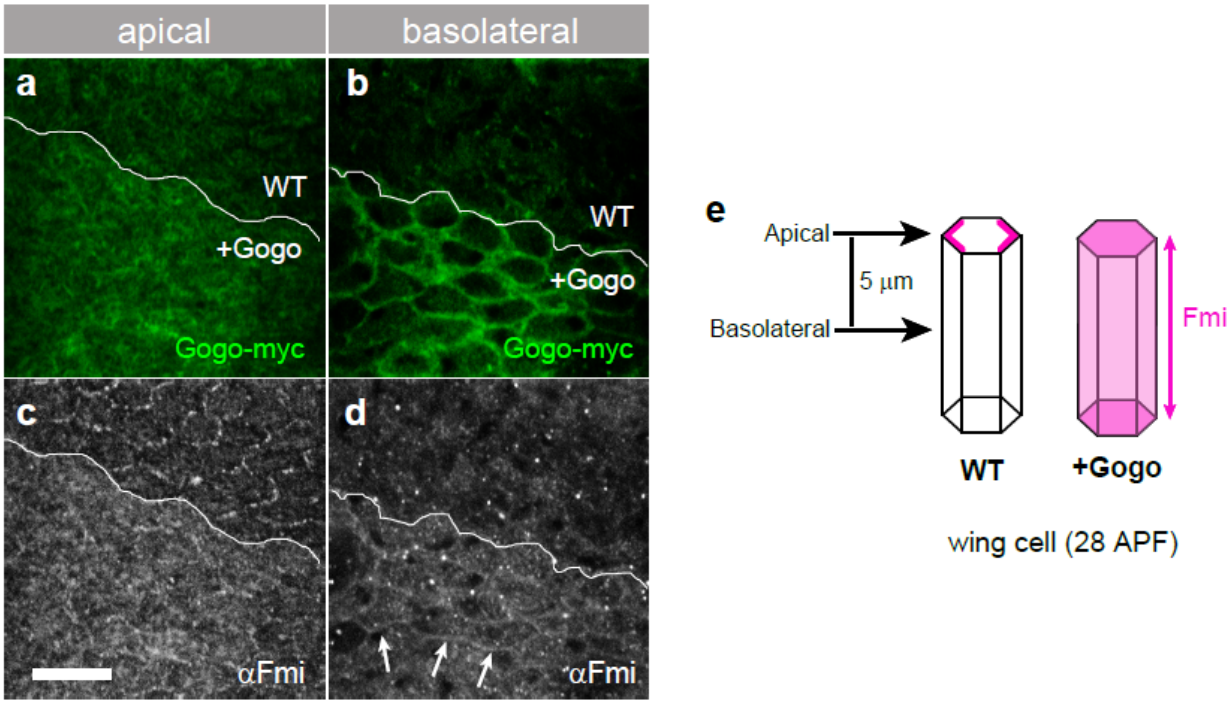


**Figure 3.4 Gogo interacts with Fmi in wing epithelial cells**
(**a**–**d**) Images of *gogo*-overexpression clones in 28h APF wing cells from the apical surface (**a**,**c**) and 5 µm beneath the surface (**b**,**d**). Subcellular localization of Gogo-myc (green in **a,b**) and Fmi (white in **c,d**) is detected with anti-myc and anti-Fmi. The clone border is marked with a white line. At the apical surface, the localization of Fmi at the proximal and distal membranes becomes disrupted in *gogo*-overexpressing clones (**c**). More basally, Fmi localizes on the lateral membranes of wing cells (arrows in **d**), similarly to Gogo (**b**). A schematic explanation is shown in (**e**). Scale bar: 10µm.

To verify that Gogo ectopic expression in pupal wing cells does not generate a pleiotrophic effect on membrane proteins, we stained E-Cadherin, which is a major component of adherens junction in epithelial cells (Kirkpatrick and Peifer, 1995). E-Cad membrane localization at the apical pole of wing cells was not disrupted in *gogo*-overexpressing clones, suggesting that the effect of Gogo on Fmi localization is specific (**Fig3.5**).

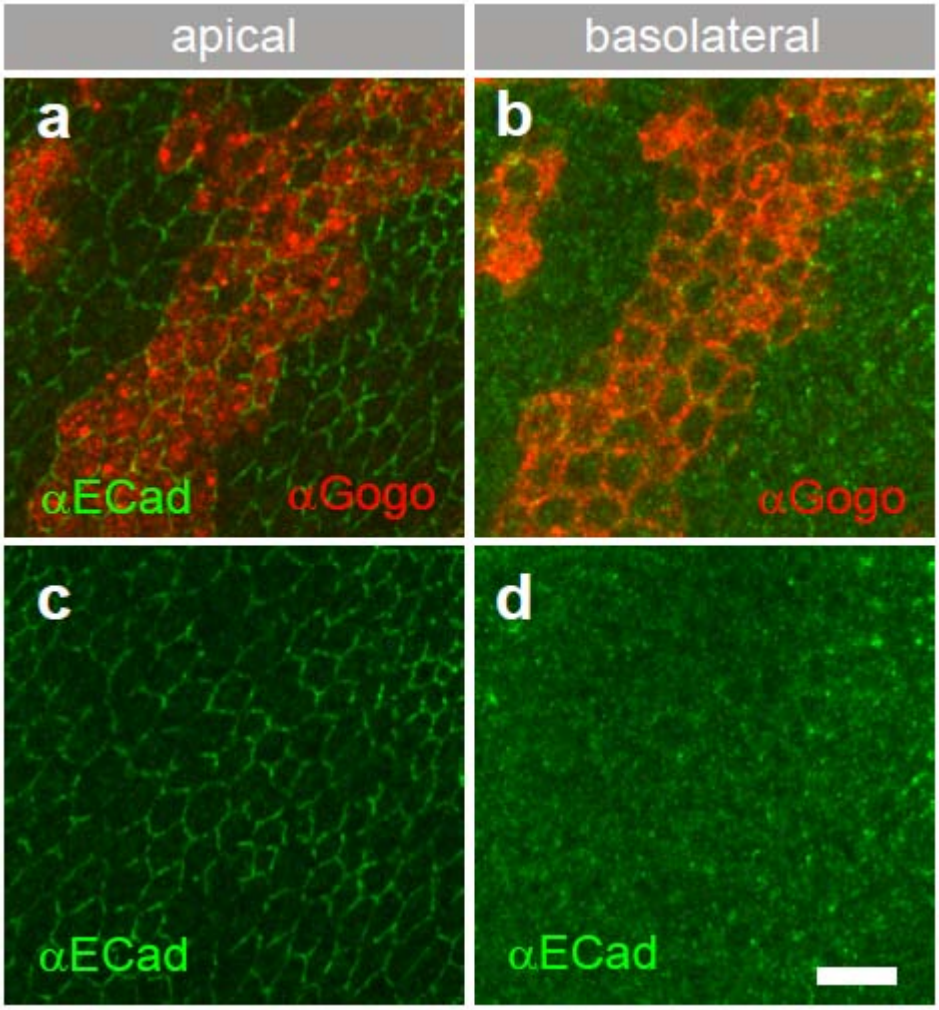


**Figure 3.5 Adherens junctions are not disrupted in *gogo*-overexpressing cells**
(**a**–**d**) Images of *gogo*-overexpression clones in 28h APF wing epithelial cells at the apical surface (**a**,**c**) and 5µm beneath the surface (**b**,**d**). Wing discs were stained with anti-E-Cadherin (green) and anti-Gogo (red). The E-Cad staining is shown separately (**c**,**d**). E-Cad localization is indistinguishable between *gogo*-overexpressing cells and WT cells at the apical surface (**a**,**c**). Basally, E-Cad is not detectable in both cases (**b**,**d**) indicating that adherens junctions are not disrupted in *gogo*-overexpressing cells. Scale bar: 10µm.

### 3.5 Gogo and Fmi interact in *cis*

To investigate whether Gogo and Fmi mediates heterotypic interactions in *trans*, we performed an aggregation assay by mixing two populations of S2 cells: one transfected with Gogo, and the other one transfected with Fmi. As a control, we mixed Fmi-expressing cells with mCD8-expressing cells. Cells that expressed Gogo were not included in the aggregates generated by Fmi, similarly to the control cells expressing mCD8 (**Fig3.6**). This result suggests that Gogo and Fmi do not mediate cell adhesion in *trans*.

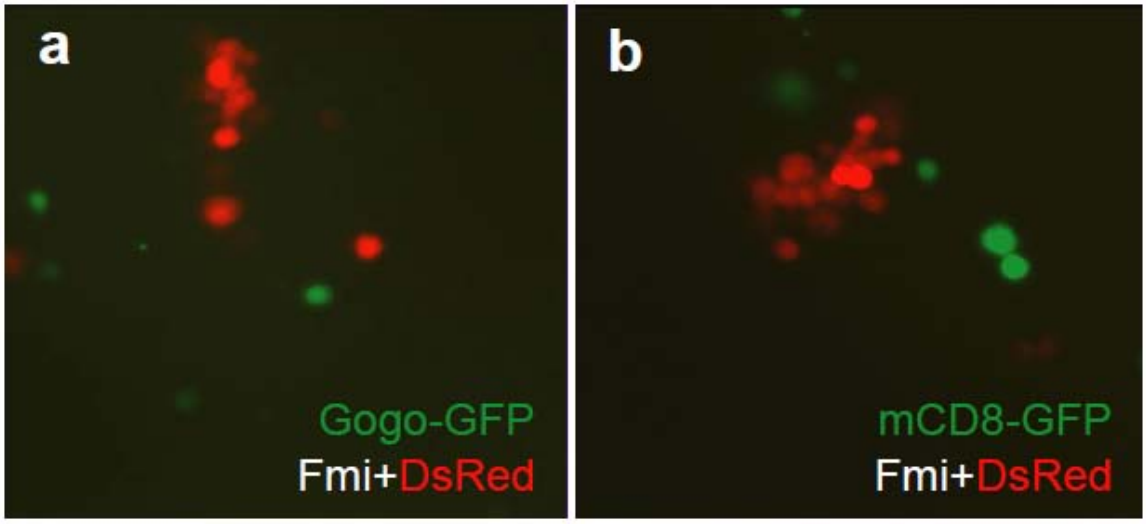


**Figure 3.6 Gogo and Fmi do not interact in *trans* in S2 cells**
(**a**,**b**) A population of cells transfected with Fmi (labeled by co-transfection with UAS-Dsred) was mixed with cells expressing Gogo-GFP (**a**) and mCD8-GFP (**b**). Gogo-expressing cells are not included in aggregates mediated by Fmi (**a**), similarly to the control cell population expressing mCD8 (**b**), suggesting that Gogo and Fmi do not interact in *trans* in cultured cells.

It was not possible to test whether Gogo and Fmi interact in *cis* with the co-localization assay in S2 cells. Indeed, protein accumulation at cell-cell borders requires Fmi homophilic interaction in *trans*, thus Fmi has to be present in a cell that express Gogo and in an adjacent cell, what does not allow to distinguish between *cis* or *trans* interaction. Therefore, we used the wing epithelial cells to test if Gogo can relocalize Fmi in *trans* or in *cis*. To determine whether mislocalized Fmi comes from the clones that expressed Gogo or from the adjacent cells, we had to generate *fmi* mutant clones.

To check whether Gogo can recruit Fmi to lateral membranes in *trans*, we generated wing cell clones that were mutant for *fmi* and overexpressed Gogo. We reasoned that if the interaction occurs in *trans*, we should observe Fmi staining at the border of the clones in the basal part of wing cells (**Fig3.7e**). Fmi was not relocalized to the basolateral membrane of the abutting cells when *fmi* was absent from the Gogo-overexpressing cells (**Fig3.7a–d**). This data suggests that Gogo does not interact with Fmi in *trans*, corroborating the results obtained in S2 cells.

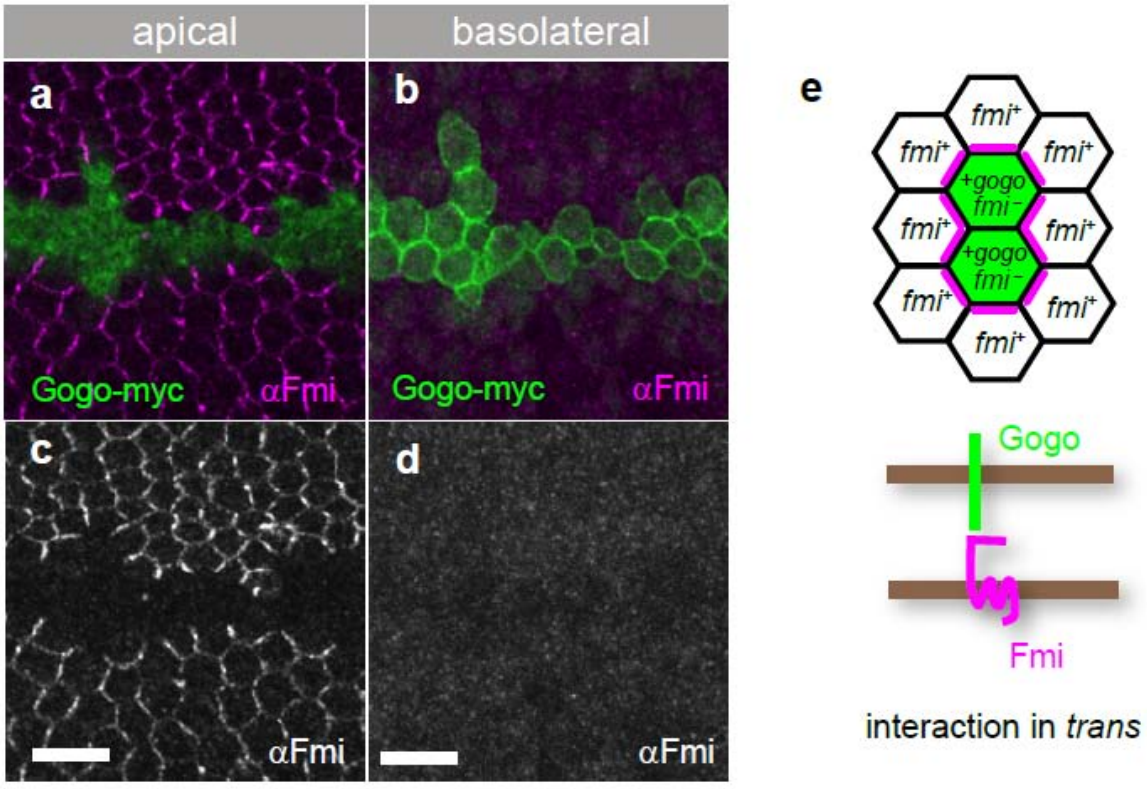


**Figure 3.7 Gogo does not relocalize Fmi in *trans* in wing cells**
(**a**–**d**) Overexpression of *gogo* in *fmi* mutant clones. Gogo-myc staining is shown in green (**a**,**b**) and Fmi staining in magenta (**a**,**b**) or white (**c**,**d**). Fmi does not localize on the lateral membrane of Gogo-overexpressing cells between $fmi^{+}$ and $fmi^{-}$ cells (**b,d**), indicating that Gogo cannot recruit Fmi in the neighboring cells (in *trans*). (**e**) Schematic explanation of (**b**,**d**). The magenta lines represent the theoretical localization of Fmi if Gogo could relocalize Fmi in *trans*, which is not the case. Scale bars: 10µm.

To test the hypothesis of a *cis* interaction, we generated *fmi* mutant clones adjacent to Gogo-overexpressing clones (**Fig3.8**). Fmi staining on lateral membranes was observed at cell membranes abutting *fmi* mutant clones (**Fig3.8b**,**d**), indicating that Gogo

is able to relocalize Fmi in *cis*. Since Fmi mislocalization occurs even if Fmi is absent in the neighboring membranes, it also suggests that Fmi homophilic *trans* interaction is not a prerequisite for Gogo to bind to Fmi in *cis*. Overall, these results indicate that Gogo and Fmi physically interact in *cis* (directly or indirectly) *in vivo*, and suggest that they collaborate in R8s for axon targeting.

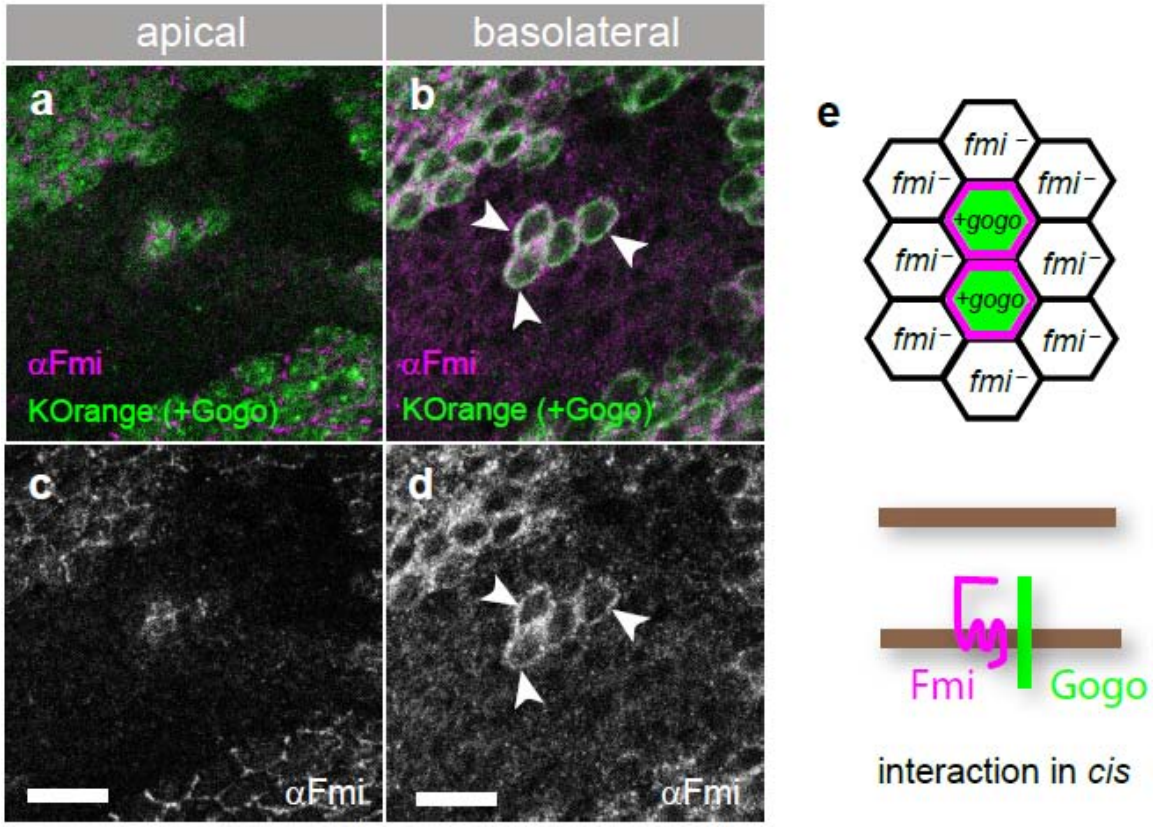


**Figure 3.8 Gogo recruits Fmi on lateral membranes of wing cells in *cis***
(**a**–**d**) apical (**a**,**c**) and basolateral (**b**,**d**) localization of Fmi in *gogo*-overexpressing clones (marked by mKOrange) surrounded by *fmi* mutant clones. mKO fluorescent signal is shown in green (**a**,**b**) and Fmi staining in magenta (**a**,**b**) or white (**c**,**d**). Fmi localizes on the lateral membranes of Gogo-overexpressing cells between $fmi^{+}$ and $fmi^{-}$ cells (arrowheads), indicating that Gogo recruits Fmi in *cis*. (**e**) Schematic explanation of **b**,**d**. Relocalized Fmi on lateral membranes of wing cells in the case of *cis* interaction is shown in magenta. Scale bars: 10μm.

### 3.6 Gogo/Fmi direct interaction could not be detected by co-immunopreciptation

The fact that Gogo and Fmi can influence their localization in cultured cells and *in vivo* strongly suggests that these two proteins physically interact. We thus tried to co-immunoprecipitate Gogo and Fmi in S2 cells. Cultured cells were transfected with Gogo-myc and Fmi, and the immunoprecipitation was performed with anti-myc beads. Unfortunately, Fmi could not be detected in the immunoprecipitate (**Fig3.9a**).

Since Fmi is a seven-pass transmembrane protein, it is very difficult to extract from the cell membrane in mild conditions which are necessary to preserve protein interactions in co-immunoprecipitation experiments. Therefore, we thought that it could be easier to perform the immunoprecipitation from the Fmi side. We thus pulled down Fmi-V5, but Gogo was not co-immunoprecipitated (**Fig3.9b**).

We then thought that the Gogo/Fmi interaction could be transient and unstable. We thus used the crosslinker DTSSP to create covalent bonds between interacting proteins before the co-immunoprecipitation. Protein cross-linking did not result in co-immunoprecipitation of Gogo with Fmi (**Fig3.9c**). Other attempts using different extraction buffers (ProteoExtract® Transmembrane Protein Extraction Kit, Novagen) or milder conditions (0.5% Triton X100, 1% Brij97) did not improve the co-immunoprecipitation (data not shown).

Fmi is an extremely large protein, whose molecular weight is estimated to be higher than 400kD. Since it is technically difficult to maintain large protein complexes during the immunoprecipitation procedure, we decided to generate a shorter Fmi construct (pUAS-HA-Fmi$^{Ecto\Delta Cad}$). As the Gogo-Fmi co-accumulation at cell-cell contacts is mediated by their extracellular domains, we deleted the intracellular and transmembrane domains. We also removed the cadherin repeats, which are supposed to mediate Fmi homophilic interaction. When we immunoprecipitated Gogo, we detected a faint band corresponding to the truncated Fmi in the immunoprecipitate (**Fig3.9d**). Since the interaction seemed to be weak, we used other negative controls to test whether this faint band was not an artifact. We immunoprecipitated mCD8-myc (supposed to be a neutral protein) and Gogo lacking its extracellular domain (which should not bind the Fmi extracellular construct). A faint band corresponding to Fmi was also observed in the immunoprecipitate of these two myc-tagged proteins (**Fig3.9e**), indicating that Fmi has more affinity to beads when they bind with any myc-tagged proteins.

Since all our attempts to co-immunoprecipitate Gogo and Fmi in S2 cells failed, we wondered if the Fmi-Gogo interaction needs to be stabilized by other factors which are absent in S2 cells. Consequently, we tried to perform the co-immunoprecipitation in *vivo*. We dissected brains from 3$^{rd}$ instar larvae containing 6 copies of GMR-*gogo*-myc (GMR is a promoter that drives expression in photoreceptor cells). Again, Fmi could not be co-immunoprecipitated with Gogo (**Fig3.9f**).

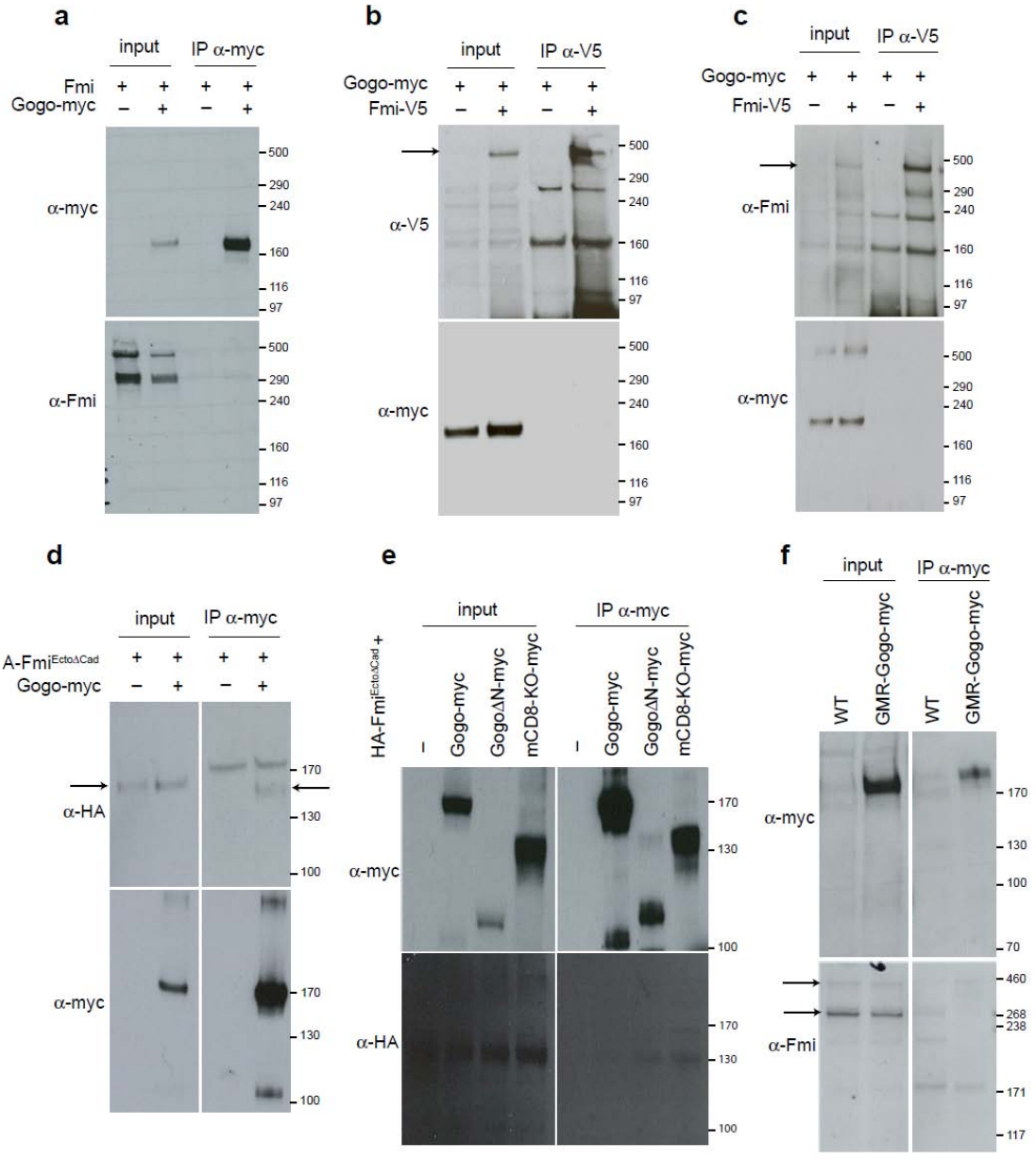


**Figure 3.9 Attempts to co-immunoprecipitate Gogo and Fmi**
(**a**) S2 cells were transfected with Fmi +/- Gogo-myc. Gogo-myc was immoprecipitated with anti-myc beads. Fmi could not be detected in the immunoprecipitate. (**b**) S2 cells were transfected

with Gogo-myc +/- Fmi-V5. Fmi-V5 was immunoprecipitated from cell lysates with anti-V5 beads. Gogo did not co-immunoprecipitate with Fmi. (**c**) S2 cells were transfected with Gogo-myc +/- Fmi-V5, and incubated with the crosslinker DTSSP before immunoprecipitation with anti-V5 beads. Gogo was not co-immunoprecipitated. (**d**,**e**) Since the large size of Fmi can make the co-immunoprecipitation difficult, we transfected S2 cells with a truncated version of Fmi, $Fmi^{EctoΔCad}$. When Gogo-myc was immunoprecipitated, a faint band corresponding to the truncated Fmi could be detected (**d**), but this band was also visible in the negative controls where GogoΔN-myc or mCD8-KO-myc were immunoprecipitated (**e**). (**f**) Brains were dissected from WT and 6x-GMR-Gogo-myc larvae, and the tissue lysates were immunoprecipitated with anti-myc. Fmi was not found in the immunoprecipitate. When unspecific bands were also detected, the expected bands are indicated with arrows. Note that Fmi appeared as two bands (>400 and 300kD), except when the anti-V5 antibody was used to recognize Fmi tagged at the C-terminal (only >400kD).

## 3.7 Gogo forms oligomers

In the co-immunoprecipitation experiments, we used the crosslinkers DSP and DTSSP to covalently bind interacting proteins. These crosslinkers are thiol-cleavable, leading to the disruption of protein complexes in reduced samples. In the lysates of cells transfected with *gogo*, we observed that the band corresponding to Gogo, usually seen at 170kD, was shifted to more than 500kD when the samples were not reduced with DTT (**Fig3.10a**). This indicated that Gogo binds to another protein or forms oligomers.

To test the second hypothesis, we performed co-immunoprecipitation in S2 cells transfected with Gogo fused to two different tags (myc and GFP). We pulled down Gogo-myc, and detected a strong band corresponding to Gogo-GFP in the co-immunoprecipitate (**Fig3.10b**). This indicates that Gogo undergo oligomerization.

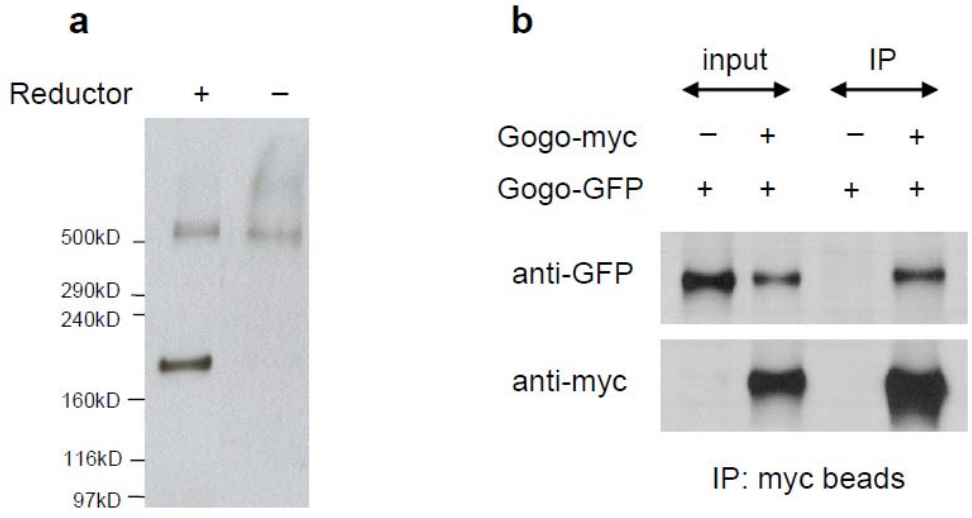


**Figure 3.10 Gogo forms oligomers in S2 cells**
(**a**) S2 cells transfected with Gogo were subjected to crosslinking with DTSSP for 30min. The crosslinker was cleaved by the reductor DTT (first lane) or not (second lane). The band corresponding to Gogo in the non-reduced sample (~170kD) was completely shifted up to more than 500kD. This indicated that Gogo forms oligomers or binds to another protein in S2 cells. Note that the band at 500kD was also present in the sample reduced with DTT, as well as in non-crosslinked samples (data not shown), suggesting that a fraction of the Gogo proteins remained associated with other molecules even without crosslink. (**b**) S2 cells were transfected with Gogo-GFP alone (control) or Gogo-GFP and Gogo-myc. Immunoprecipitations were performed using anti-myc agarose beads. Gogo-GFP was co-immunoprecipitated with Gogo-myc, indicating that Gogo forms homo-oligomers in S2 cells.

### 3.8 The BiFC assay showed unspecific fluorescent signal

As mentioned above, Fmi is a very large protein with 7 transmembrane domains, which render co-immunoprecipitation experiments technically challenging. Moreover, we showed that Gogo forms oligomers, resulting in a large protein complex of more than 500kD. Fmi is also known to bind homophilically in *cis* (Kimura et al., 2006). It is thus possible that Gogo and Fmi interact in a very large protein complex, making the co-immunoprecipitation extremely difficult. Consequently, we tried to demonstrate the physical interaction between Gogo and Fmi using alternative methods in living cells to avoid biochemical procedures.

Techniques to detect protein-protein interaction in intact cells include Protein Complementation Assays (PCAs). In PCAs, two halves of a reporter protein are separately fused to the putative interaction partners. If the protein interaction occurs, the split reporter is reconstituted and reporter activity can be detected. To test the physical interaction between Gogo and Fmi, we used the Bimolecular Fluorescence Complementation (BiFC) technique, which is a PCA in which the split reporter is a fluorescence protein (**Fig3.11a**, (Kerppola, 2006; Plaza et al., 2008). As a reporter, we chose an improved version of the Yellow Fluorescent Protein (YFP) called Venus. We used a mutated version of Venus (T153M) to avoid spontaneous interaction between the N- and C-terminal fragments (Saka et al., 2008).

Fmi was fused to the N-terminal part of Venus (Fmi-VN) and Gogo with the C-terminal fragment (Gogo-VC). When these constructs were transfected separately, no fluorescent signal could be detected (**Fig3.11b,c,f,g,j,k**). If Gogo-VC and Fmi-VN were co-transfected, S2 cells started to shine 24h after transfection. Fluorescence signal was intense in intracellular compartements located close to the nucleus, as well as in the plasma membrane at cell-cell contacts where Gogo and Fmi co-accumulated (**Fig3.11e,i,m**). However, we also observed BiFC signal in control cells co-transfected with Fmi-VN and mCD8-VC (**Fig3.11d,h,l**). Like in Gogo-VC and Fmi-VN transfected cells, the Venus fluorescent signal was mostly observed in cellular compartments adjacent to the nucleus (**Fig3.11d**), what suggests that unspecific binding occurs essentially in these compartments. However, BiFC signal was sometimes also detected at the plasma membrane in control cells. Since the split fragments have some affinity to each other and that their association is irreversible, it is likely that the fluorescent background is due to unspecific binding of the two halves of Venus. This unspecific

association can be enhanced by the fact that transmembrane proteins are in close proximity at the cell surface and in intracellular compartments when they are highly overexpressed. Therefore, we were not able to conclude unambiguously on the physical binding between Gogo and Fmi with this assay.

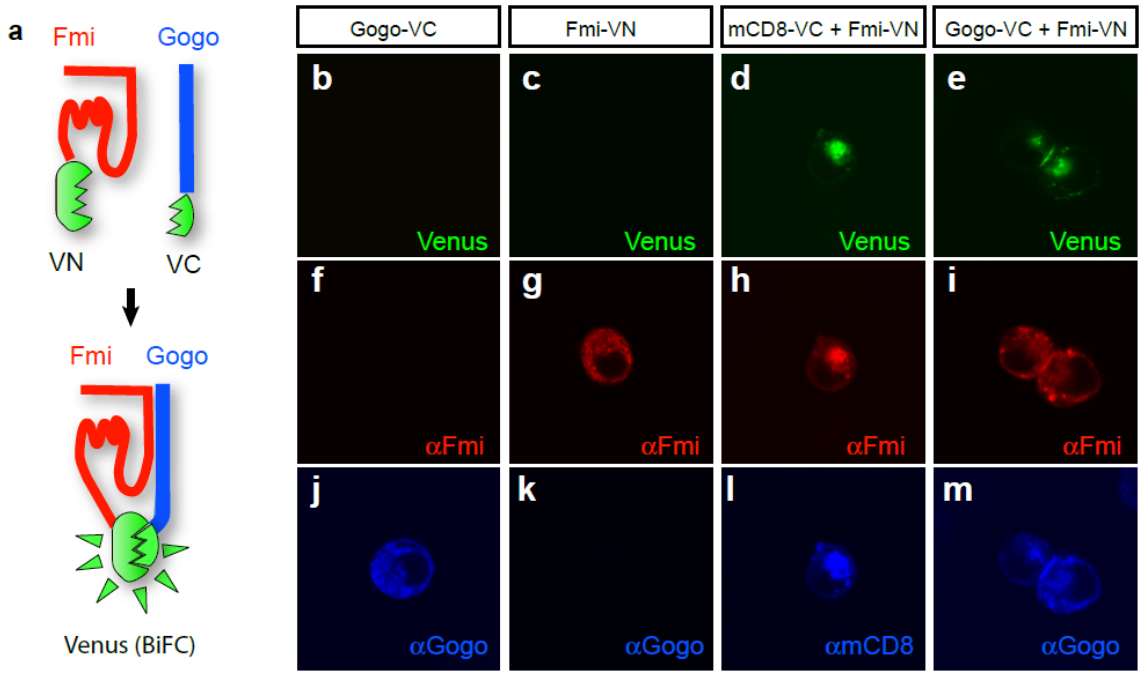


**Figure 3.11 The BiFC assay generates unspecific signal in transfected S2 cells**
(**a**) Schematic representation of the BiFC assay. Fmi and Gogo are fused with the N-terminal part (VN) and the C-terminal part (VC) of the fluorescent protein Venus, respectively. The interaction of Gogo and Fmi allows the association of the two fragments of the split Venus, and generates a fluorescent signal. (**b–m**) S2 cells were transfected with the indicated constructs. The transfection efficiency was monitored with anti-Fmi (**f–i**), anti-Gogo (**j**,**k**,**m**) or anti-mCD8 (**l**). The BiFC signal is show in green (**b**–**e**). Control cells expressing Gogo-VC or Fmi-VN alone did not produce a fluorescent signal (**b**,**c**). Venus fluorescence was observed in cells co-expressing Gogo-VC and Fmi-VN (**e**), especially in intracellular compartments situated close to the nucleus and at cell-cell contacts where Gogo and Fmi co-accumulated. However, BiFC signal was also visible in cells co-transfected with mCD8-VC and Fmi-VN (**d**). This suggested that intrinsic affinity between the two Venus fragments generates false positives.

### 3.9 *in situ* PLA generates unspecific background signal in S2 cells

Since the BiFC assay could not be used for assessing the binding between Gogo and Fmi, we tried a new strategy to detect protein-protein interactions called *in situ* proximity ligation assay (PLA) (**Fig3.12a**; (Soderberg et al., 2008). The PLA technology uses antibodies attached to oligonucleotides. If these antibodies are in close proximity, the oligonucleotides are ligated, and DNA amplification of the ligated fragment can occur, serving as a read-out of the assay. PLA was initially developed in solution phase, and DNA amplification was done by PCR (Fredriksson et al., 2002). *In situ* PLA is a modified version which allows the detection of proteins and their interactions in cells and tissues (Soderberg et al., 2006). In this case, the ligation of the pair of oligonucleotides generates a circular DNA that serves as a template for rolling-circle amplification. The oligonucleotide conjugated to one of the antibody acts as a primer, and the amplified DNA stay attached to the antibody, allowing *in situ* detection of protein interactions. A concatemeric single-stranded DNA is thus produced and is detected by fluorescently labeled oligonucleotides that can hybridize to a specific DNA sequence. The PLA signal appears as little dots in the cells (**Fig3.12b–k**).

We used this assay to check the interaction between Gogo and Fmi in cultured cells. As a control, we transfected S2 cells with Gogo or Fmi separately, and performed the PLA assay using both antibodies. These controls gave a very low background (less than 1 dot/cells, **Fig3.12b,g,c,h,l**). In cells co-transfected with Gogo and Fmi, we obtained a substantial signal (26 dots/cells, **Fig3.12f,k,l**). As a negative control, we performed the PLA with Gogo and N-cad, or with Fmi and mCD8. We also observed a positive signal in these two cases (14.7 and 21.2 dots/cells, respectively). Since we did not observe a background signal in the case of single protein expression, the high signal in the samples co-transfected with a control protein is probably not due to the technique itself. Instead, it seems that transmembrane proteins overexpressed in S2 cells are crowded at the cell surface, and are consequently in close proximity. This may explain why we see a high background in negative controls. In any case, this method was not suitable to test the physical interaction of Gogo and Fmi in S2 cells.

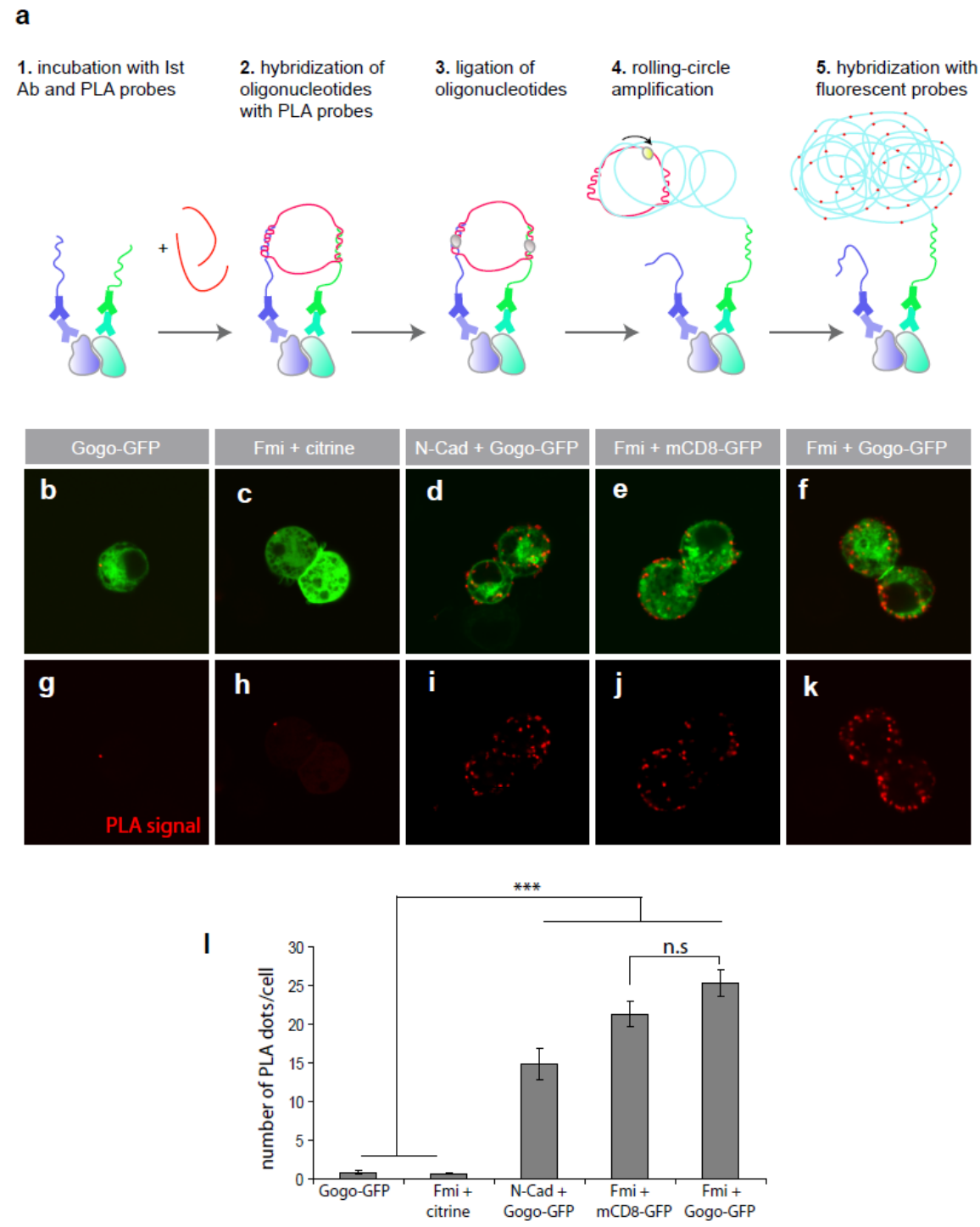


**Figure 3.12 *in situ* PLA show unspecific interactions of transmembrane proteins**
(**a**) In the PLA assay, the sample is first incubated with primary antibodies directed against the two putative protein partners. The secondary antibodies coupled with oligonucleotides (PLA probes) recognize their respective primary antibody. Two oligonucleotides that contain a sequence complementary to the DNA of each PLA probes hybridize to their complementary sequence. If the oligonucleotides are in close proximity, the ligation of the pair of oligonucleotides allows the formation of a close DNA circle. This circular DNA serves as a template for rolling-

circle amplification (RCA) and the nucleotide of one arm of the PLA probes acts as a primer for amplification. A polymerase then generates a single-stranded concatemeric RCA product. Oligonucleotides complementary to the RCA product and labeled with fluorophores hybridize and allow the detection of the PLA by fluorescence microscopy. (**b–k**) S2 cells were transfected with the indicated constructs, and subjected to PLA using the following primary antibodies: α-Gogo and α-Fmi (**b**,**c**,**f**,**g**,**h**,**k**), α-NCad and α-Gogo (**d**,**i**), α-Fmi and α-mCD8 (**e**,**j**). Transfected cells were visualized with GFP-tagged constructs or by co-transfection with citrine (green in **b–f**), and PLA signal, appearing as a dotty staining, is shown in red (**b**–**k**). PLA signal was detected in cells co-transfected with Gogo and Fmi (**k**), but not in cells expressing only one of the protein (**b**,**c**,**g**,**h**). However, we obtained a similar PLA signal with transmembrane proteins which are not supposed to physically interact (**d**,**e**,**i**,**j**). The number of PLA dots per cell was quantified on at least 60 cells in three independent experiments (**l**).The quantification was analyzed with a $\chi^2$ test.

### 3.10 Gogo does not modify the adhesive properties of Fmi in cultured cells

Even though a direct binding of Gogo and Fmi could not be demonstrated unambiguously, the fact that these two proteins can influence their localization in S2 cells and *in vivo* strongly suggests that they interact. We wondered what could be the role of this interaction in R8 photoreceptor cells. Since Fmi is known to mediate homophilic adhesion, and since Fmi is expressed in both photoreceptor and target cells, it is possible that Fmi homotypic interactions regulate R8 axon pathfinding. Therefore, we asked whether Gogo, by interacting with Fmi in *cis*, could modulate the strength of cell adhesion mediated by Fmi-Fmi interactions. To test this hypothesis, we performed an aggregation assay by mixing a population of cells co-transfected with Gogo and Fmi with another population transfected with Fmi alone. As a control, we replaced Gogo with mCD8. If Gogo inhibits Fmi-Fmi interaction, we should observe less Gogo-expressing cells in the aggregates mediated by Fmi. On the contrary, if Gogo promotes Fmi-Fmi *trans* interaction, the aggregation rate should be higher in Gogo co-transfected cells, and these cells should form a core in the aggregates, which should be surrounded by cells expressing Fmi alone. We did not observe any of these trends, and the composition of the aggregates was similar to the control (**Fig3.13a,b**). This result suggest that Gogo does not modulate Fmi homophilic adhesion, at least in S2 cells.

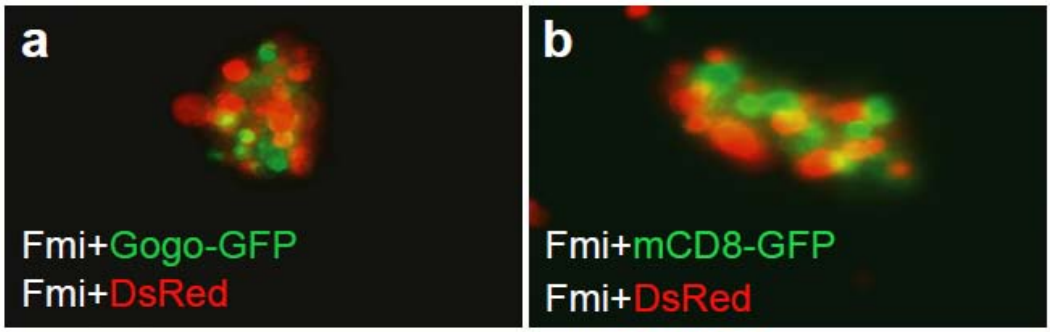


**Figure 3.13 Gogo does not modulate Fmi homophilic interactions in S2 cells**
Fmi-expressing cells (labeled with Dsred, shown in red) were mixed with cells expressing Gogo-GFP and Fmi (**a**) or mCD8-GFP and Fmi (**b**) (shown in green). The two populations of cells were equally distributed in the aggregates, suggesting that Gogo does not modify the adhesive properties of Fmi in S2 cells.

### 3.11 Gogo and Fmi collaborate to mediate M3 recognition

To get insight on the way Gogo and Fmi collaborate in R8 axon targeting, we tested the effect of co-overexpressing these proteins in photoreceptor cells. When we overexpressed Fmi or Gogo separately in photoreceptor cells using the GMR-Gal4 driver, we observed a mild rough eye phenotype (**Fig3.14a,b)**. Strikingly, the eye morphology was completely disrupted in flies co-overexpressing Gogo and Fmi (**Fig3.14c**). We then looked at the effect of Gogo and Fmi overexpression on medulla axon targeting. The overexpression of Fmi led to a very mild phenotype in R7s, which extended thin filopodia beyond M6 (**Fig3.14d**). When we overexpressed Gogo, R7 axons looked similar to the wild type (**Fig3.14e**). Since the eyes of flies that co-overexpressed Gogo and Fmi were severely affected, photoreceptor axon targeting analysis was precluded due to strongly disrupted axonal connections. As the Gal4/UAS system is temperature-dependent, we raised these flies at 20°C to induce a milder overexpression of Gogo and Fmi. This way, the photoreceptor targeting phenotype could be analyzed. Strikingly, approximately half of R7 axons were redirected to the M3 layer, which R8 normally target (**Fig3.14f,i**). This result suggested that Gogo and Fmi collaborate to guide photoreceptor axons to the M3 layer.

Since Gogo and Fmi were overexpressed in both R7 and R8 photoreceptors in the previous experiments, we could not conclude whether the R7 premature stopping phenotype is due to axon-axon interactions between R7 and R8 from the same column, or to axon-target interactions between R7 and the M3 layer (**Fig3.14h**). To distinguish between these two hypotheses, we overexpressed Gogo and Fmi only in R7 photoreceptors. To this end, we used FLPase under the GMR promoter, which generates mitotic recombination only in R1, R6 and R7 photoreceptors (Lee et al., 2001). Again, R7 axons stopped at the R8-recipient layer M3 (16.5% at 20°C, **Fig3.14i**). The lower penetrance of the phenotype is probably due to the perdurance of the Gal80 repressor protein. When flies were raised at 25°C, we observed a similar strength of the phenotype to what we quantified in flies co-overexpressing Gogo and Fmi in all photoreceptor cells at 20°C (**Fig3.14g,i**), suggesting that the expression level rather than the expression in R8 is important for redirecting R7 to the M3 layer, even though we cannot exclude that axon-axon interactions participate in generating R7 premature stopping at M3. In summary, these data suggest that Gogo and Fmi work together in R8s to recognize and adhere to their target layer M3.

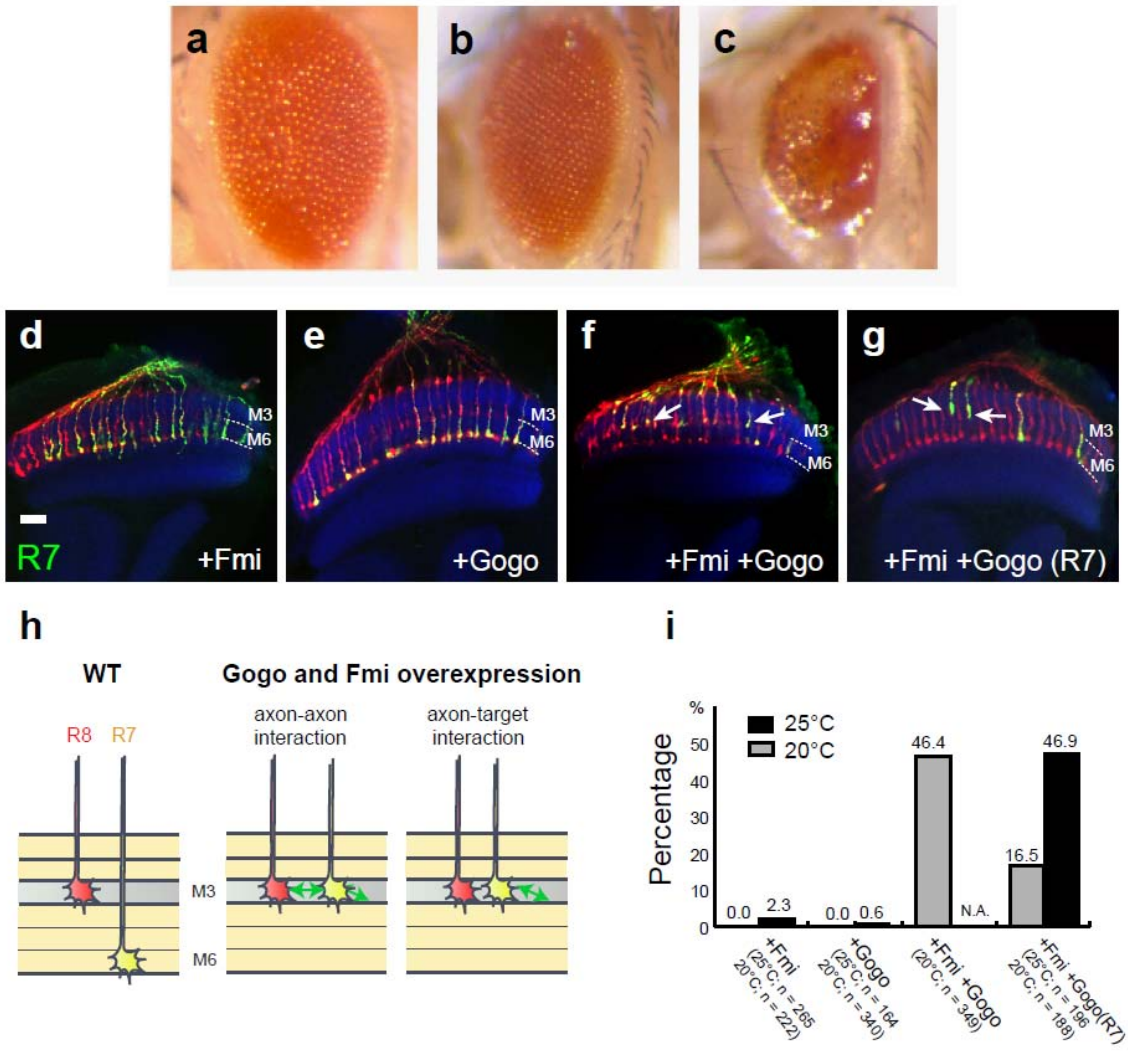


**Figure 3.14 Gogo and Fmi collaborate in the recognition of the M3 layer**
(**a–c**) Pictures of the eye of flies overexpressing Fmi (**a**), Gogo (**b**), or both proteins (**c**) with the GMR-Gal4 driver. The mild rough eye phenotype seen in the case of Fmi or Gogo overexpression is very strongly enhanced when Gogo and Fmi are co-overexpressed. (**d–f**) R7 and R8 axons in the medulla are stained with 24B10 antibody (red), R7s with *Rh4*-GFP (green), and medulla layers with anti-NCad (blue). Flies overexpressing Fmi (**d**) or Gogo (**e**) using the GMR-Gal4 driver did not show a phenotype in R7 photoreceptor targeting. When both proteins were overexpressed, almost half of R7 axons targeted the M3 layer, where R8 axons normally stop (**f**) (20°C). R7-specific clones that overexpress Gogo and Fmi are labeled with GFP (green in **g**). R7 mistargeted the M3 layer even when Fmi and Gogo were not co-overexpressed in R8 photoreceptors. (**h**) Schematic explaining that the R7 mistargeting phenotype can be explained by axon-axon interactions between R7 and R8 from the same column, or R7-target interactions. (**i**) Quantification of the R7 stopping phenotype at M3 at 20°C and 25°C. Note that the eye is severely disrupted when Gogo and Fmi are overexpressed at 25°C in all photoreceptor neurons, preventing the analysis of the axon targeting phenotype (N.A in **i**). Scale bar: 20µm.

### 3.12 Fmi is required in L3 for R8 axon targeting

Since Fmi functions through homophilic interactions *in vitro* and *in vivo* in wing cells, we wondered whether Gogo and Fmi in R8 axons bind to Fmi in their target cells to achieve the proper innervation of R8s. Therefore, we wanted to test the requirement of Fmi in the brain for R8 axon targeting. It was tentatively shown by Bazigou et al. using the ELF system that Fmi seems to be required in the target area, but the phenotype was very mild (5.6□% bundling, 0.4□% stopping) (Bazigou et al., 2007). We used the FLICK technique to knock-out *fmi* in the target cells more efficiently (see material and methods). Several Gal4 lines were tested to drive FLPase expression in lamina and/or medulla neurons. We obtained a substantial R8 stopping phenotype at M1 (18,0%) with the *gcm* (*glial cells missing*) promoter (Chotard et al., 2005) (**Fig3.15b,f,i**).

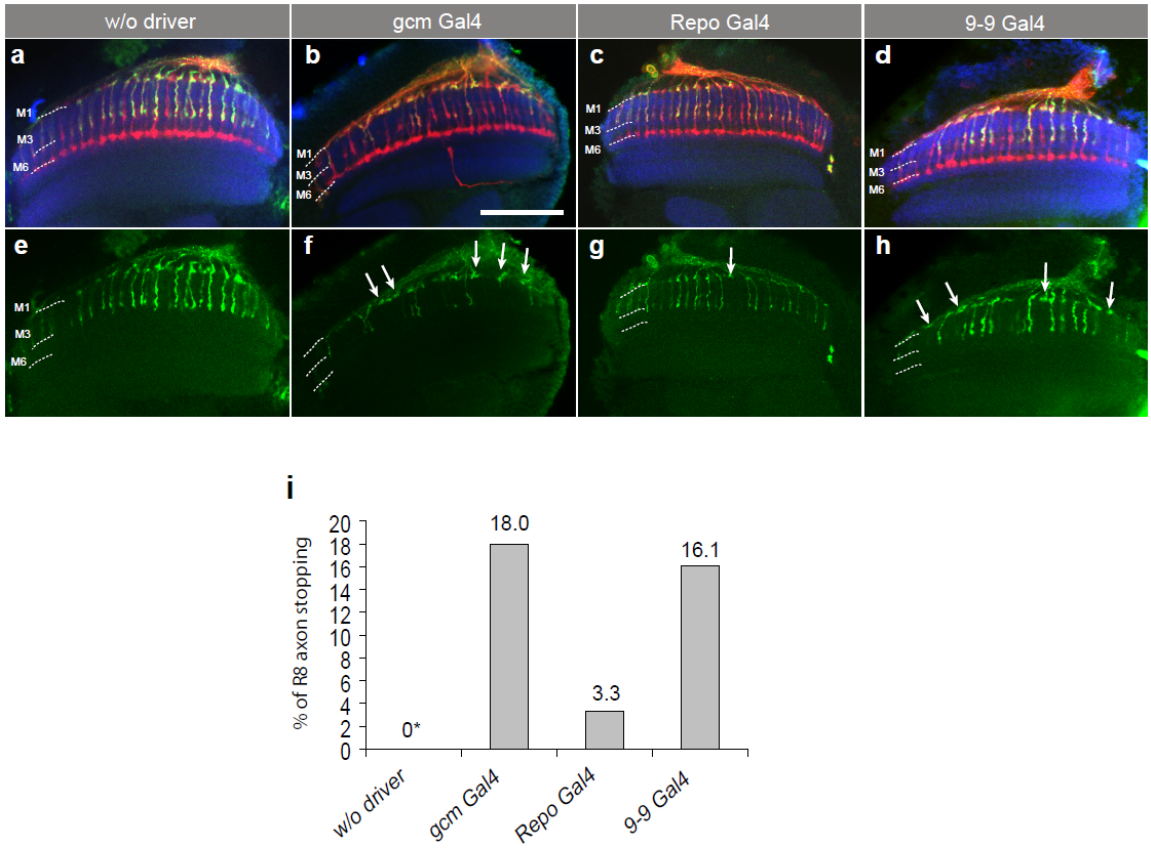


**Figure 3.15 Fmi is required in L3 neurons for R8 axon targeting to M3**
(**a**–**h**) Horizontal sections of adult medulla in *fmi* FLICK flies. R7 and R8 photoreceptor axons are stained with mAb24B10 (red), R8 are marked with Rh6-GFP, and medulla layers are visualized with anti-N-Cadherin (blue). (**a**,**e**) In control flies lacking the Gal4 driver, R8 showed a bundling phenotype but did not stop at the M1 layer. (**b**,**f**) When Fmi was removed from the target area using the *gcm*-Gal4 driver, we observed a substantial R8 stopping phenotype at the M1 layer

(arrows). (**c**,**g**) Removing Fmi from glial cells with *Repo*-Gal4 led to a mild R8 stopping phenotype. (**d**,**h**) Fmi FLICK driven by 9-9-Gal4, a driver known to be expressed in lamina neurons L3, induced R8 retargeting to M1 (arrows). (**i**) Quantification of the R8 stopping phenotype at the M1 layer. The percentage of R8 stopping was estimated by the absence of R8 axons innervating the medulla relatively to the control. Scale bar: 20µm.

To monitor the cells that underwent FLP-out, we used the Act<stop<nLacZ transgene (Struhl et al., 1993). If the stop cassette is excised by FLPase, LacZ is expressed in the nuclei under the *actin* promoter. All neuronal cells were stained with ElaV (*embryonic lethal abnormal vision*; (Robinow et al., 1988) antibody. We observed that using the *gcm*-Gal4 driver, FLP-out occurred in almost all lamina neurons, in lamina and medulla glial cells, and in a few medulla cells (**Fig3.16b,d**). Importantly, nLacZ was not detected in photoreceptor cells, indicating that *fmi* was specifically removed from the brain but not from R cells in the FLICK experiment. In summary, we showed that *fmi* is required specifically in the target region for R8 photoreceptor axon targeting, and that when Fmi is reduced in the target area, R8 axons tend to stop at the M1 layer. This phenotype resembles the one observed in flies lacking *fmi* in photoreceptor cells. This suggests that Fmi homophilic interactions between R8 growth cones and their target layer M3 mediate R8 synaptic-layer targeting.

We then asked in which brain cells *fmi* is required for correct R8 axon targeting. Since FLICK using the *gcm*-Gal4 driver occurred mostly in lamina neurons and glial cells, we first wanted to check whether *fmi* is important in lamina and medulla glia for R8 targeting. To do so, we generated FLICK only in glial cells using the *repo* (*reversed polarity*) driver (Xiong et al., 1994). We observed a very mild R8 stopping phenotype (3.3%, **Fig3.15c,g,i**) when *fmi* was knocked out in glial cells, indicating that glia play a minor role in guiding R8 growth cones. Again, we checked in which cells FLP-out occurred and monitored its efficiency with Act<stop<nLacZ. We found that most of glial cells expressed nLacZ (**Fig3.15c,e**).

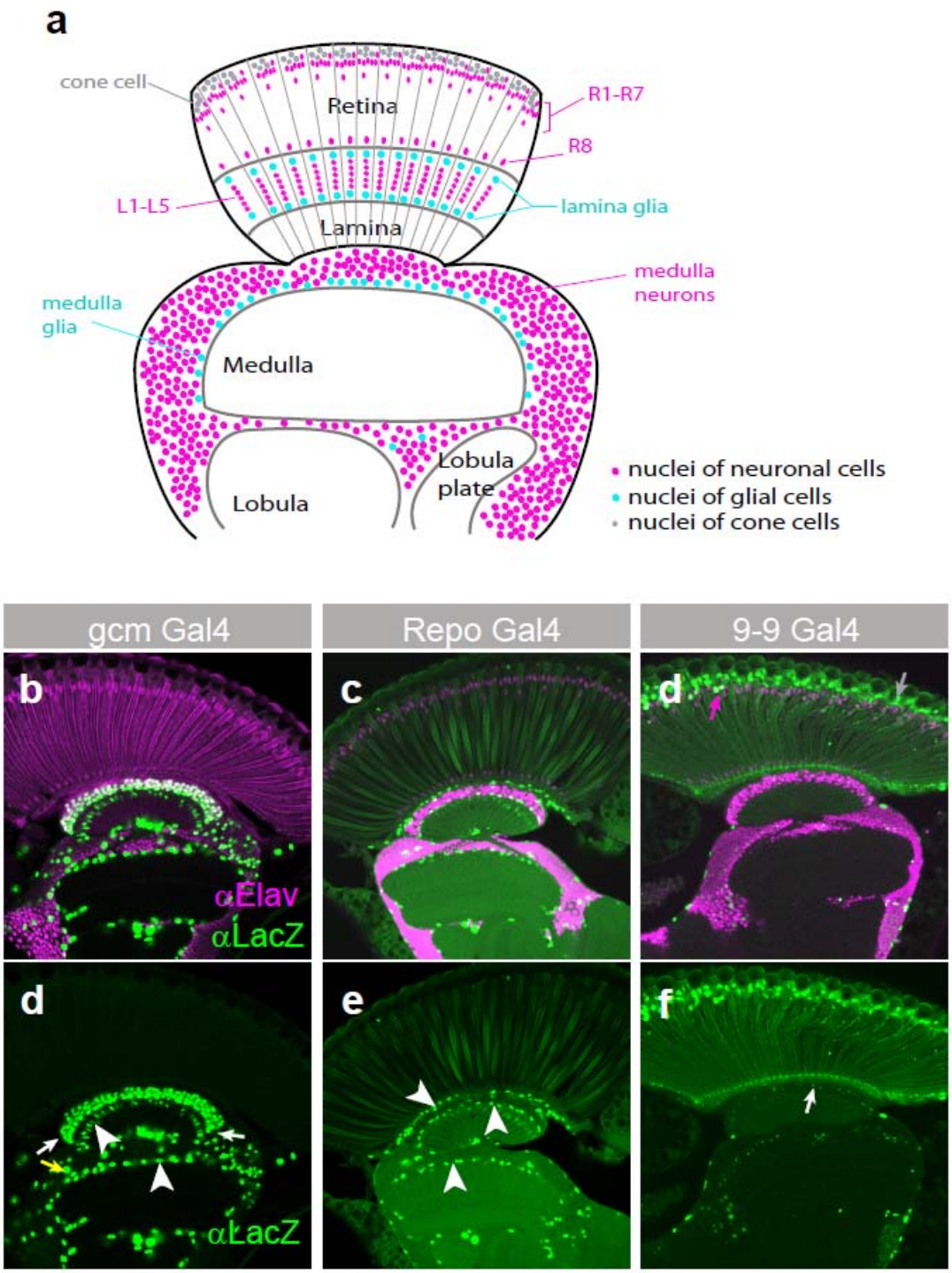


**Figure 3.16 Monitoring cells that undergo FLP-out with drivers used in *fmi* brain FLICK**
(**a**) Schematic representation the nuclei localization of the different cell types of the adult visual system. Nuclei of cone cells are represented in grey, nuclei of neurons in magenta, and glial nuclei in cyan. (**b**–**f**) Agarose sections of the adult visual system stained with anti-ElaV (magenta) and anti-LacZ (green). The excision of the stop cassette in the Act<stop<nLacZ transgene allows the visualization of the nuclei of cells that undergo FLP-out using different Gal4 lines. (**b**,**d**) The *gcm*-Gal4 driver generated FLP-out in almost all lamina neurons (white arrows), in a few medulla neurons (yellow arrow) and in lamina and medulla glial cells (arrowheads). (**c**,**e**) *repo*-Gal4 induced FLP-out in many glial cells (arrowheads). (**d**,**f**) In flies carrying the *9-9*-Gal4 driver, FLP-

out occurred in lamina neurons L3 (white arrow), in a few photoreceptor cells (magenta arrow) and in many cone cells (grey arrow).

Since glial cells seem not to play a major role in the guidance of R8 axons, lamina neurons are likely to be involved. From the morphology of lamina neurons arborization in the medulla layers, L3 is a good candidate for presenting Fmi to R8 growth cones: L3 axons terminate at the M3 layer and form a flat structure at the bottom of this layer (Takemura et al., 2008). To test the requirement of *fmi* in L3 lamina neurons, we used the *9-9*-Gal4 driver to induce FLICK (Nern et al., 2008). This driver gave a significant R8 phenotype (16.1% axon stopping, **Fig3.15d,h,i**), indicating that L3 neurons play a crucial role in R8 axon targeting. When we checked in which cells FLP-out occurred, we observed that nLacZ was expressed in half of L3 neurons, in cone cells, and in a few photoreceptor cells, but never in R8s (**Fig3.16d,f**). This confirms that the driver line used for knocking-out *fmi* from L3 neurons is rather specific, and that the R8 targeting phenotype is not due to FLPase expression in R8 photoreceptors.

To confirm that that the medulla layers were not affected in the *fmi* brain FLICK flies, we performed N-Cad antibody staining at mid-pupal stage (48h APF) when the second targeting step starts. We did not observe any difference in the medulla layers stained with anti-N-Cad between the control and the *fmi* brain FLICK flies (**Fig3.17a–c**), indicating that the R8 axon targeting phenotype is not due to the disruption of the medulla layers. To further test whether the requirement of *fmi* in L3 for R8 targeting is not a consequence of the mistargeting of L3 neurons when they lack *fmi*, we performed MARCM in lamina neurons using FLPase under the control of the *dac* promoter (Millard et al., 2007), and marked L3 neurons using the 9-9-Gal4 driver. *fmi* mutant L3 axons targeted normally the M3 layer (**Fig3.17d**), indicating that *fmi* is not autonomously required in these neurons for axon targeting, but is non-autonomously required for R8 targeting.

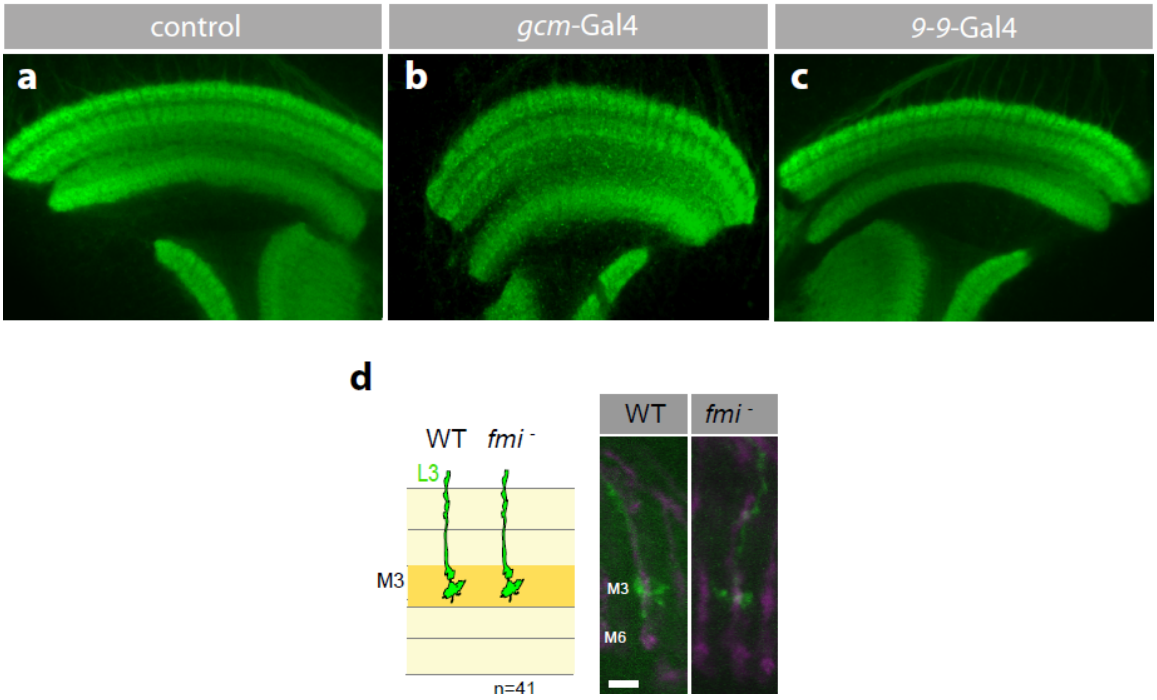


**Figure 3.17 The synaptic layers of the medulla are not disrupted in *fmi* brain FLICK flies**
(**a**–**c**) Synaptic layers in the medulla at 48h APF are stained with N-Cad antibody in control flies (**a**), and in *fmi* brain FLICK flies generated with the *gcm*-Gal4 driver (**b**) or the *9-9*-Gal4 driver (**c**). The medulla layers appeared to be normal in each case. (**d**) Wild type and *fmi* mutant L3 neurons were labeled using dacFLP and the *9-9*-Gal4 driver (green), and R7 and R8 axons with 24B10 antibody (magenta). *fmi* mutant L3 targeted the proper layer M3 in the adult. The scale bar represents 5µm.

Finally, we checked whether Fmi was efficiently reduced from the target cells in *fmi* brain FLICK flies. Fmi antibody stainings at 48h APF showed that it was strongly reduced in the distal part of medulla in *fmi gcm*-FLICK flies compared to the control (**Fig3.18a**,**b**,**d**,**e**,**g**,**h**). In *fmi 9-9*-FLICK flies, we could see some patchy areas were the fluorescence intensity was reduced in the M3 layer (**Fig3.18c**,**f**,**i**). Since the difference was mild (maybe due to Fmi staining in the processes of other neurons running through the medulla), these results should be confirmed by monitoring the FLICK occurrence during larval stages or beginning of pupal stage using the Act<stop<nLacZ cassette.

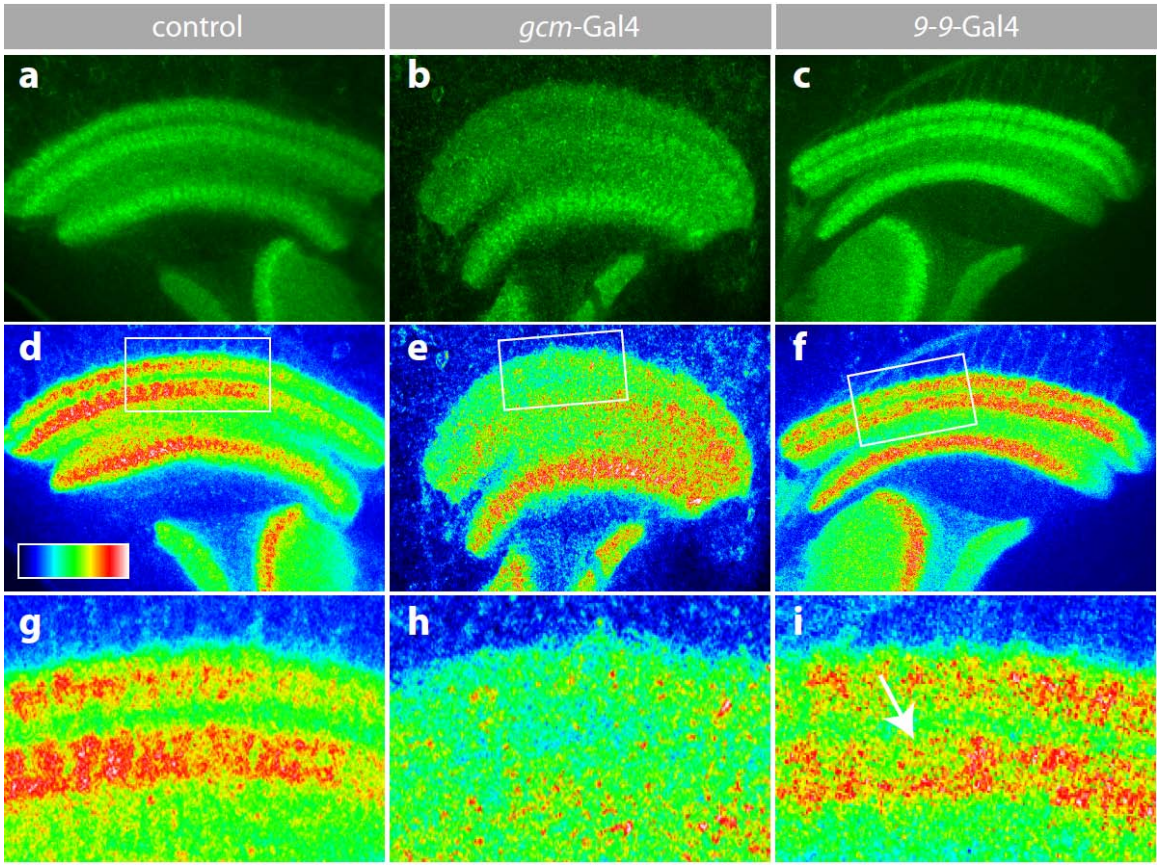


**Figure 3.18 Fmi staining at the mid-pupal stage in *fmi* brain FLICK flies**
(**a**–**i**) Fmi antibody staining at 48h APF in control flies (**a**,**d**,**g**), and in *fmi* FLICK flies carrying the *gcm*-Gal4 (**b**,**e**,**h**) and the *9-9*-Gal4 drivers (**c**,**f**,**i**). (**d**–**i**) The intensity of the Fmi antibody staining is shown in pseudocolors. (**g**–**i**) Magnification of the regions shown in (**d**–**f**). Fmi is strongly reduced with the *gcm*-Gal4 driver. With the *9-9*-Gal4 driver, some areas at the M3 layer showed a reduced Fmi expression compared to the underlying layer (arrow).

Overall, the requirement of *fmi* in the target area strongly suggests that Gogo and Fmi on R8 axons interact with Fmi in target cells in *trans*.

# 4. DISCUSSION

## 4.1 Gogo and Fmi interaction in neuronal development

Fmi is a multifunctional protein involved in different processes of *Drosophila* development. In planar cell polarity, Fmi acts together with the core PCP proteins including Fz and Vang. In neuronal development, on the other hand, the molecular pathway in which Fmi is involved was not known. In photoreceptor axons, Fmi regulates layer-targeting in the medulla and cartridge selection in the lamina (Lee et al., 2003; Senti et al., 2003). Fmi also controls dendritic field formation in the embryo and during larval stage (Gao et al., 2000; Kimura et al., 2006). The phenotypic similarities between *gogo* and *fmi* in all these developmental aspects and the genetic interaction of *gogo* and *fmi* in R8 targeting and dendritic field formation suggests that the collaboration between Gogo and Fmi is a general molecular mechanism in neuronal development.

Do Gogo and Fmi work in a similar way in R8 axon targeting compared with other neuronal systems? We can already observe some differences in the way Fmi regulates diverse aspects of neuronal development. Unlike in R8 targeting, Fmi has a non-autonomous function but not an autonomous function in R1-R6 lamina cartridge selection (Chen and Clandinin, 2008). An intriguing model has been proposed, in which Fmi homophilically interact in *trans* between R axons, and the balance of adhesion forces between R axons shapes the targeting pattern of lamina cartridges. *gogo* mutants have a similar phenotype in photoreceptor targeting in the lamina (Hakeda-Suzuki et al., 2011). It will be interesting to determine whether *gogo* functions in an autonomous or non-autonomous fashion and if it interacts with *fmi* in this context. In either case, the molecular mechanisms underlying R1-R6 target selection is likely to be different from R8 axon pathfinding, since Fmi exerts a non-autonomous function in lamina targeting and an autonomous function in medulla targeting.

The function of Fmi seems to be also different between dendritic field formation and photoreceptor axon targeting. Fmi is an ambivalent protein about its structural domains: due to its cadherin repeats and homophilic properties, Fmi is considered as a cell adhesion molecule. On the other hand, its hormone receptor domain and 7-pass transmembrane domain (similar to GPCR) suggests that Fmi functions as a receptor.

Interestingly, it has been reported that a Fmi deletion consisting of the intracellular, transmembrane, and hormone receptor domain (FmiΔN) is able to partially rescue the *fmi* dendritic overgrowth phenotype (Kimura et al., 2006). This indicates that Fmi does not mediate dendritic field formation by homophilic interactions. Moreover, a Fmi deletion lacking the intracellular domain (FmiΔC) fails to rescue the dendritic phenotype, suggesting that intracellular signaling is crucial in this context. On the contrary, in R8 axons, FmiΔN cannot rescue the *fmi* targeting phenotype, whereas the Fmi intracellular deletion FmiΔIntra rescues to the same extend as the full length protein (Hakeda-Suzuki et al., 2011). These rescue experiments, together with the fact that Fmi is required in the target of R8 axons, suggest that Fmi rather acts as a cell adhesion molecule in R8 targeting and as a receptor in dendritic field formation. It will be therefore interesting to investigate how Gogo regulates the formation of dendrites to decipher the general principles versus unique mechanisms mediated by the interaction between Gogo and Fmi.

Fmi has been shown to play a role also in synaptogenesis at the neuromuscular junction (Bao et al., 2007). It would be interesting to test whether *gogo* mutants have a similar phenotype and interact with *fmi* in this context.

## 4.2 Physical interaction between Gogo and Fmi

Our study indicates that Gogo and Fmi physically interact in *cis* in R8 growth cones to guide them to their proper final layer M3. Two results support the physical interaction between Gogo and Fmi. First, when Gogo was co-expressed with Fmi in cultured cells, Gogo co-accumulated with Fmi at cell-cell contacts. Second, if Gogo was ectopically expressed in pupal wing epithelial cells, Fmi localization was disrupted at the apical pole the cells, and Fmi colocalized with Gogo at the lateral membranes. Even though these experiments provide only an indirect way to show the physical interaction between Gogo and Fmi, it is difficult to imagine that Gogo and Fmi mutually influence their localization without binding to each other (directly or indirectly). The reason why Fmi recruits Gogo in cultured cells whereas Gogo recruits Fmi in wing cells is unclear. In wing cells, Fmi localization at the distal and proximal membranes is dependent on the localization of other PCP proteins and relies on a feed-back loop involving endocytic trafficking (Mottola et al., 2010; Tree et al., 2002). This sophisticated mechanism is probably easily disrupted when Gogo binds to Fmi. On the contrary, Fmi accumulation at cell-cell contacts in S2 cells may occur only by simple diffusion in the plasma membrane, which could explain why Gogo cannot disrupt Fmi localization and Fmi recruits Gogo in this case. In the endogenous situation, although the trafficking and axonal transport of Gogo and Fmi seem to be largely independent on each other in R8 axons, we observed a decrease in Gogo accumulation at the growth cones in *fmi* mutant in third instar larvae (**Supplementary Fig1**). This data supports the idea that Gogo and Fmi interact endogenously in R8 photoreceptor growth cones.

The most common way to demonstrate a physical interaction between two proteins is by co-immunoprecipitation. Unfortunately, all our attempts to co-immunoprecipitate Gogo and Fmi failed. It is noteworthy that this co-immunoprecipitation is technically challenging. Indeed, Fmi possesses a 7-transmembrane domain which makes its extraction from the plasma membrane difficult. Moreover, Fmi is a very large protein (>400kD) and can form dimers in *cis* (Kimura et al., 2006). In addition, Gogo is also a large molecule (170kD) and can oligomerize. Consequently, it is possible that Gogo and Fmi form a gigantic complex, which is thus very difficult to pull-down. Alternatively, it is possible that some factors that allow the formation and/or the stabilization of the Gogo-Fmi complex are not expressed in S2 cells.

However, since we still observed a co-accumulation of Gogo and Fmi at cell-cell borders in S2 cells, this hypothesis is less probable. Another explanation would be that Gogo and Fmi do not bind directly even though they are in proximity, what prevents Gogo and Fmi to be pull-down in the same protein complex.

In some cases, we observed a faint band corresponding to the co-immunoprecipitated protein when we compared with control cells expressing only one of the proteins. However, a faint band also appeared when we co-transfected Gogo or Fmi with a control protein immunoprecipitated with the same tag. This indicates that in co-immunoprecipitation experiments, it is crucial to design a proper negative control. Ideally, it is more thorough to perform the co-immunoprecipitation with an irrelevant protein fused with the same tag.

Since the co-immunoprecipitation of Gogo and Fmi is technically difficult, we tried to demonstrate the interaction between Gogo and Fmi in living cells. A common method for detecting protein-protein interactions in intact cells is Förster resonance energy transfer (FRET). In this technique, two fluorophores that have compatible emission and excitation spectra are fused to the putative interacting partners. If the fluorophores are in close proximity, energy is transferred from one fluorophore to the other, and the change in fluorescence intensity is the read-out of the assay (Masi et al.). An important drawback of FRET is that it is difficult to get a positive signal and to design a proper negative control. Indeed, for the energy transfer to occur, the two fluorophores have to be in close proximity and have a permissive relative orientation. Since Fmi and Gogo both have a large cytoplasmic domain and nothing is known about their structures, it will be probably difficult to obtain the proper fusion site and fluorophore orientation to allow energy transfer. In addition, a lower FRET signal in the negative control compared to the putative interacting partners can be simply due to a sterical impairment of energy transfer. FRET is thus suitable for inducible protein interactions, but results showing new protein-protein interactions with FRET should be interpreted with caution. In addition, the sensitivity of the FRET assay is lower than other methods: FRET requires high protein concentrations, and a large fraction of the fluorophores must be in close proximity to obtain a positive signal. Since we could not detect a binding between Fmi and Gogo by co-immunoprecipitation, their interaction might be too weak to be assessed by FRET. For all these reasons, we chose other techniques to check the interaction between Gogo and Fmi in intact cells.

We tried to use a protein complementation assay (PCAs) in which the split reporter is a fluorescent protein (BiFC). In this assay, each of the putative interactors is fused to a half of a fluorescent protein, which is reconstituted if the tested proteins actually interact, generating a fluorescent signal. We observed an unspecific BiFC signal also with the control protein mCD8 which is supposed to be neutral in *Drosophila* and is commonly used as a cell-membrane marker *in vivo*. The fluorescent signal was mainly observed in intracellular compartments adjacent to the nucleus. These compartments could correspond to lysosomes, and the strong unspecific signal in these vesicles may come from the self assembly of the split Venus after cleavage of the fusion proteins. However, a faint BiFC signal was also sometimes visible in the plasma membrane in control cells, indicating that unspecific association also occurred at the cell surface. Although we saw a very strong BiFC signal at cell-cell borders in cells expressing Gogo-VC and Fmi-VN, it is difficult to say whether this fluorescence is due to the actual binding of Gogo and Fmi, or if Gogo and Fmi are spatially restricted, increasing the probability that they encounter. Since the association of the two halves of Venus is irreversible, even very transient interactions or simple protein encounters may be seen with this assay. Besides, the complementary Venus parts may have a high affinity to each other, which may be responsible for the high background signal that we observed. Consequently, it was not possible to conclude unambiguously about the actual binding of Gogo and Fmi using the BiFC assay.

PCAs are known to generate a high rate of false positives and false negatives. False positives are often due to high intrinsic affinity between the two halves of the reporter protein. False negatives can be found if the fusion with the split reporter prevents protein interactions, or the fusion site does not sterically allow reporter recombination. We therefore tried to use PLA, a recently developed assay based on antibodies, to test the Gogo-Fmi interaction (Fredriksson et al., 2002; Soderberg et al., 2008). In this assay, two antibodies directed against each of the putative interacting proteins are conjugated with two different DNA nucleotides. If the proteins are in close proximity, the ligation of the oligonucleotides allows rolling-circle amplification of the DNA, which is then detected by fluorescently labeled oligonucleotides. We obtained a positive PLA signal in S2 cells expressing Gogo and Fmi, but unfortunately also when an irrelevant protein was used as a control. However, we did not observe background PLA fluorescence when only Gogo

or Fmi was transfected, indicating that the unspecific signal seen in the negative controls is really due to unspecific transient interactions or just proximity between the two overexpressed proteins. The maximum distance between the interacting proteins to obtain a PLA signal is estimated to be 30-40nm when secondary PLA probes are used (manufacturer's information), which is much larger than in FRET (1-10nm). Since the PLA system is based on DNA amplification, a PLA signal can be detected even if only a small amount of the two tested protein are transiently and rarely in close proximity. Therefore, it seems that the PLA system is too sensitive for detecting protein-protein interactions in S2 cells when proteins are overexpressed. We tried to perform the PLA assay in endogenous conditions on agarose slices and whole mount brain in 3$^{rd}$ instar larvae and pupal stage, but we were not able to detect a specific signal (data not shown).

Overall, the techniques that we tried for the detection of protein interactions in intact cells (BiFC and PLA) may be too sensitive for testing interactions between transmembrane proteins in S2 cells in an overexpression situation. Novel techniques or improvements of the existing one are necessary for the reliable detection of protein interactions in intact cells.

## 4.3 How does Gogo collaborate with Fmi in R8 axons?

Even though we were not able to show a direct binding of Gogo and Fmi, the dependency of their localization and the genetic interaction in R8 photoreceptors in both loss-of-function and gain-of-function situations strongly suggest that they collaborate to guide R8 axons to their correct medulla layer. What is the functional role of the interaction between Gogo and Fmi in R8 photoreceptor axons? Three different hypotheses can be proposed, which are not mutually exclusive.

First, by binding to Fmi in *cis*, Gogo could modify the *trans* homophilic adhesion properties of Fmi. We tested this possibility using the aggregation assay in S2 cells, but we could not observe a difference between cells expressing only Fmi and cells co-expressing Fmi and Gogo. Nevertheless, we can not rule out this hypothesis, since the sensibility of this assay is probably not high enough to detect subtle changes in cell adhesion and might not reflect the endogenous situation. Alternatively, one can imagine that the Gogo-Fmi complex in R8 photoreceptor cells binds specifically with a Fmi-FactorX complex in the target cells. Indeed, a comparable situation exists in wing epithelial cells, where the Fmi-Vang complex at proximal membranes interacts in *trans* with the Fmi-Fz complex situated at the distal border (see paragraph **4.5**).

The second possibility we envisioned is that Gogo could transmit the extracellular guidance information received by Fmi inside the growth cone. Fmi intracellular domain is not required for R8 axon targeting, suggesting that it could act as a cell adhesion molecule, or that a co-receptor transduces the axon guidance signal intracellularly. Since the cytoplasmic domain of Gogo is required and Gogo interacts with Fmi in R8 axon targeting, Gogo could be a signaling component acting with Fmi for the recognition of the M3 layer. One experiment support this hypothesis, in which different combinations of cytoplasmic deletions of Gogo and Fmi were tested for their ability to generate R7 retargeting to M3 (**Supplementary Fig2**). As shown above, co-overexpression of the full length versions of Gogo and Fmi induced R7 mistargeting to the R8 recipient-layer M3. When both cytoplasmic deletions of Fmi and Gogo were co-overexpressed in photoreceptors, R7 targeted normally the M6 layer, suggesting that Gogo and Fmi interacts with intracellular components to mediate M3 recognition. A mild R7 stopping phenotype was induced by co-overexpression of GogoΔC with Fmi full length (7.2% of

R7 axons), whereas co-expression of Gogo full length with FmiΔIntra generated 41.0% of R7 stopping at M3 (**Supplementary Fig2**). These results indicate that Gogo intracellular domain plays an essential role in intracellular transduction of the M3 guidance signal. However, as mentioned above, Fmi possesses a 7-pass transmembrane domain similar to GPCR, indicating that Fmi could transduce the guidance signal even without cytoplasmic domain. Moreover, in dendrites, the HRM, transmembrane and intracellular domains are sufficient to partially rescue the dendritic phenotype, indicating that these domains are functional in dendritic tiling. It is unfortunately difficult to test the requirement of the 7-transmembrane domain for R8 photoreceptor targeting, since the trafficking of Fmi does not occur properly when this domain is replaced by other transmembrane domains (Tadashi Uemura, personal communication). Since we still observed a mild R7 stopping phenotype when Gogo cytoplasmic domain is removed in the co-overexpression experiment, it seems that some intracellular signaling is also mediated through Fmi, although Gogo cytoplasmic domain appears to be more essential for M3 layer recognition.

Finally, the third hypothesis is that Gogo and Fmi collaborate to add the specificity code necessary for guiding R8 photoreceptor axons to the M3 layer. This scenario is supported by the fact that overexpression of both Gogo and Fmi specifically in R7 axons induced their mistargeting to the R8-recipient layer. Although it is not clear how the specificity of these connections is achieved (see paragraph **4.5**), this result strongly indicates that both Gogo and Fmi are necessary in R8 photoreceptor growth cones to recognize and adhere specifically to their target layer.

## 4.4 Asymmetric Fmi homophilic interactions between R8s and their target cells

Which guidance cue is recognized by Gogo and Fmi at the M3 layer? Since Fmi is a homophilic adhesion molecule and R8 axon targeting is affected when Fmi is reduced in the target area, it is highly probable that Fmi homotypic interactions govern the guidance of R8 axons to M3. Qualitatively, the R8 axon targeting phenotype is similar when Fmi is removed specifically from the photoreceptors or from the target region: R8 axons often stop prematurely at the M1 layer. This corroborates the hypothesis that Fmi in R8 growth cones recognizes Fmi in the target cells. To confirm the homophilic asymmetric interaction between Gogo-Fmi in R8 axons and Fmi in the target cells, one interesting experiment would be to remove *fmi* from the brain and overexpress Gogo and Fmi in photoreceptor cells to see whether *fmi* is needed in the target cells for retargeting R7 to the M3 layer. Nevertheless, this experiment is technically difficult, since it requires an expression system independent of Gal4/UAS.

We tried to determine in which cell subtypes of the target area Fmi is required. We showed that Fmi seems not to be essential in glial cells. Since lamina neurons L3 form branches in the M3 layer in adults, they were good candidates for guiding R8 axons to their target layer. We could obtain a substantial R8 stopping phenotype when we removed Fmi from L3, indicating that Fmi in these cells is an important cue for R8 axons. However, it was difficult to confirm that Fmi was efficiently removed from the L3 axonal termini, possibly because they are surrounded by other neuronal processes that run through the medulla and express Fmi. It is thus necessary to check whether FLICK happened already during larval or early pupal stages. Several experiments can be envisioned to confirm that L3 are the target cells of R8 axons. First, using specific markers to monitor R8 and L3 simultaneously, one could observe the behavior of R8 axons at critical time points when they extend filopodia toward the future M3 layer, and check whether R8 filopodia contact L3 processes in wild type flies. Besides, to further test the importance of L3 for R8 targeting, one could induce apoptosis specifically in these neurons by expressing *reaper* of *head involution defective* (Zhou et al., 1997), and look at the R8 targeting phenotype. With this strategy, we may be able to obtain a stronger phenotype in R8 axons, since the complete elimination of L3 could allow the suppression of other redundant guidance molecules. However, the death of L3 neurons may have other unexpected consequences that indirectly influence R8 axon targeting. A

milder way to show that L3 are the target cells of R8 axons would be to make L3 retarget the M5 and M6 layers by generating *N-Cad* mutant L3 neurons (Nern et al., 2008). One problem can be that even if Fmi is required in L3, other guidance molecules for R8s can be sufficient in other lamina or medulla neuronal subtypes to guide R8 axons, making it difficult to obtain a penetrant R8 targeting phenotype in this experiment.

As mentioned above, the R8 targeting phenotypes when Fmi is absent from photoreceptors or from the target region are qualitatively similar, suggesting Fmi homophilic interactions between axons and target cells. However, the penetrance is lower when Fmi is removed from the target area (less than 20% R8 stopping at M1, against ~65% in *fmi* mutant photoreceptor clones). Two possibilities could account for this observation. First, when we removed Fmi from the target area, we could still see a residual amount of Fmi protein in the target layer, which could be sufficient to guide a portion of R8 axons. This remaining Fmi expression could be due to the fact that the FLICK occurs too late and to the perdurance of Fmi protein. Another assumption is that Fmi may be required in some medulla neurons, which were mostly not mutant for *fmi* with the drivers used in the *fmi* brain FLICK. This should be assessed in the future by using drivers that are expressed in medulla neurons. In any case, we showed that Fmi has an important role in L3 for R8 targeting.

Interestingly, although L3 are the guidance targets for R8 axons, it seems that they are not their synaptic partners. Medulla reconstruction studies using electron microscopy suggest that R8 make synaptic connections with L1 and L5, but not L3 (Takemura et al., 2008). Moreover, when R8 synapses are visualized with Bruchpilot tagged with mCherry, fluorescence can be seen along the axon shaft between M1 and M3 (unpublished data). Consequently, L3 neurons seem to attract R8 filopodia via Fmi, but probably do not form synapses with R8s. It would be interesting to screen for molecules required for synapse formation, which are probably different from those discovered in screenings for photoreceptor axon guidance.

In summary, we propose that during the second targeting step, Gogo and Fmi in R8 axons recognize Fmi in their target layer. This model is supported by three main observations. First, in *gogo* and *fmi* mutants, R8 axons fail to extend protrusions towards their final target layer. Second, *fmi* is required in the target area for the proper targeting of

R8 axons. Third, overexpression of Gogo and Fmi in R7s induce their mistargeting to the R8-recipient layer (**Fig 4.1**).

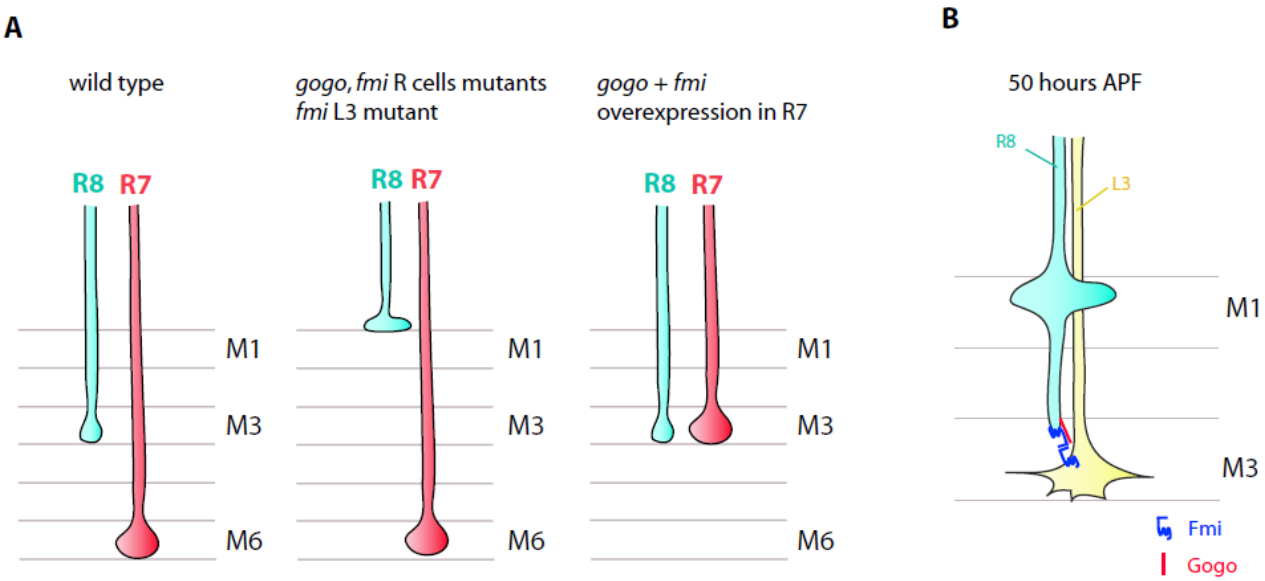


**Figure 4.1 Phenotypes summary and model**
(**A**) In wild type flies, R8 axons terminate at the medulla layer M3 and R7 at M6. When photoreceptors are mutant for *gogo* or *fmi*, R8 axons stop prematurely at the intermediate target layer M1. A similar phenotype is observed when *fmi* is removed from L3 target neurons. Overexpression of both *gogo* and *fmi* in photoreceptors redirect R7 axons to the M3 layer. (**B**) Model explaining how Gogo and Fmi may regulate R8 targeting specificity to the M3 layer. During the second targeting step (50h APF), Gogo and Fmi collaborate in R8 photoreceptors to recognize Fmi on the processes of L3 lamina neurons.

## 4.5 How do Gogo and Fmi confer synaptic-layer specificity?

### 4.5.1 Specificity from the photoreceptor side

Two arguments support the idea that Gogo and Fmi in photoreceptors mediate the targeting specificity of R8 axons to the M3 layer. First, *gogo* or *fmi* mutant R8 axons fail to extend to the M3 layer, whereas R7 mutant axons behave normally. Second, co-overexpression of Gogo and Fmi in R7 axons induces their mistargeting to the R8-recipient layer. However, since both R7s and R8s express Gogo and Fmi during early pupal stages, why do R7 axons target the M6 layer whereas R8 axons terminate at M3?

One possibility is that the interaction between Gogo and Fmi is differentially regulated in distinct photoreceptor cell types. In the case of Gogo and Fmi co-overexpression in R7 photoreceptors, it is possible that even if their interaction is not positively regulated in R7s, the interaction still occurs because the protein level is much higher than the endogenous situation.

The activity of Gogo and/or Fmi could also be modulated differentially in R7 and R8 axons by protein regulation. Nothing is known about how Fmi could be regulated. On the other hand, Gogo contains a conserved YYD motif in its intracellular domain that is a putative tyrosine phosphorylation site. Rescue experiments indicate that Gogo has to be non-phosophorylated in this motif to be functional in R8 axon guidance (unpublished data). It would be interesting to check in the future if Gogo is dephosphorylated only in R8 axons, and whether the YYD motif is involved in the interaction between Gogo and Fmi or in the formation of Gogo dimers (which could influence Gogo signaling). However, since the expression of the non-phosphorylated form of Gogo in *gogo* mutant photoreceptors did not retarget R7 to the M3 layer (unpublished data), the targeting specificity of R8 axons can not rely only on Gogo dephosphorylation.

Another explanation would be that even if Gogo and Fmi are functioning in R7s during mid-pupal stages, R7 growth cones already overtook the R8-recipient layer and are located in a deeper layer in the medulla. The molecular cues encountered by R7 growth cones could thus be different from the ones received in more superficial layers by R8 axons. For instance, there could be imbalanced adhesion forces at the R8 and R7 recipient layers, and R7s would be more attracted by guidance cues in their recipient layer, while R8 axonal termini are too far to sense these cues. Co-overexpression of Gogo

and Fmi would change the balance of attraction forces towards the R8-recipient layer, thus generating the observed R7 stopping phenotype.

### 4.5.2 Specificity in the target medulla layers

In this study, we could demonstrate that *fmi* is necessary in the target area for R8 targeting, and that R8 axons tend to remain at the M1 layer when *fmi* is absent from the target cells. However, since Fmi is expressed in several layers in the medulla during the second targeting step, it is again difficult to understand why R8 axons select the M3 layer instead of other Fmi-expressing layers. Many attempts to overexpress Fmi in the target area did not lead to an R8 axon targeting phenotype (data not shown), what supports the idea that Fmi in the brain cannot determine synaptic-layer specificity alone. One explanation could be that Fmi in the target cells has only a permissive role for R8 targeting. Alternatively, one speculative but interesting idea would be that Fmi could have an instructive role in combination with another molecule expressed specifically in the R8-recepient layer. Planar cell polarity is established via specific homophilic interactions between asymmetric complexes that include Fmi: the Fmi-Fz complex in the distal part of pupal wing cells recruits Fmi-Vang on the proximal side. It would be intriguing if the Fmi-Gogo complex in R8 photoreceptor axons would interact with Fmi-FactorX in the target cells. This FactorX cannot be Gogo, since it is not detectable in the medulla by antibody staining and not required in the brain for R8 targeting (Tomasi et al., 2008).

## 4.6 Redundant mechanisms for R8 targeting

Even if *gogo* and *fmi* mutant have a strong phenotype, the percentage of R8 axon stopping at the M1 layer is not 100%, suggesting that redundant mechanisms act in parallel to mediate the targeting of R8 axons to the M3 layer. The cell adhesion molecule Caps and the axon guidance molecules Netrin and Frazzled are also involved in the targeting specificity of R8 axons.

Since Caps is a homophilic cell adhesion molecule and it is expressed specifically in R8 and several medulla layers including the R8-recipient layer, it has been proposed that homophilic Caps interactions between R8 axons and their target mediates the layer-targeting of R8s. However, Caps requirement in the target area has still not been demonstrated, and Caps does not act homophilically in the olfactory system. The phenotype of *caps* mutants is different from *gogo* and *fmi* mutants: R8 axons stop between M3 and M6 with a higher frequency (22%) than at more superficial layers than M3 (8%), indicating that the underlying mechanisms are distinct. The analysis of *caps* mutant R8 axons during early pupal stage showed that the phenotype starts to be visible between the first and second targeting step. However, the *caps* mutant phenotype has not been analyzed at the beginning of the second targeting step. It would be interesting to test whether R8 axons can not send filopodia to the M3 layer like in *fmi* and *gogo* mutants. However, since R7s that ectopically express Caps retarget the R8-recepient layer already at 30h APF, it seems that *caps* functions earlier than *gogo* and *fmi* in R8 axon targeting.

Netrin and Frazzled also play a role in R8 photoreceptor axon targeting. Since Netrin is located specifically in the R8-recepient layer during pupal stage, it is likely to participate in the specificity of R8 targeting (Katarina Timofev, Neurofly 2010).

To check whether these three molecular pathways are the key mechanisms that ensure the synaptic-layer specificity of R8s, it would be interesting to test if all R8 axons mistarget their correct layer in the triple knock-out.

Why is it necessary to have several redundant mechanisms for synaptic-layer specificity in the fly visual system? The redundancy seems to be needed to add robustness to the system. Visual perception is very important in flies, and the visual system represents half of the *Drosophila* brain. Therefore, it seems to be crucial that visual circuits are established with extreme precision. Even if the phenotypes are rather mild in the *caps* or *netrin* mutant, it probably already impairs proper visual information

processing in the brain, which could affect the survival of the flies. The model of synaptic molecular matchmaking, which propose that one molecule expressed specifically in a small subset of axons recognize another molecule specifically expressed in their target is probably a simplified vision of what is really occurring during nervous system development. In the *Drosophila* visual system, it seems that the superposition and complementarity of several mechanisms orchestrate the specificity of axonal targeting. These molecular mechanisms act at different temporal stages and in different subset of cells, and the combination of these distinct mechanisms allows the formation of precise connection patterns in the fly brain.

## 4.7 Concluding remarks and general considerations about axon targeting

Although the detailed mechanisms involved in the targeting of photoreceptor axons to precise layers in the medulla are not completely uncovered, the main goal of our work is to shed light on the general mechanisms of targeting specificity. Studies in the *Drosophila* visual system, including the work presented in this dissertation, led to the discovery of general principles of synaptic specificity that can be summarized as follow:

- Gradient of diffusible guidance cues, combined with the sequential cell differentiation of afferents and their synchronization with their target cells are the driving forces for topographic mapping.

- Some cell adhesion molecules are expressed only in a subset of cells, allowing matchmaking between axons and targets, but most of the transmembrane proteins involved in axon targeting are expressed widely.

- Temporally restricted axon competence to respond to broadly expressed guidance cues contribute to the specificity of synaptic-layer formation.

- What our study suggests is that the combination of cell surface molecules confers targeting specificity.

These general concepts found in the *Drosophila* visual system are mainly applicable to vertebrates. Nevertheless, one important difference is that the development of visual circuits in flies is defined exclusively genetically, whereas wiring up the nervous system in mammals comprises a higher level of complexity, since synaptic connectivity is refined by electrical activity. It will be interesting to determine whether neuronal activity ultimately leads to the same molecular mechanisms than those involved in earlier activity-independent steps of axonal targeting.

## SUPPLEMENTAL FIGURES

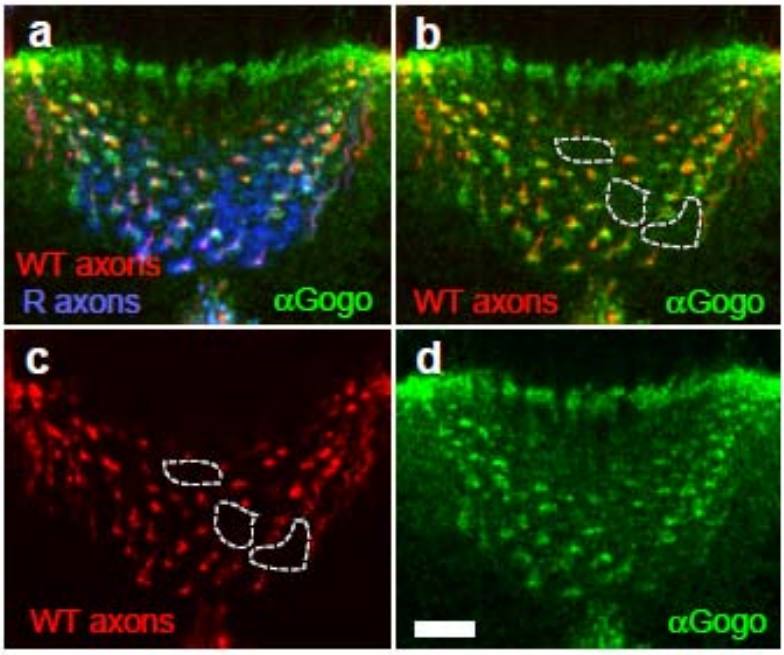


**Supplementary Fig1. Gogo accumulation at growth cones is reduced in *fmi* mutant axons.**
(**a-d**) *fmi* mutant R axon clones in the third instar larval optic lobe. WT axons are labeled in red, all R axons in blue, and Gogo in green. Gogo accumulation is reduced in *fmi* mutant growth cones (demarcated with dashed white lines). Scale bar: 10µm.

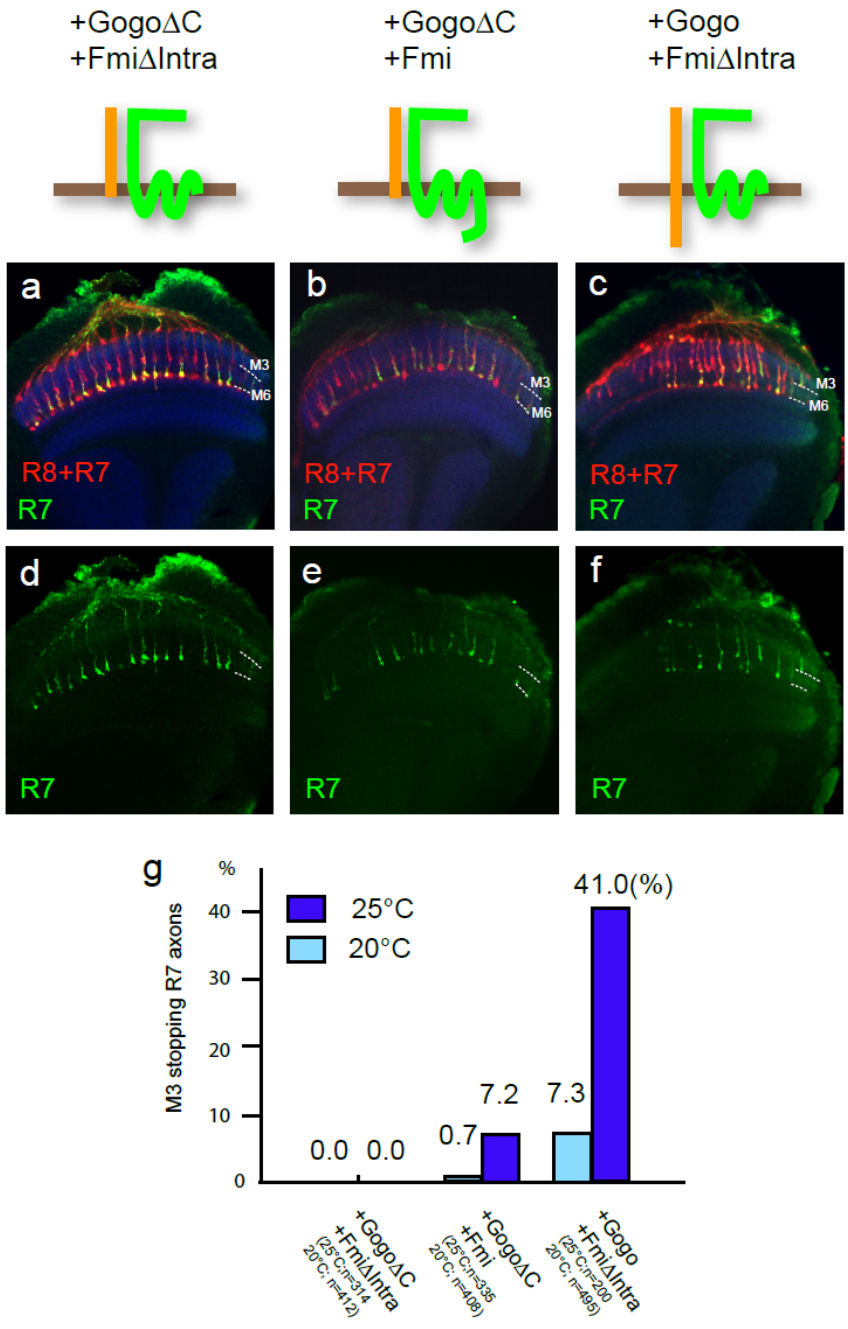


**Supplementary Fig2. Gogo and Fmi interact with intracellular components through the Gogo cytoplasmic domain.**
R7 and R8 axons in the medulla are stained with 24B10 antibody (red), R7s with *Rh4*-GFP (green), and medulla layers with anti-NCad (blue). (**a-f**) Phenotypes of R7 axons overexpressing different combinations of Gogo, Fmi and their cytoplasmic truncations. Overexpressed proteins are indicated above each panel. (**a**,**d**) R7 photoreceptors overexpressing GogoΔC and FmiΔIntra target normally to the M6 layer. (**b**,**e**) When GogoΔC and Fmi were overexpressed, few R7 axons stop at the M3 layer. (**c**,**f**) In flies overexpressing Gogo full length and FmiΔIntra, almost half of R7s stop at the M3 layer. (**g**) Quantification of the R7 stopping phenotype at the M3 layer. The cytoplasmic domain of Gogo is crucial to generate the R7 premature stopping phenotype.

## REFRERENCES

**Andrews, G. L., Tanglao, S., Farmer, W. T., Morin, S., Brotman, S., Berberoglu, M. A., Price, H., Fernandez, G. C., Mastick, G. S., Charron, F. et al.** (2008). Dscam guides embryonic axons by Netrin-dependent and -independent functions. *Development* **135**, 3839-48.

**Astigarraga, S., Hofmeyer, K. and Treisman, J. E.** Missed connections: photoreceptor axon seeks target neuron for synaptogenesis. *Curr Opin Genet Dev* **20**, 400-7.

**Augsburger, A., Schuchardt, A., Hoskins, S., Dodd, J. and Butler, S.** (1999). BMPs as mediators of roof plate repulsion of commissural neurons. *Neuron* **24**, 127-41.

**Bao, H., Berlanga, M. L., Xue, M., Hapip, S. M., Daniels, R. W., Mendenhall, J. M., Alcantara, A. A. and Zhang, B.** (2007). The atypical cadherin flamingo regulates synaptogenesis and helps prevent axonal and synaptic degeneration in Drosophila. *Mol Cell Neurosci* **34**, 662-78.

**Bashaw, G. J. and Klein, R.** (2010). Signaling from axon guidance receptors. *Cold Spring Harb Perspect Biol* **2**, a001941.

**Battye, R., Stevens, A. and Jacobs, J. R.** (1999). Axon repulsion from the midline of the Drosophila CNS requires slit function. *Development* **126**, 2475-81.

**Bazigou, E., Apitz, H., Johansson, J., Loren, C. E., Hirst, E. M., Chen, P. L., Palmer, R. H. and Salecker, I.** (2007). Anterograde Jelly belly and Alk receptor tyrosine kinase signaling mediates retinal axon targeting in Drosophila. *Cell* **128**, 961-75.

**Berger, J., Senti, K. A., Senti, G., Newsome, T. P., Asling, B., Dickson, B. J. and Suzuki, T.** (2008). Systematic identification of genes that regulate neuronal wiring in the Drosophila visual system. *PLoS Genet* **4**, e1000085.

**Bouquet, C. and Nothias, F.** (2007). Molecular mechanisms of axonal growth. *Adv Exp Med Biol* **621**, 1-16.

**Cajal, S. and Sanchez, D.** (1915). Contribucion al conocimiento de los centros nerviosos de los insectos. In *Trabajos del Laboratorio de Investigaciones biológicas de la Universidad de Madrid,* vol. 13 (ed., pp. 1-167.

**Chae, J., Kim, M. J., Goo, J. H., Collier, S., Gubb, D., Charlton, J., Adler, P. N. and Park, W. J.** (1999). The Drosophila tissue polarity gene starry night encodes a member of the protocadherin family. *Development* **126**, 5421-9.

**Charron, F., Stein, E., Jeong, J., McMahon, A. P. and Tessier-Lavigne, M.** (2003). The morphogen sonic hedgehog is an axonal chemoattractant that collaborates with netrin-1 in midline axon guidance. *Cell* **113**, 11-23.

**Chen, P. L. and Clandinin, T. R.** (2008). The cadherin Flamingo mediates level-dependent interactions that guide photoreceptor target choice in Drosophila. *Neuron* **58**, 26-33.

**Chotard, C., Leung, W. and Salecker, I.** (2005). glial cells missing and gcm2 cell autonomously regulate both glial and neuronal development in the visual system of Drosophila. *Neuron* **48**, 237-51.

**Clandinin, T. R., Lee, C. H., Herman, T., Lee, R. C., Yang, A. Y., Ovasapyan, S. and Zipursky, S. L.** (2001). Drosophila LAR regulates R1-R6 and R7 target specificity in the visual system. *Neuron* **32**, 237-48.

**Clandinin, T. R. and Zipursky, S. L.** (2000). Afferent growth cone interactions control synaptic specificity in the Drosophila visual system. *Neuron* **28**, 427-36.

**Culotti, J. G. and Merz, D. C.** (1998). DCC and netrins. *Curr Opin Cell Biol* **10**, 609-13.
**Dickson, B. J.** (2002). Molecular mechanisms of axon guidance. *Science* **298**, 1959-64.

**Dworak, H. A., Charles, M. A., Pellerano, L. B. and Sink, H.** (2001). Characterization of Drosophila hibris, a gene related to human nephrin. *Development* **128**, 4265-76.

**Fischbach, K. F.** (1983). Neural cell types surviving congenital sensory deprivation in the optic lobes of Drosophila melanogaster. *Dev Biol* **95**, 1-18.

**Fredriksson, S., Gullberg, M., Jarvius, J., Olsson, C., Pietras, K., Gustafsdottir, S. M., Ostman, A. and Landegren, U.** (2002). Protein detection using proximity-dependent DNA ligation assays. *Nat Biotechnol* **20**, 473-7.

**Gao, F. B., Kohwi, M., Brenman, J. E., Jan, L. Y. and Jan, Y. N.** (2000). Control of dendritic field formation in Drosophila: the roles of flamingo and competition between homologous neurons. *Neuron* **28**, 91-101.

**Garrity, P. A., Lee, C. H., Salecker, I., Robertson, H. C., Desai, C. J., Zinn, K. and Zipursky, S. L.** (1999). Retinal axon target selection in Drosophila is regulated by a receptor protein tyrosine phosphatase. *Neuron* **22**, 707-17.

**Hakeda-Suzuki, S., Berger-Muller, S., Tomasi, T., Usui, T., Horiuchi, S. Y., Uemura, T. and Suzuki, T.** (2011). Golden Goal collaborates with Flamingo in conferring synaptic-layer specificity in the visual system. *Nat Neurosci* **14**, 314-23.

**Harrelson, A. L. and Goodman, C. S.** (1988). Growth cone guidance in insects: fasciclin II is a member of the immunoglobulin superfamily. *Science* **242**, 700-8.

**Hedgecock, E. M., Culotti, J. G. and Hall, D. H.** (1990). The unc-5, unc-6, and unc-40 genes guide circumferential migrations of pioneer axons and mesodermal cells on the epidermis in C. elegans. *Neuron* **4**, 61-85.

**Hiesinger, P. R., Zhai, R. G., Zhou, Y., Koh, T. W., Mehta, S. Q., Schulze, K. L., Cao, Y., Verstreken, P., Clandinin, T. R., Fischbach, K. F. et al.** (2006). Activity-independent prespecification of synaptic partners in the visual map of Drosophila. *Curr Biol* **16**, 1835-43.

**Hong, W., Zhu, H., Potter, C. J., Barsh, G., Kurusu, M., Zinn, K. and Luo, L.** (2009). Leucine-rich repeat transmembrane proteins instruct discrete dendrite targeting in an olfactory map. *Nat Neurosci* **12**, 1542-50.

**Huang, Z. and Kunes, S.** (1996). Hedgehog, transmitted along retinal axons, triggers neurogenesis in the developing visual centers of the Drosophila brain. *Cell* **86**, 411-22.

**Huang, Z., Shilo, B. Z. and Kunes, S.** (1998). A retinal axon fascicle uses spitz, an EGF receptor ligand, to construct a synaptic cartridge in the brain of Drosophila. *Cell* **95**, 693-703.

**Huberman, A. D., Clandinin, T. R. and Baier, H.** Molecular and cellular mechanisms of lamina-specific axon targeting. *Cold Spring Harb Perspect Biol* **2**, a001743.

**Kaneko-Goto, T., Yoshihara, S., Miyazaki, H. and Yoshihara, Y.** (2008). BIG-2 mediates olfactory axon convergence to target glomeruli. *Neuron* **57**, 834-46.

**Keleman, K. and Dickson, B. J.** (2001). Short- and long-range repulsion by the Drosophila Unc5 netrin receptor. *Neuron* **32**, 605-17.

**Kerppola, T. K.** (2006). Design and implementation of bimolecular fluorescence complementation (BiFC) assays for the visualization of protein interactions in living cells. *Nat Protoc* **1**, 1278-86.

**Kidd, T., Bland, K. S. and Goodman, C. S.** (1999). Slit is the midline repellent for the robo receptor in Drosophila. *Cell* **96**, 785-94.

**Kidd, T., Brose, K., Mitchell, K. J., Fetter, R. D., Tessier-Lavigne, M., Goodman, C. S. and Tear, G.** (1998). Roundabout controls axon crossing of the CNS midline and defines a novel subfamily of evolutionarily conserved guidance receptors. *Cell* **92**, 205-15.

**Kimura, H., Usui, T., Tsubouchi, A. and Uemura, T.** (2006). Potential dual molecular interaction of the Drosophila 7-pass transmembrane cadherin Flamingo in dendritic morphogenesis. *J Cell Sci* **119**, 1118-29.

**Kirkpatrick, C. and Peifer, M.** (1995). Not just glue: cell-cell junctions as cellular signaling centers. *Curr Opin Genet Dev* **5**, 56-65.

**Lee, C. H., Herman, T., Clandinin, T. R., Lee, R. and Zipursky, S. L.** (2001). N-cadherin regulates target specificity in the Drosophila visual system. *Neuron* **30**, 437-50.

**Lee, R. C., Clandinin, T. R., Lee, C. H., Chen, P. L., Meinertzhagen, I. A. and Zipursky, S. L.** (2003). The protocadherin Flamingo is required for axon target selection in the Drosophila visual system. *Nat Neurosci* **6**, 557-63.

**Leung, K. M., van Horck, F. P., Lin, A. C., Allison, R., Standart, N. and Holt, C. E.** (2006). Asymmetrical beta-actin mRNA translation in growth cones mediates attractive turning to netrin-1. *Nat Neurosci* **9**, 1247-56.

**Luo, L. and Flanagan, J. G.** (2007). Development of continuous and discrete neural maps. *Neuron* **56**, 284-300.

**Ly, A., Nikolaev, A., Suresh, G., Zheng, Y., Tessier-Lavigne, M. and Stein, E.** (2008). DSCAM is a netrin receptor that collaborates with DCC in mediating turning responses to netrin-1. *Cell* **133**, 1241-54.

**Lyuksyutova, A. I., Lu, C. C., Milanesio, N., King, L. A., Guo, N., Wang, Y., Nathans, J., Tessier-Lavigne, M. and Zou, Y.** (2003). Anterior-posterior guidance of commissural axons by Wnt-frizzled signaling. *Science* **302**, 1984-8.

**Malaga-Trillo, E., Solis, G. P., Schrock, Y., Geiss, C., Luncz, L., Thomanetz, V. and Stuermer, C. A.** (2009). Regulation of embryonic cell adhesion by the prion protein. *PLoS Biol* **7**, e55.

**Masi, A., Cicchi, R., Carloni, A., Pavone, F. S. and Arcangeli, A.** Optical methods in the study of protein-protein interactions. *Adv Exp Med Biol* **674**, 33-42.

**Mast, J. D., Prakash, S., Chen, P. L. and Clandinin, T. R.** (2006). The mechanisms and molecules that connect photoreceptor axons to their targets in Drosophila. *Semin Cell Dev Biol* **17**, 42-9.

**Maurel-Zaffran, C., Suzuki, T., Gahmon, G., Treisman, J. E. and Dickson, B. J.** (2001). Cell-autonomous and -nonautonomous functions of LAR in R7 photoreceptor axon targeting. *Neuron* **32**, 225-35.

**Meinertzhagen, I. A. and Sorra, K. E.** (2001). Synaptic organization in the fly's optic lamina: few cells, many synapses and divergent microcircuits. *Prog Brain Res* **131**, 53-69.

**Millard, S. S., Flanagan, J. J., Pappu, K. S., Wu, W. and Zipursky, S. L.** (2007). Dscam2 mediates axonal tiling in the Drosophila visual system. *Nature* **447**, 720-4.

**Mitchell, K. J., Doyle, J. L., Serafini, T., Kennedy, T. E., Tessier-Lavigne, M., Goodman, C. S. and Dickson, B. J.** (1996). Genetic analysis of Netrin genes in Drosophila: Netrins guide CNS commissural axons and peripheral motor axons. *Neuron* **17**, 203-15.

**Mottola, G., Classen, A. K., Gonzalez-Gaitan, M., Eaton, S. and Zerial, M.** (2010). A novel function for the Rab5 effector Rabenosyn-5 in planar cell polarity. *Development* **137**, 2353-64.

**Nern, A., Nguyen, L. V., Herman, T., Prakash, S., Clandinin, T. R. and Zipursky, S. L.** (2005). An isoform-specific allele of Drosophila N-cadherin disrupts a late step of R7 targeting. *Proc Natl Acad Sci U S A* **102**, 12944-9.

**Nern, A., Zhu, Y. and Zipursky, S. L.** (2008). Local N-cadherin interactions mediate distinct steps in the targeting of lamina neurons. *Neuron* **58**, 34-41.

**Newsome, T. P., Asling, B. and Dickson, B. J.** (2000). Analysis of Drosophila photoreceptor axon guidance in eye-specific mosaics. *Development* **127**, 851-60.

**Pecho-Vrieseling, E., Sigrist, M., Yoshida, Y., Jessell, T. M. and Arber, S.** (2009). Specificity of sensory-motor connections encoded by Sema3e-Plxnd1 recognition. *Nature* **459**, 842-6.

**Petrovic, M. and Hummel, T.** (2008). Temporal identity in axonal target layer recognition. *Nature* **456**, 800-3.

**Plaza, S., Prince, F., Adachi, Y., Punzo, C., Cribbs, D. L. and Gehring, W. J.** (2008). Cross-regulatory protein-protein interactions between Hox and Pax transcription factors. *Proc Natl Acad Sci U S A* **105**, 13439-44.

**Poeck, B., Fischer, S., Gunning, D., Zipursky, S. L. and Salecker, I.** (2001). Glial cells mediate target layer selection of retinal axons in the developing visual system of Drosophila. *Neuron* **29**, 99-113.

**Prakash, S., Caldwell, J. C., Eberl, D. F. and Clandinin, T. R.** (2005). Drosophila N-cadherin mediates an attractive interaction between photoreceptor axons and their targets. *Nat Neurosci* **8**, 443-50.

**Prakash, S., McLendon, H. M., Dubreuil, C. I., Ghose, A., Hwa, J., Dennehy, K. A., Tomalty, K. M., Clark, K. L., Van Vactor, D. and Clandinin, T. R.** (2009). Complex interactions amongst N-cadherin, DLAR, and Liprin-alpha regulate Drosophila photoreceptor axon targeting. *Dev Biol* **336**, 10-9.

**Robinow, S., Campos, A. R., Yao, K. M. and White, K.** (1988). The elav gene product of Drosophila, required in neurons, has three RNP consensus motifs. *Science* **242**, 1570-2.

**Saka, Y., Hagemann, A. I. and Smith, J. C.** (2008). Visualizing protein interactions by bimolecular fluorescence complementation in Xenopus. *Methods* **45**, 192-5.

**Sanes, J. R. and Yamagata, M.** (2009). Many paths to synaptic specificity. *Annu Rev Cell Dev Biol* **25**, 161-95.

**Sanes, J. R. and Zipursky, S. L.** (2010). Design principles of insect and vertebrate visual systems. *Neuron* **66**, 15-36.

**Sato, M., Umetsu, D., Murakami, S., Yasugi, T. and Tabata, T.** (2006). DWnt4 regulates the dorsoventral specificity of retinal projections in the Drosophila melanogaster visual system. *Nat Neurosci* **9**, 67-75.

**Seeger, M., Tear, G., Ferres-Marco, D. and Goodman, C. S.** (1993). Mutations affecting growth cone guidance in Drosophila: genes necessary for guidance toward or away from the midline. *Neuron* **10**, 409-26.

**Senti, K. A., Usui, T., Boucke, K., Greber, U., Uemura, T. and Dickson, B. J.** (2003). Flamingo regulates R8 axon-axon and axon-target interactions in the Drosophila visual system. *Curr Biol* **13**, 828-32.

**Serafini, T., Colamarino, S. A., Leonardo, E. D., Wang, H., Beddington, R., Skarnes, W. C. and Tessier-Lavigne, M.** (1996). Netrin-1 is required for commissural axon guidance in the developing vertebrate nervous system. *Cell* **87**, 1001-14.

**Serizawa, S., Miyamichi, K., Takeuchi, H., Yamagishi, Y., Suzuki, M. and Sakano, H.** (2006). A neuronal identity code for the odorant receptor-specific and activity-dependent axon sorting. *Cell* **127**, 1057-69.

**Shapiro, L., Love, J. and Colman, D. R.** (2007). Adhesion molecules in the nervous system: structural insights into function and diversity. *Annu Rev Neurosci* **30**, 451-74.

**Shinza-Kameda, M., Takasu, E., Sakurai, K., Hayashi, S. and Nose, A.** (2006). Regulation of layer-specific targeting by reciprocal expression of a cell adhesion molecule, capricious. *Neuron* **49**, 205-13.

**Shishido, E., Takeichi, M. and Nose, A.** (1998). Drosophila synapse formation: regulation by transmembrane protein with Leu-rich repeats, CAPRICIOUS. *Science* **280**, 2118-21.

**Siebert, M., Banovic, D., Goellner, B. and Aberle, H.** (2009). Drosophila motor axons recognize and follow a Sidestep-labeled substrate pathway to reach their target fields. *Genes Dev* **23**, 1052-62.

**Soderberg, O., Gullberg, M., Jarvius, M., Ridderstrale, K., Leuchowius, K. J., Jarvius, J., Wester, K., Hydbring, P., Bahram, F., Larsson, L. G. et al.** (2006). Direct observation of individual endogenous protein complexes in situ by proximity ligation. *Nat Methods* **3**, 995-1000.

**Soderberg, O., Leuchowius, K. J., Gullberg, M., Jarvius, M., Weibrecht, I., Larsson, L. G. and Landegren, U.** (2008). Characterizing proteins and their interactions in cells and tissues using the in situ proximity ligation assay. *Methods* **45**, 227-32.

**Strutt, H. and Strutt, D.** (2008). Differential stability of flamingo protein complexes underlies the establishment of planar polarity. *Curr Biol* **18**, 1555-64.

**Takeichi, M.** (2007). The cadherin superfamily in neuronal connections and interactions. *Nat Rev Neurosci* **8**, 11-20.

**Takemura, S. Y., Lu, Z. and Meinertzhagen, I. A.** (2008). Synaptic circuits of the Drosophila optic lobe: the input terminals to the medulla. *J Comp Neurol* **509**, 493-513.

**Ting, C. Y., Yonekura, S., Chung, P., Hsu, S. N., Robertson, H. M., Chiba, A. and Lee, C. H.** (2005). Drosophila N-cadherin functions in the first stage of the two-stage layer-selection process of R7 photoreceptor afferents. *Development* **132**, 953-63.

**Tojima, T., Akiyama, H., Itofusa, R., Li, Y., Katayama, H., Miyawaki, A. and Kamiguchi, H.** (2007). Attractive axon guidance involves asymmetric membrane transport and exocytosis in the growth cone. *Nat Neurosci* **10**, 58-66.

**Tojima, T., Itofusa, R. and Kamiguchi, H.** (2010). Asymmetric clathrin-mediated endocytosis drives repulsive growth cone guidance. *Neuron* **66**, 370-7.

**Tomasi, T., Hakeda-Suzuki, S., Ohler, S., Schleiffer, A. and Suzuki, T.** (2008). The transmembrane protein Golden goal regulates R8 photoreceptor axon-axon and axon-target interactions. *Neuron* **57**, 691-704.

**Tree, D. R., Shulman, J. M., Rousset, R., Scott, M. P., Gubb, D. and Axelrod, J. D.** (2002). Prickle mediates feedback amplification to generate asymmetric planar cell polarity signaling. *Cell* **109**, 371-81.

**Usui, T., Shima, Y., Shimada, Y., Hirano, S., Burgess, R. W., Schwarz, T. L., Takeichi, M. and Uemura, T.** (1999). Flamingo, a seven-pass transmembrane cadherin, regulates planar cell polarity under the control of Frizzled. *Cell* **98**, 585-95.

**Xiong, W. C., Okano, H., Patel, N. H., Blendy, J. A. and Montell, C.** (1994). repo encodes a glial-specific homeo domain protein required in the Drosophila nervous system. *Genes Dev* **8**, 981-94.

**Yamagata, M. and Sanes, J. R.** (2008). Dscam and Sidekick proteins direct lamina-specific synaptic connections in vertebrate retina. *Nature* **451**, 465-9.

**Yamagata, M., Weiner, J. A. and Sanes, J. R.** (2002). Sidekicks: synaptic adhesion molecules that promote lamina-specific connectivity in the retina. *Cell* **110**, 649-60.

**Yao, J., Sasaki, Y., Wen, Z., Bassell, G. J. and Zheng, J. Q.** (2006). An essential role for beta-actin mRNA localization and translation in Ca2+-dependent growth cone guidance. *Nat Neurosci* **9**, 1265-73.

**Yazdani, U. and Terman, J. R.** (2006). The semaphorins. *Genome Biol* **7**, 211.

**Yonekura, S., Ting, C. Y., Neves, G., Hung, K., Hsu, S. N., Chiba, A., Chess, A. and Lee, C. H.** (2006). The variable transmembrane domain of Drosophila N-cadherin regulates adhesive activity. *Mol Cell Biol* **26**, 6598-608.

**Zhou, L., Schnitzler, A., Agapite, J., Schwartz, L. M., Steller, H. and Nambu, J. R.** (1997). Cooperative functions of the reaper and head involution defective genes in the programmed cell death of Drosophila central nervous system midline cells. *Proc Natl Acad Sci U S A* **94**, 5131-6.

**Zou, D. J., Feinstein, P., Rivers, A. L., Mathews, G. A., Kim, A., Greer, C. A., Mombaerts, P. and Firestein, S.** (2004). Postnatal refinement of peripheral olfactory projections. *Science* **304**, 1976-9.

**Zou, Y. and Lyuksyutova, A. I.** (2007). Morphogens as conserved axon guidance cues. *Curr Opin Neurobiol* **17**, 22-8.

## ACKNOWLEDGMENTS

First of all, I would like to thank Takashi Suzuki for allowing me to work in his lab on this exciting project. Thank you for your constant support and supervising, and for giving me the opportunity to present my work at several conferences.

I am thankful to Satoko Suzuki for her collaboration in this project (her contribution is detailed at the end of the introduction). I would like to thank you for your precious advice and great expertise in Drosophila genetics. I also thank Narin Hengrung and Birgit Schuster for their help in the BiFC experiment.

I am grateful to my thesis committee members, Rüdiger Klein and Frank Schnorrer, for their helpful suggestions. I especially thank Rüdiger Klein for being my official Doktovater.

Thanks to all the Suzuki lab members, for scientific discussions and the nice atmosphere in the lab. I especially want to thank Cristina for muffin and ice cream breaks, Klaudiusz for the beautiful drawings on the cell culture flasks, and Irina for intense chatting and playing motivating music in the fly room.

I would like to thank all the friends I made at the Institute during my PhD. Especially, I want to thank Sarah, Lindita, Thorben, Arnab, Jörg, Farida, Dodo, Vanessa, Frank, Michi, Kevyn, Kathrin, Igor, Julia, and Pontus for the nice “working” atmosphere and the funny after-work parties and PhD retreats. I had a wonderful time with you!

I want to thank my husband Jörg for his love and his support in the moments of frustration which are not so rare during a PhD thesis.

Enfin, je souhaite dire un immense merci à mes parents pour leur engagement et leur support durant toutes mes études. Je n’aurais jamais pu arriver là sans votre aide précieuse, vos encouragements et votre amour.

# CURRICULUM VITAE

## PERSONAL INFORMATION


| | |
|---|---|
| Name: | Sandra Müller |
| Email address: | Sandra.muller@gmx.de |
| Date of birth: | 29.04.1984 |
| Nationality: | French |


## EDUCATIONAL BACKGROUND

| | |
|---|---|
| 2007-2011 | **PH.D. AT THE MAX PLANCK INSTITUTE OF NEUROBIOLOGY** (Munich, Germany). |
| 2004-2007 | **INSTITUT NATIONAL AGRONOMIQUE** (Paris-Grignon, France). Master with major in molecular biology/biochemistry. |
| 2002-2004 | **CLASSES PREPARATOIRES BCPST OZENNE** (Toulouse, France). Intensive coursework in biology, physics, chemistry and mathematics for the preparation of the national entrance examination for French engineering schools. |
| June 2002 | **LYCEE FERMAT** (Toulouse, France). Scientific High School diploma. |

## PROFESSIONAL EXPERIENCE

| | |
|---|---|
| Oct 2007- 2011 | **PH.D. AT THE MAX PLANCK INSTITUTE OF NEUROBIOLOGY** (Munich, Germany).<br>*Study of mechanisms underlying axon guidance and neuronal connectivity*<br>Laboratory techniques: molecular cloning, cell culture, western blot, co-immunoprecipitation, confocal microscopy, Drosophila genetics |
| Mars-Sept 2007 | **DIPLOMA THESIS AT SANOFI-AVENTIS** (Labège, France).<br>*Evaluation of the cytotoxicity of an anti-depressive drug*<br>Techniques used: culture of hepatic cells, cytotoxicity test, western blot, Free Flow Electrophoresis |
| June-August 2006 | **INTERNSHIP AT THE STOWERS INSTITUTE** (Kansas City, USA).<br>*Role of the glycosylation of a protein involved in the fusion of muscle cells in Drosophila* |

## PUBLICATIONS AND CONFERENCES

| | |
|---|---|
| Publications: | - Hakeda-Suzuki S*, Berger-Mueller S*, Usui T, Horiuchi S, Uemura T, Suzuki T (2011). Golden Goal Collaborates with Flamingo in Conferring Synaptic-Layer Specificity in the Visual System. *Nature Neuroscience* **14**, 314–323<br>- Berger-Mueller S, Suzuki T. Seven-pass transmembrane cadherins: roles and emerging mechanisms in axonal and dendritic patterning. *Molecular Neurobiology (*in press). |
| Main conferences: | - Oral presentation at the Cold Spring Harbor Laboratory conference on "Axon guidance, synaptic plasticity and regeneration", Sept. 2010 (New York, USA)<br>- Poster presentation at the Neurofly, Sept. 2010 (Manchester, UK)<br>- Poster at the European Drosophila Research Conference, Nov. 2009 (Nice, France) |